Laboratory Performance Characterization of Asphalt Mixtures Containing Aging-Resistant Technologies

by

Josue Adrian Garita-Jimenez

A thesis submitted to the Graduate Faculty of
Auburn University
in partial fulfillment of the
requirements for the Degree of
Master of Science

Auburn, Alabama
May 03, 2024

Keywords: Asphalt aging, aging resistance,
asphalt mixtures, asphalt modification.

Approved by

Nam Hoai Tran, Chair, PhD, Civil and Environmental Engineering
Randy West, PhD, Civil and Environmental Engineering
Fan Yin, PhD, Civil and Environmental Engineering
Raquel Moraes Puchalski, PhD, Civil and Environmental Engineering
Carolina Rodezno, PhD, Civil and Environmental Engineering

ABSTRACT

Incorporating various aging-resistant technologies to prevent the adverse effects of aging into asphalt mixtures is believed to slow down the oxidative aging process of asphalt binders and, therefore, asphalt mixtures. Effective technologies would make asphalt mixtures less susceptible to fatigue cracking and extend pavement's service life. There is a necessity for the asphalt pavement industry to efficiently evaluate the effectiveness of additive technologies so that they can be implemented.

The primary purpose of this study is to evaluate through laboratory testing if five anti-aging additive technologies reduce aging susceptibility and increase the cracking resistance of asphalt mixtures. The additives included (1) a thermosetting two-phase epoxy polymer and oil-based modifiers, (2) a hybrid ground tire rubber powder and a polymeric compound system, (3) a hybrid high-content polymer with pine-based chemical-based recycling agent, (4) a bio-polymer from epoxidized soybean oil, and (5) a biosynthetic, petroleum-based, and rheology modifiers blend.

For this evaluation, mixtures containing two selected base binders (i.e., B1 and B5) from different sources and characteristics were modified with the additives and aged at three aging levels (i.e., Short-Term Oven Aging (STOA), Long-Term Oven Aging (LTOA), and NCAT Accelerated Weathering System(NAWS)). The effect of the additive technology on the fatigue cracking performance of the mixes after aging was evaluated through Dynamic Modulus ($|E^*|$) and Cyclic Fatigue testing results. The Cyclic Fatigue Index (S_{app}) and Glover-Rowe mix Index ($G\text{-}R_m$) were calculated to determine the mixtures' fatigue cracking resistance and aging susceptibility after aging. Pavement structural analysis was performed using the FlexPAVE^{TM} software to determine the percent cracking damage evolution of the mixtures for an analysis period of 20 years. Finally, the Asphalt Mixture Aging-Cracking (AMAC) model predicted 5-day oven aging at 95°C. The

predicted data was compared to the experimental LTOA results for the model evaluation. The same model was also used to determine the degree of aging induced by the NAWS method in terms of days of loose mixture aging at 95°C.

The results indicated that the additives effectively improved the properties related to increased cracking resistance after extended aging compared to the control mixtures. However, the effectiveness of the additive depended on the base binder and aging method.

ACKNOWLEDGMENTS

I couldn't be more grateful to god and all the people at NCAT who trusted me with the opportunity to contribute to this project, which allowed me to be a better professional, researcher, and engineer.

I want to thank my advisor, Dr. Nam Tran, for his support, encouragement, confidence, and guidance during this project. I appreciate the guidance and support of my committee members, Dr. Randy West, Dr. Fan Yin, Dr. Carolina Rodezno, and Dr. Raquel Moraes, whom I admire and who contributed to the completion of this project. And not less important, to every professor I had during the program, which provided me with the knowledge and skills to complete this study. I couldn't imagine this project succeeding without the key work and support on the performance testing from Adam Taylor and Tina at NCAT.

My personal experience during the Master's program has been enriched by the support, company, and joy shared with my closest friends—Anthony Brenes, Fernando Cordero, Luis Munoz, Orlando Fiallos, Javier Lopez, Andrew Szydel, Henry Alter, Kayleen McCafferty, and all the people with whom I created unforgettable experiences during this time in Auburn.

Finally, thanks to my parents and brother, the most influential figures in my life, for inspiring me daily to find joy in my work and life. This achievement is the realization of years of incomparable effort from my parents, to whom I couldn't be more grateful for their love and guidance in everything I do.

TABLE OF CONTENTS

LIST OF TABLES

LIST OF FIGURES

CHAPTER 1 - INTRODUCTION

1.1. Background

The first observations of the detrimental effects of aging on asphalt pavements were made around the 1900s (Sirin, Paul, & Kassem, 2018a). Subsequent studies have consistently demonstrated that aging plays a significant role in the performance of asphalt mixtures and pavements (Baek, Underwood, & Kim, 2012).

The aging process alters the rheological and chemical properties of asphalt binders, impacting the behavior of asphalt mixtures and, consequently, the long-term performance of asphalt pavements (Barghabany, Zhang, Mohammad, Cooper, & Cooper, 2022). These changes lead to embrittlement and hardening of asphalt mixtures, making pavements more susceptible to cracking (Huh & Robertson, 1996). The increased stiffness and brittleness of aged mixtures have raised concerns among agencies and contractors about potential long-term performance issues (Hand, 2021).

With the increasing use of recycled materials, such as recycled asphalt pavement (RAP) and recycled asphalt shingles (RAS), in asphalt mixes, minimizing aging effects becomes more important (Copeland, 2011). The oxidation that occurs during the previous service life of these recycled components introduces an aged binder to the mix, resulting in a hardening effect upon their incorporation (Ahmed & Hossain, 2020; W. Mogawer et al., 2012).

In response to these concerns, aging-resistant technologies have been developed as additives for asphalt mixtures to enhance pavement performance by mitigating the effects of aging on asphalt binder properties (Camargo, Dhia, Loulizi, Hofko, & Mirwald, 2021). Several innovative technologies have demonstrated potential in slowing the oxidative aging of asphalt binders and, in some cases, improving asphalt binder properties, both of which lead to enhanced

pavement performance (I. G. D. Camargo, T. Ben Dhia, A. Loulizi, B. Hofko, & J. Mirwald, 2021; Feng, Xu, Sun, & Yu, 2012; Sirin et al., 2018a). Therefore, evaluating the effectiveness of these technologies in asphalt mixtures is an essential step.

While field performance evaluation is considered the most reliable method for assessing the impact of these additives (Timm, Yin, Tran, Foshee, & Rodezno, 2022), it often requires substantial costs and complex procedures, making it less efficient for the industry to evaluate these technologies. Laboratory-based testing offers a practical alternative for efficiently gathering crucial insights into the cracking performance of asphalt binders and mixtures. The material properties of the asphalt layer can be determined through various tests, such as dynamic modulus and cyclic fatigue tests. These properties are the basis for calculating performance indexes like Glover-Rowe (G-R) and S_{app}, which are directly linked to the fatigue cracking performance of asphalt pavements (Glover, 2005; Y. R. Y. W. B. S. U. Kim, 2019).

Furthermore, the properties of both binder and mixtures obtained through laboratory testing can be used to model the performance of pavements throughout their service life. This modeling is facilitated by the use of the Layered Viscoelastic Pavement Design software, known as FlexPave™. Previous research has demonstrated that results from the FlexPave™ software exhibit reasonable trends and a strong correlation with field performance (Cao, Mohammad, Barghabany, & Cooper, 2019; Cao, Norouzi, & Kim, 2016; Park, Eslaminia, & Kim, 2014; Y. D. Wang, Keshavarzi, & Kim, 2018).

1.2. Research Hypothesis

Incorporating selected aging-resistant technologies into asphalt mixes with RAP can reduce their susceptibility to aging and sustain their resistance to cracking.

1.3. Research Objective

The objective of this research was to assess whether selected aging-resistant technologies can mitigate the aging susceptibility of asphalt mixtures and enhance their fatigue cracking performance following long-term aging. This assessment employed fatigue cracking performance indicators and predicted damage curves derived from laboratory test results and pavement analysis.

1.4. Research Scope

This study consisted of three main experiments. The initial experiment focused on selecting two base binders to evaluate the chosen aging-resistant technologies. The second experiment aimed to assess the binders with and without aging-resistant technologies. Finally, the last experiment described in this thesis aimed to evaluate the asphalt mixtures with the base binders and those modified with the selected aging-resistant technologies.

Asphalt mixture specimens were fabricated using five additive technologies with two distinct base binders. These mixtures were subjected to three aging conditions and compared to control mixes without aging-resistant additives. A set of small specimens was fabricated for each base binder, additive technology, and aging condition. The aging conditions included Short-Term-Oven Aging (STOA), Long-term-oven aging (LTOA), and the NCAT Accelerated Weathering System (NAWS), which were used to simulate aging effects on the mixtures analyzed in this study.

All variables, including mix design, volumetric properties, binder content, and testing conditions, remained consistent for each tested mixture. The sole variations between sets were the type of additive integrated into the mix and the dosage of the additive blended with the binder, with dosages selected according to manufacturers' recommendations.

Dynamic modulus ($|E^*|$) and phase angle tests were executed on these samples using the Asphalt Mixture Performance Tester (AMPT). These tests provided the data necessary for the

computation of the mixture Glover-Rowe (G-R_m) parameters for each mix, allowing the characterization of the mixtures through master curves and black space diagrams. Subsequently, the S_{app} parameter was derived from the AMPT results to assess fatigue-cracking performance. Aging and effectiveness indexes were then computed using G-R_m and S_{app} to evaluate cracking and aging susceptibility.

Furthermore, performance simulations, considering environmental factors and varying load conditions, were executed using the FlexPave1.1™ software. These simulations generated damage curves for each mixture and estimated the pavement structure's damage by the end of the analysis period. These results facilitated the assessment of the life extension benefits associated with implementing these technologies.

The two base binders employed in this experiment were chosen based on prior evaluations conducted by the manufacturers, considering their compatibility with the aging technology and distinct aging susceptibility indicated by the rheological properties of the binders. It's worth noting that the scope of this study does not include a comparison of the effectiveness of each additive technology between the two base binders.

While the selected testing procedures for this project are not inherently complex, they did require experienced testers to prepare the samples, set the specimens adequately, and operate the equipment effectively to obtain reliable results. Balancing the need to reduce fabrication times while maintaining reliability, a minimum of three samples were tested for the dynamic modulus and fatigue cracking tests. Results were considered valid only if they demonstrated low variability, addressing the limitation of the number of samples tested. In cases where the variation in results exceeded acceptable limits, additional specimens were tested until the desired level of variability

was achieved. For cyclic fatigue testing, only results demonstrating a mid-level failure mode were accepted, as this indicated adequate specimen fabrication and setup for the test.

CHAPTER 2 - LITERATURE REVIEW

2.1. Introduction

Asphalt mixture properties change over time due to aging, caused mainly by volatilization, thermal and ultraviolet oxidation, and other chemical reactions during production, construction, and service stages (Randy C. West, 2018). The oxidation process has an irreversible stiffening effect on the mix, negatively impacting cracking performance, increasing maintenance costs, and reducing service life (Das, 2014). Incorporating high percentages of recycled material (i.e.,>20%) into asphalt mixtures significantly affects cracking susceptibility and long-term performance compared to mixes only containing virgin binder (Obaid et al., 2019). Alternatives such as the use of a softer virgin binder, increasing the total mixture binder content, and using rejuvenators or softening agents have been implemented to address this issue and offset the effects of incorporating aged binder into the mix (Zaumanis & Mallick, 2015). Increasing the amount of binder is not an economical solution. In contrast, using a softer virgin binder has been determined to be less effective than some rejuvenators in improving the asphalt mixture performance, leaving rejuvenators as a promising alternative for avoiding the negative effects of aging in asphalt mixtures (Ziari, Moniri, Bahri, & Saghafi, 2019a). The positive effects of some rejuvenators are evident in the reduction of stiffness of resulting asphalt mixtures. Still, the effects on the mixture performance are poorly understood, and more research is needed (Epps Martin et al., 2020). To address these challenges, this literature review explores the current state of research on aging in asphalt mixtures, the impact of recycled materials, and the effectiveness of various rejuvenators in mitigating these effects.

2.1.1 Asphalt Binder Aging

Asphalt binder is commonly described as a colloidal substance base composed of an asphaltene fraction dispersed in a continuous oily matrix known as the maltenes fraction (i.e., saturates, aromatics, and resins) (Lesueur, 2009; Pfeiffer & Saal, 1940). The composition of asphalt binder is characterized by a wide variation in the polarity of its components. The physical properties of asphalt binders are intricately linked to the balance between these polar and non-polar components. Polar molecules within the binder significantly alter the distribution of asphalt components within the oily matrix, thereby affecting the binder's mobility (J C Petersen, Harnsberger, & Robertson, 1996). The presence of polar molecules is associated with the elastic response in the viscoelastic behavior of the binder, whereas non-polar molecules contribute to the viscous response (Sultana & Bhasin, 2014).

Asphalt binders undergo aging processes during various stages of their service life, as illustrated in Figure 1. The initial phase is characterized by a rapid aging period known as short-term aging. This phase primarily results from losing volatile components within the binder during production and construction, leading to significant changes in the chemical composition and rheological properties (Roberts, 1996). Figure 2 illustrates the impact of aging on the mass percentages of individual SARA fractions during the early stages of service life. Notably, there is a substantial decrease in the mass of certain light gaseous components within the oily fractions, specifically saturates and resins. Concurrently, the mass of asphaltenes and aromatics increases as they react with oxygen. While high production and construction temperatures have traditionally been attributed as the primary causes of short-term aging, it is essential to recognize that factors such as binder source, binder type, aggregate absorption, plant type, production temperature, and silo storage time also play roles in influencing the short-term aging process (Newcomb et al., 2019).

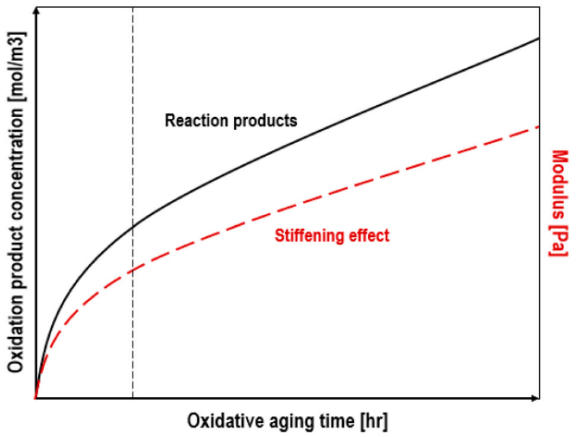

Figure 1. Schematic illustration of a typical asphalt oxidation in-service condition (Apostolidis, Liu, Erkens, & Scarpas, 2022)

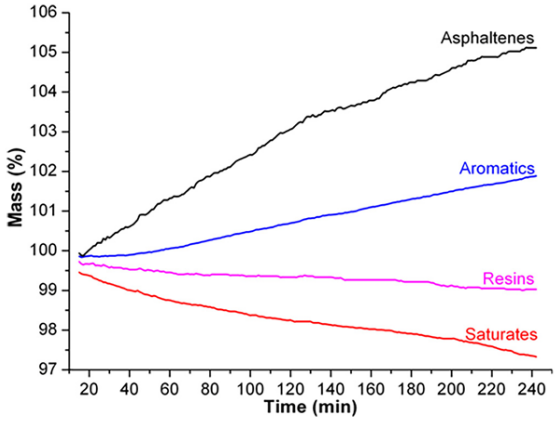

Figure 2. SARA fractions during isothermal-oxidative aging at 163°C for 4 hours (Hu, Zhang, Wang, & Xu, 2020)

Subsequently, the long-term aging of asphalt concrete is characterized by a progressive constant-rate oxidation process that occurs throughout the service life. Unlike short-term aging, long-term aging is primarily driven by oxidation—a chemical reaction between asphalt molecules and environmental oxygen (C. J. Glover, 2009). During oxidative aging, asphalt binder components transform less polar fractions into more polar fractions. These polar components correspond to the development of oxygen-containing functional groups within the asphalt

molecules, contributing to the reduced viscosity of binders following aging (Joseph C. Petersen, 2009).

Oxidative aging involves the replacement of hydrogen atoms in asphalt molecules with oxygen atoms, resulting in changes in asphalt binder density, viscosity, cohesive energy density, and surface-free energy. The effects of oxidative aging on binder behavior can be attributed to the increased molecular size of asphaltene, resin, and aromatics, accompanied by a reduction in available free space for saturated fractions (Xu & Wang, 2017). To simulate these two aging phases in the laboratory, the Rolling Thin Film Oven (RTFO) test is employed for short-term aging, while the Pressure Aging Vessel (PAV) test replicates long-term aging. These tests provide valuable insights into aging mechanisms and enable ranking binder aging rates. Figure 3 illustrates the expected increase in asphaltene and resin fractions and the reduction in saturate and aromatics fractions due to these aging processes.

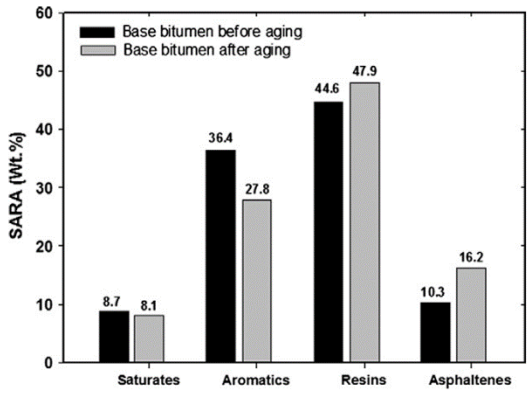

Figure 3. SARA analysis of virgin binder before and after thermos-oxidative aging (Dehouche, Kaci, & Mokhtar, 2012)

2.1.2 Asphalt Mixture Aging

Oxidative aging of asphalt binders significantly influences age-related pavement damage by altering the time-temperature behavior of the binder, which behaves as a viscoelastic material (Moraes & Bahia, 2015). The effects of aging on asphalt mixtures can be assessed by examining changes in the binder and the mix's physical and rheological properties (Saleh et al., 2020).

Aged asphalt binders have the capacity to withstand higher shear stress due to increased elastic stiffness while exhibiting reduced stress relaxation properties resulting from decreased viscous flow. These dual effects on viscoelastic behavior collectively lead to a hardening effect on the binder and the asphalt mix. This phenomenon typically manifests in the asphalt mixture's properties as an increase in elastic modulus ($|E^*|$) and a decrease in phase angle, as illustrated in Figure 4. Saleh et al. (2020) conducted aging tests on various asphalt mixes over short-term (STA) periods of five, eleven, and 21 days, observing a consistent trend of $|E^*|$ increase and phase angle reduction with aging.

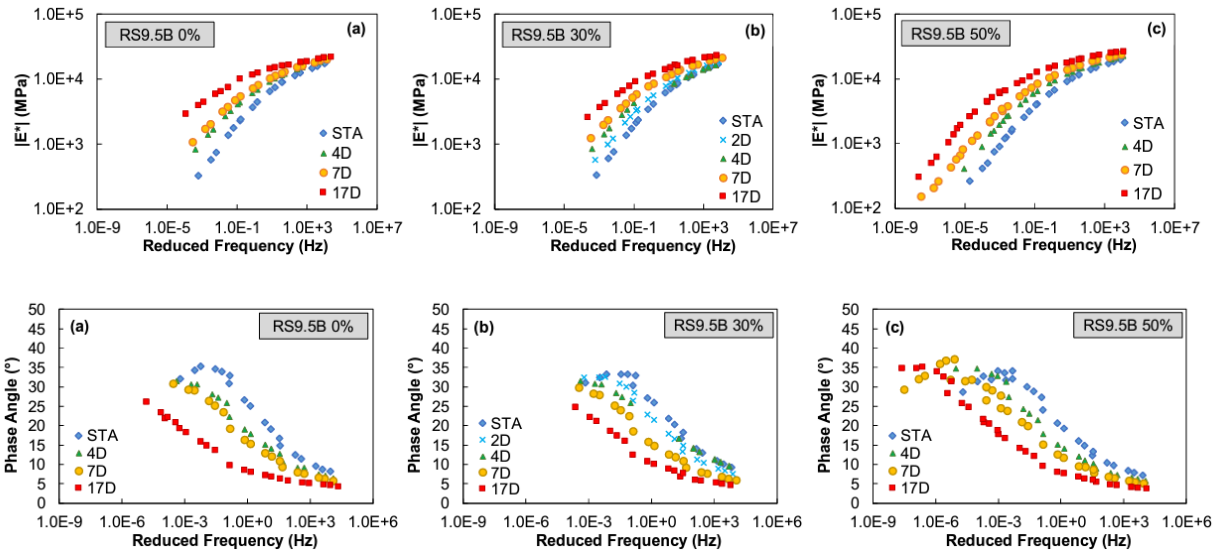

Figure 4. Dynamic modulus evolution of asphalt mixtures with long-term oven aging (Saleh et al., 2020).

The aging-induced hardening effect makes asphalt mixtures more susceptible to various distresses, with fatigue cracking a prominent concern (Moraes & Bahia, 2018). This heightened susceptibility arises from the asphalt binder's reduced ability to relieve stresses under repeated loading and during cooling cycles, making it more brittle and prone to cracking distresses (Jing, Varveri, Liu, Scarpas, & Erkens, 2021). Additionally, excessive stiffening of asphalt mixtures due to aging can reduce adhesion between the asphalt binder and aggregates, resulting in loss of surface material (Moraes, 2014). This, in turn, affects wear resistance and moisture susceptibility, ultimately impacting the pavement structure's durability (Bell, 1989b).

The aging of asphalt pavement involves numerous interconnected variables that can make the analysis quite complex. Some of the key variables encompass the chemical composition of the asphalt, the processing methodology, binder content in the mix, the nature of aggregates and their gradation, void content within the mix, production-related factors, temperature, and time (Lu & Isacsson, 2002).

2.2. Aging-resistant Technologies for Asphalt Mixtures

Additives can be incorporated into asphalt mixtures to mitigate or reverse the aging process and restore the mechanical properties affected by aging, which are closely linked to poor pavement performance (I. G. d. N. Camargo, T. Ben Dhia, A. Loulizi, B. Hofko, & J. Mirwald, 2021). Numerous innovative technologies have emerged, showing promise in delaying the oxidation-related aging of asphalt binders and enhancing their rheological and mechanical properties (Behnood, 2019; I. G. D. Camargo et al., 2021; Sirin, Paul, & Kassem, 2018b). However, the development of these products beyond the proof-of-concept stage is often slow or may not progress due to the high costs associated with full-scale implementation testing. The significant expenses involved in full-scale implementation testing underscore the importance of determining the

effectiveness of these additives through more cost-effective alternatives, such as laboratory testing (Timm et al., 2022).

This project focuses on evaluating the effectiveness of five distinct technologies when incorporated into asphalt mixtures to measure their impact on fatigue performance. These additives are commonly referred to as recycling agents, rejuvenators, anti-aging agents, or antioxidant technologies, depending on their specific mechanisms and their ultimate effects on the mixture's performance (Apeagyei, 2011; Behnood, 2019; Feng et al., 2012; Sirin et al., 2018b).

2.2.1 Rejuvenators

Rejuvenators, often referred to as recycling agents, are specialized products designed to restore the rheological properties of aged asphalt binders from recycled asphalt pavement (RAP) and recycled asphalt shingles (RAS) while also enhancing the engineering characteristics of naturally hard binders (Behnood, 2019). These additives aim to reduce the viscosity, stiffness, and embrittlement of aged binders by improving the asphaltene-to-maltene ratio, reducing the size of asphaltene clusters, or enhancing the dispersing power of the maltene phase (Kaseer, Martin, & Arámbula-Mercado, 2019a). The careful selection and proper incorporation of a rejuvenator into the mixture enable the realization of economic and environmental benefits associated with recycled components, all while maintaining pavement performance standards (Im, Zhou, Lee, & Scullion, 2014).

Aging harms the fatigue cracking resistance of asphalt mixtures due to the stiffening effect it induces. Cracking susceptibility intensifies when recycled asphalt pavement (RAP) is incorporated into the mix. Despite higher RAP percentages' economic and environmental advantages, agencies establish maximum limits to prevent cracking distress (Rathore, Zaumanis, & Haritonovs, 2019). Rejuvenators, while not preventing the oxidative aging process in asphalt

binders, counteract its effects by restoring the rheological properties of aged binders (Behnood, 2019; Ongel & Hugener, 2015). However, it's worth noting that rejuvenators may increase the proportion of aged binders in asphalt mixtures (W. S. Mogawer et al., 2015).

Rejuvenators, including recycled coal tar, waste vegetable oil, aromatic extracts, tall oils, and soybean-derived products, have demonstrated their effectiveness in restoring the essential properties of aged bitumens (Ziari, Moniri, Bahri, & Saghafi, 2019b). Im et al. (2014) conducted a comprehensive investigation of various commercial rejuvenators to assess their impact on the performance and engineering properties of Hot Mix Asphalt (HMA) containing recycled materials like Recycled Asphalt Pavement (RAP) and Recycled Asphalt Shingles (RAS). The study compared results from multiple tests, including Hamburg, overlay, dynamic modulus, and repeated load testing. The findings indicated that while the ranking of rejuvenators varied for different distress factors, all rejuvenators led to improvements in cracking performance, moisture susceptibility, and rutting resistance compared to control mixes without rejuvenators (Im et al., 2014).

Another study by Zaumanis et al. (2015) focused on evaluating the performance of different rejuvenators in mixtures composed entirely of 100% recycled asphalt. The research revealed that organic products required lower dosages than petroleum-based products to achieve similar effects. Organic oils and waste vegetable products exhibited outstanding binder and mixture fatigue resistance performance, as measured by linear amplitude sweep and fracture work density, respectively (Zaumanis, Mallick, & Frank, 2015).

Furthermore, organic rejuvenators like soybean-derived oil have demonstrated the ability to enhance asphalt mixture moisture damage resistance while reducing stiffness. This reduction in

stiffness is thought to contribute to improved cracking performance, making organic rejuvenators a promising additive for asphalt mixes (Tarar, Khan, & Rehman, 2022).

However, the effectiveness of a rejuvenator is influenced by various factors. These factors include the type, source, and properties of the virgin binder, characteristics of the aged binder, type and dosage of rejuvenator, mixing and preparation conditions, and the characteristics and amount of recycled materials. Studies have shown that these factors play a significant role in determining the effectiveness of rejuvenators when incorporated into the mix (Behnood, 2019).

The dosage of the rejuvenator used in the mix plays a significant role in determining the behavior of the rejuvenated binder and, consequently, the overall performance of the mixture. In a study conducted by Zaumanis et al. (2015), the favorable performance of organic rejuvenators over petroleum-based additives was partly attributed to less-than-optimal dosages (Zaumanis et al., 2015). Shen et al. (2007) researched to investigate the impact of rejuvenator dosage on the performance-based properties of rejuvenated asphalt binders and mixtures. Their findings revealed that the percentage of rejuvenators directly influenced performance indicators. Specifically, increasing the content of the rejuvenator led to improvements in fatigue resistance and shrinkage parameters, while rutting resistance parameters decreased, as expected, due to the softening effects of the rejuvenator on the binder (Shen, Amirkhanian, & Tang, 2007).

The softening effect of rejuvenators highlights the critical importance of selecting an optimal dosage to avoid issues with rutting performance in the mix, as excessive rejuvenator usage can compromise cracking performance (Kaseer, Martin, & Arámbula-Mercado, 2019b; Lin et al., 2021). Conversely, insufficient dosage may impact the mixture's stiffness without improving performance (Kaseer et al., 2019b). To address this, Zaumanis et al. (2014) proposed a procedure for optimizing the rejuvenator percentage based on the binder's Superpave PG requirements,

successfully determining the optimal dosage required to restore the PG characteristics of an aged binder to match those of a virgin binder (Zaumanis, Mallick, & Frank, 2014). Nsengiyuma et al. (2020) conducted a mechanical-chemical characterization to study the effects of rejuvenators' type, dosage, and treatment methods on aged binders and mixtures. They found that PG parameters are valuable for defining dosage ranges of rejuvenators related to improved asphalt mix performance. Still, chemical characterization of rejuvenated binders can offer insights into more material-specific rejuvenation processes (Nsengiyumva, Haghshenas, Kim, & Kommidi, 2020). Factors like the source of the virgin binder, the level of aging in recycled materials, and the percentage of recycled materials also influence the rejuvenator dosage. Therefore, it is advisable to conduct mixture-level assessments of cracking and rutting performance to determine the effectiveness of rejuvenators (Arámbula-Mercado, Kaseer, Epps Martin, Yin, & Garcia Cucalon, 2018).

The same dosages of rejuvenators can yield different mixture performances when applied to mixtures with different base binders (i.e., source and grade) (Kaseer et al., 2019b). Elkashef et al. (2018) evaluated the impact of asphalt binder grade and source on the rheological changes of rejuvenated binders using a soybean-derived additive. The findings of this study indicated that although the effects of the rejuvenator were similar across different binder sources, the extent of rejuvenation was correlated with the stiffness of the base binder. Specifically, rejuvenation was more pronounced in stiffer binders (Elkashef, Williams, & Cochran, 2018). Other research studies have also established that rejuvenators tend to have more favorable effects on the properties of rejuvenated binders when combined with higher-quality base binders, which can be characterized by parameters like ΔT_C and *G-R* (Garcia Cucalon et al., 2019; Kaseer, Garcia Cucalon, Arambula, Epps Martin, & Epps, 2018).

When incorporating rejuvenating technologies into asphalt binders, there are notable differences in the chemical composition and the ratio of asphaltenes to maltenes in the rejuvenated binder compared to the virgin binder. Although the rejuvenated binder exhibits behavior similar to that of the virgin binder, these differences in chemical composition may have implications for the long-term performance of the aged binder mix (Kaseer et al., 2019a). Several studies have indicated that the beneficial effects of rejuvenators in reducing the stiffness of mixes with high recycled material contents may diminish with aging (Arámbula-Mercado et al., 2018; Kaseer, Yin, Arámbula-Mercado, & Epps Martin, 2017; Yin, Kaseer, Arámbula-Mercado, & Epps Martin, 2017). For instance, Tran et al. (2012) observed that rejuvenators effectively enhanced cracking resistance without negatively impacting moisture susceptibility and rutting resistance. However, dynamic modulus testing results from short-term and long-term aging revealed that the rejuvenated mixtures experienced a more rapid increase in stiffness after aging compared to the virgin binder (Tran, Taylor, & Willis, 2012). This aging-induced stiffness increase is illustrated in Figure 5 and Figure 6. While the short-term aged curves of modified binder mixes are stiffer than the virgin ones, they are still relatively close to the unmodified condition, as shown in Figure 5. Conversely, Figure 6 demonstrates that all the modified binder mixes exhibit higher stiffness and greater separation than the unmodified binder mix, indicating a more substantial increase in stiffness in the modified mixes compared to the control mix after aging.

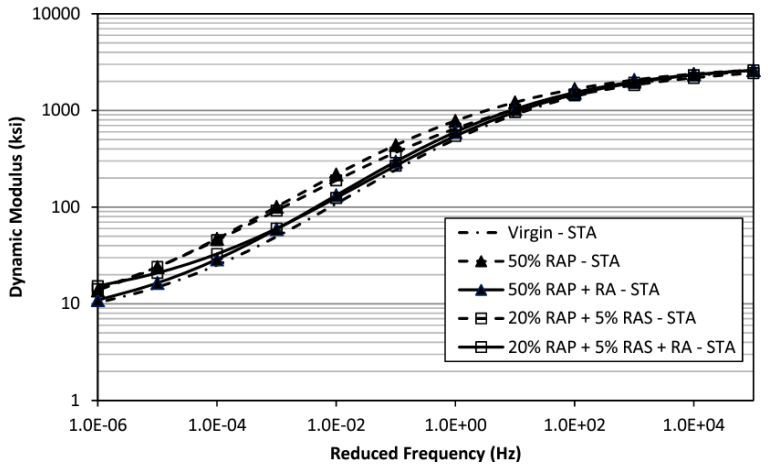

Figure 5. Comparison of |*E**| Test Results for Short-Term Aged Specimens (Tran et al., 2012)

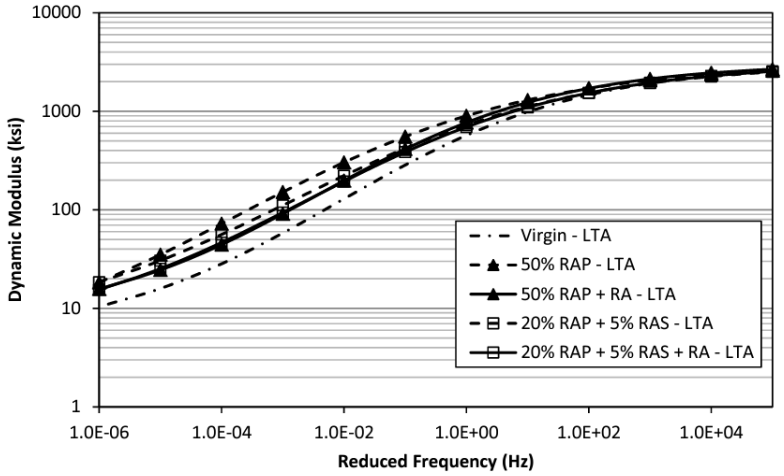

Figure 6. Comparison of |*E**| Test Results for Long-Term Aged Specimens (Tran et al., 2012)

In a study conducted by Kasser et al. (2017), the effectiveness of rejuvenators in asphalt mixtures with a high percentage of recycled materials and recycling agents was assessed using an effectiveness parameter defined as the percent reduction in stiffness compared to the control mix. The results indicated that certain rejuvenators could reduce stiffness by 15% to 40% when used at optimal dosages. However, after subjecting the mixtures to Long-Term Oven Aging (LTOA) for five days at 85°C, the effectiveness of these rejuvenators diminished, reducing the stiffness by only 5% to 20% (Kaseer et al., 2017).

Similarly, Yin et al. (2017) evaluated the long-term effectiveness of tall oil and aromatic extract rejuvenators in mixtures containing high percentages of Recycled Asphalt Pavement (RAP) and Recycled Asphalt Shingles (RAS). Their findings showed that while the studied rejuvenators could initially restore the properties of the recycled materials, their effectiveness decreased with aging. However, the study also revealed that the rejuvenated mixtures with these rejuvenators achieved similar or even better rheological properties and cracking performance than mixtures with recycled materials but without rejuvenators, even after aging (Yin et al., 2017).

Mogawer et al. (2015) evaluated the impact of aging on the fatigue characteristics of high Recycled Asphalt Pavement (RAP) asphalt mixtures that contained various types of rejuvenators, including aromatic oil, paraffinic oil, and organic blends. This assessment utilized various testing methods, such as a four-point flexural beam fatigue test, the Hot Mix Asphalt (HMA) fracture mechanical model, the simplified viscoelastic continuum damage model, and the semi-circular bending test. Although the results from the fatigue tests did not consistently agree with each other, it was noted that there was no significant difference in the outcomes when comparing mixtures with and without rejuvenators after long-term aging. This aligns with findings from other studies demonstrating that the softening effect of rejuvenators was observed in the short term but diminished after prolonged exposure to aging (W. S. Mogawer et al., 2015).

In another study by Ziari et al. (2019), the effects of rejuvenators on the aging resistance of asphalt mixtures were investigated. The study revealed that the rejuvenator type significantly influenced the mixtures' aging susceptibility. In this case, the rejuvenated mixtures exhibited more aging when compared to the unmodified control mix. These findings contradicted previous research that suggested organic rejuvenators should perform better in terms of aging susceptibility than petroleum-based rejuvenators (Behnood, 2019; Cavalli, Zaumanis, Mazza, Partl, &

Poulikakos, 2018). It is believed that the higher oxygen content in organic rejuvenators, such as bio-oils, may contribute to their increased susceptibility to aging compared to petroleum asphalt (Behnood, 2019). Consequently, additional studies are needed to comprehensively evaluate the aging susceptibility of asphalt mixtures rejuvenated with various additives. The long-term effectiveness of these additives remains a significant concern, emphasizing the importance of characterizing the actual cracking resistance of asphalt mixtures containing Recycled Asphalt Pavement (RAP) and rejuvenators over extended periods rather than focusing solely on their immediate softening effects (Rathore et al., 2019).

2.2.2 Polymer Modifiers

Various polymeric additives, generally categorized as elastomers and plastomers, have been employed to enhance asphalt mixtures (Tarar et al., 2022). Elastomers such as styrene-butadiene-styrene (SBS), styrene-isoprene-styrene (SIS), and styrene-ethylene/butylene-styrene (SEBS) enhance the elastic recovery of the mix by improving the ability to recover the initial shape after deformation. Plastomers (i.e., ethylene vinyl acetate (EVA), polyethylene (PE), polypropylene (PP)) consist of a three-dimensional network, rigid enough to resist stresses (Zhu, Birgisson, & Kringos, 2014). Introducing these polymeric additives is closely linked to enhancing the characteristics of the asphalt binder, ultimately leading to high-performance pavements (Diab, Enieb, & Singh, 2019). Despite the evident advantages of polymer-modified asphalt mixtures, concerns remain, primarily regarding their aging resistance (Cai et al., 2019; Elkashef, Podolsky, Williams, & Cochran, 2017; Zhu et al., 2014). The selection of the appropriate polymer type, dosage, and compatibility with other mixture constituents is a critical factor in determining the success of polymer modification. Furthermore, ongoing studies and field evaluations are necessary

to comprehensively understand these innovative mixtures' long-term performance and cost-effectiveness under diverse climatic and traffic conditions.

In the pursuit of enhancing the aging resistance of polymer-modified asphalt binders, the incorporation of antioxidant additives has proven to be a valuable strategy (Li et al., 2010; Ouyang, Wang, Zhang, & Zhang, 2006; Zhu et al., 2014). A study conducted by Elkashef et al. (2017) examined the effects of incorporating a soybean oil rejuvenator into two distinct binders: a conventional PG 58-28 and a polymer-modified PG 64-28, with a small dosage of 0.75%. Binder testing results indicated a noticeable reduction in the complex shear modulus and a concurrent increase in the phase angle, indicative of reversing the aging-related effects on the binder properties. Also, the unmodified binders exhibited improved fatigue resistance upon including the soybean rejuvenator. This enhancement was discerned by a reduction in the $G^*\sin\delta$ parameter at different temperatures, as depicted in Figure 7. It is also observed that the boost in fatigue resistance was more pronounced in the polymer-modified binder than in the neat binder. This observation suggests that the interaction between the polymer modifier and the rejuvenator contributes to the enhanced performance of the binder. While the precise mechanisms underlying this interaction warrant further chemical analysis, it is evident that combining rejuvenators with polymer-modified binders holds promise to maximize the effectiveness of both technologies. This innovative approach represents a significant step in achieving superior aging resistance and performance in asphalt mixtures. However, continued research and comprehensive field evaluations are necessary to explore the potential of such combinations fully and to optimize their use in practical pavement applications (Elkashef et al., 2017)

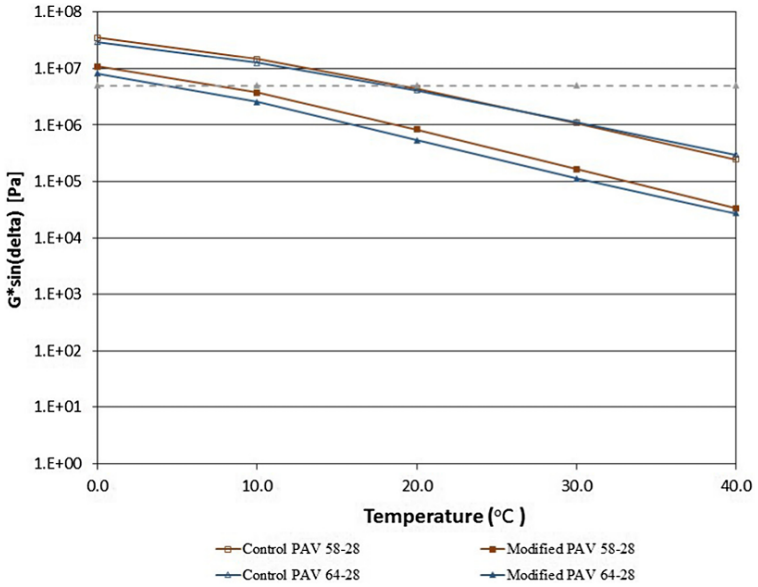

Figure 7. Variation of G*sinδ with temperature (Elkashef et al., 2017)

Researchers widely concur on the effectiveness of Styrene-Butadiene-Styrene (SBS) modification in significantly enhancing the cracking and rutting resistance of asphalt mixtures (S.-S. Kim & Sargand, 2003; S. Kim, Sholar, Byron, & Kim, 2009; Tia, Roque, Sirin, & Kim, 2002; Von Quintus, Mallela, & Buncher, 2007). Although extensive research has been performed in this area, it is important to note that a predominant focus has been on a single type of polymer modifier—SBS. Consequently, there remains a notable gap in understanding the long-term performance and behavior of various polymer modifiers when incorporated into asphalt mixtures. Furthermore, there is a pressing need for extensive investigations into the effects of aging on the chemical composition and properties of these polymers. (Wu et al., 2021). Addressing these knowledge gaps will provide invaluable insights into the optimal selection and utilization of polymer modifiers to achieve enduring and resilient asphalt pavement structures. Consequently, further research in this area is imperative to unlock the full potential of polymer modification in asphalt technology.

2.2.3 Crumb Rubber

Crumb Rubber modifiers (CRM) significantly enhance the mechanical properties of asphalt binders while addressing environmental concerns related to scrap tire disposal. These modifiers are derived from recycled tires and are integrated into asphalt mixtures through various grinding techniques, offering a sustainable solution (Lang Wang, Chang, & Xing, 2009). Crumb Rubber (CR) modification techniques primarily encompass two approaches (i.e., wet and dry processes) (Picado-Santos, Capitão, & Neves, 2020). The key distinction between these methods lies in the stage at which the rubber is introduced into the mixture. In the dry process, crumb rubber particles are directly incorporated into the mix during the mixing phase, altering the asphalt binder and partially substituting some aggregates. Conversely, crumb rubber particles are first blended with the asphalt binder in the wet process before mixing occurs (Riekstins, Baumanis, & Barbars, 2021). The wet process can be further categorized into various variations, including terminal blend, wet no agitation, wet process-high viscosity, semi-wet process, pre-treatment with wax additives, polymer-CR combinations, and other modifications (Butz, Muller, & Riebesehl, 2012; Chavez, Marcobal, & Gallego, 2019; Fornai, Sangiorgi, Mazzotta, Bermejo, & Saiz, 2016; Lo Presti, 2013). This range of methods underscores the versatility of CR incorporation techniques in asphalt mixtures, offering tailored solutions to meet specific performance and environmental objectives.

Prior investigations into binders have established that Crumb Rubber modifiers (CRM) can effectively enhance the resistance of modified asphalt binders to rutting, cracking, and aging, potentially extending the service life of asphalt pavements when incorporated into asphalt mixtures (Keuliyan, 2022). Pszczoła et al. (2017) assessed the low-temperature properties of rubberized asphalt mixtures utilizing CR and SBS-modified binders. Their findings revealed that, across all tests, the use of polymer-rubber-modified binders improved the low-temperature resilience of the mixtures, with some instances demonstrating superior performance by polymer-rubber compared

to SBS-modified mixtures (Pszczoła, Jaczewski, Szydłowski, Judycki, & Dołżycki, 2017). Similarly, in accordance with Wang et al. (2020), crumb rubber-modified asphalt mixtures (CR-MA) exhibited enhanced resistance to cracking compared to SBS-modified asphalt mixtures (SBS-MA) under identical conditions. This relationship persisted even after aging, with CR-MA displaying superior aging resistance in comparison to SBS-MA mixtures (Lan Wang, Shan, & Li, 2020). These findings underscore the potential of CR-MA as a promising option for enhancing the performance and longevity of asphalt pavements

In a recent study by Jin et al. (2023), an assessment was conducted on the pavement performance of dry-processed rubberized asphalt mixtures using a combination of laboratory and field tests. The results revealed that, while the dynamic modulus of the modified mixtures was higher than that of the unmodified mixes, as depicted in Figure 8, the indirect tensile test results indicated that including Crumb Rubber (CR) significantly enhances cracking resistance. This enhancement was evidenced by an impressive increase in failure energy, ranging from 29% to 50%, observed in the modified mixtures compared to the control, as illustrated in Figure 9. These findings also underscore the potential benefits of incorporating CR in asphalt mixtures for improved resistance to cracking and enhanced pavement performance.

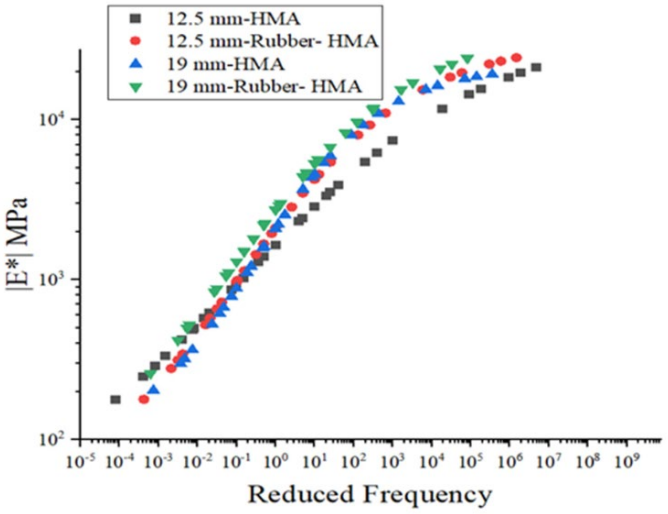

Figure 8. Dynamic modulus master curve of HMA (@21°C) (D. Jin, Ge, Wang, Malburg, & You, 2023)

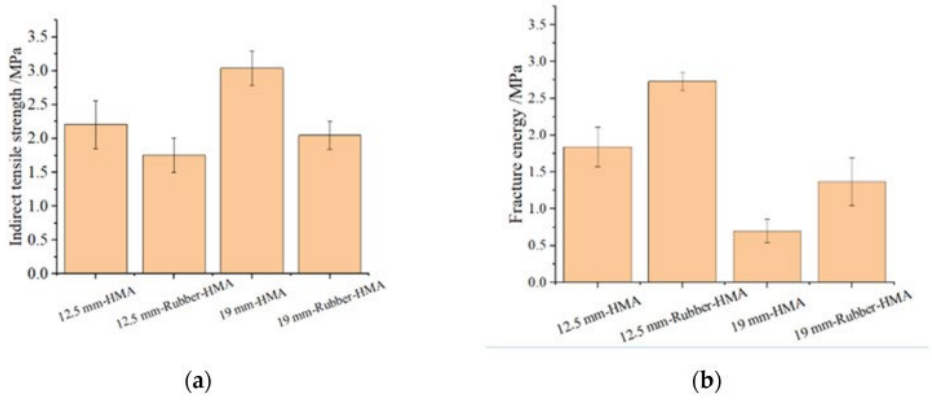

Figure 9. IDT strength and failure energy results (a) IDT strength test data; (b) failure energy results (D. Jin et al., 2023)

2.2.4 Epoxy Resins

Epoxy polymers, characterized as thermosetting materials that retain their rigidity once fully formed, undergo a curing process where monomers link covalently to create a brittle material (Apostolidis et al., 2022). Epoxy asphalt (EA) is typically employed in asphalt mixtures as a two-component system comprising epoxy resin (ER) as part A and a curing agent, diluent, filler, or

toughening agent as part B (Chen, Hossiney, Yang, Wang, & You, 2021). The incorporation of epoxy resins to produce epoxy asphalts yields improved mechanical properties, enhancing resistance to factors such as fatigue loading, moisture damage, and oxidation (Xiang & Xiao, 2020; Xiao, van de Ven, Molenaar, Su, & Zandvoort, 2011).

Youtcheff et al. (2006) assessed epoxy-modified asphalt concrete, focusing on its resistance to cracking, rutting, and moisture damage. The findings indicated that the epoxy-modified mixes exhibited superior performance in fatigue cracking compared to unmodified control mixtures. Furthermore, they outperformed polymer-modified mixtures in terms of rutting resistance. Moisture damage, assessed through the Hamburg wheel and pine rut tests, did not pose a significant issue(Youtchef, Gibson, Shenoy, & Al-Katheeb, 2006). Cong et al. (2010) examined epoxy resin-modified asphalt mixtures used for steel bridge deck paving in a separate study. The study evaluated the modified mixes' fatigue life and recovery elasticity through indirect tension fatigue and static creep tests, respectively. Their research revealed an increase in the creep stiffness modulus of the epoxy-modified mix, which was linked to enhanced resistance to permanent deformation and extended fatigue life (Cong, Chen, & Yu, 2011).

Aging resistance has been reported in epoxy-modified binders and asphalt mixtures (Alamri, Lu, & Xin, 2020). Notably, epoxy asphalt technologies stand out for their resistance to rutting, fatigue cracking, aging, and embrittlement, setting them apart from other thermosetting elastomers used as asphalt modifiers (Moraes & Yin, 2022). Apostolidis et al. (2022) also investigated the oxidative aging of epoxy asphalts, revealing that epoxy-modified binders exhibit greater resistance to oxygen-induced aging. However, it is essential to note that, owing to the nature of epoxy, modified materials may become stiffer and more brittle after aging, potentially affecting their fatigue and thermal cracking resistance in some mixtures (Apostolidis et al., 2022).

2.3. Laboratory Aging

The traditional approach to studying the effects of aging in asphalt mixtures has primarily focused on investigating the aging of asphalt binders in laboratory settings. In this method, the asphalt binders are subjected to various levels of aging severity within controlled laboratory conditions, and the resulting changes in physical properties are measured and analyzed. Previous research efforts have extensively explored this approach (Apostolidis, Liu, Kasbergen, & Scarpas, 2017).

While analyzing the aging of asphalt binders provides valuable insights into the aging mechanisms and helps assess the aging susceptibility of different binder formulations (X. Jin, Han, Cui, & Glover, 2011), it has certain limitations. Specifically, this approach does not fully account for the influence of the mineral aggregates within the asphalt mixture, and it does not directly quantify the impact of binder aging on the overall performance of the asphalt mixture itself.

Nevertheless, the knowledge gained from studying asphalt binder aging mechanisms is instrumental in developing strategies to counteract the aging effects and ultimately achieve longer-lasting pavements (Apostolidis et al., 2017). Understanding how binder properties change with aging is a critical step in designing effective technologies and additives to enhance the durability and performance of asphalt pavements.

Another approach to studying aging in asphalt mixtures involves simulating the aging process within the asphalt mixture, replicating real-world conditions to a greater extent. In this method, the asphalt mixture is subjected to various aging conditions, such as exposure to heat, moisture, and UV radiation, to mimic the effects of environmental aging. Subsequently, the changes in the physical properties of the asphalt mixture are assessed and analyzed. This approach

is considered more representative of what occurs when the asphalt mixture is in place, as it directly addresses the aging of the entire mix (Cheolmin Baek, Shane Underwood, & Richard Kim, 2012).

While this second method provides a more holistic view of the aging process in asphalt mixtures, it also introduces additional complexities. Factors such as the physicochemical interactions between the asphalt binder and mineral aggregates, as well as the presence of air voids in the pavement structure, contribute to the intricacies of this analysis. These complexities have resulted in less research and available knowledge in this area (Y. R. Kim et al., 2017). Nonetheless, this method offers insights into the aging effects on the asphalt mixture, accounting for factors beyond the binder alone. It is particularly valuable for assessing how environmental conditions and aging factors affect asphalt pavements' overall performance and durability in real-world applications.

Bell et al. (1989, 1994) conducted pioneering studies on asphalt binder aging by extracting and recovering binders from aged mixtures. However, these early investigations primarily focused on assessing changes in penetration and viscosity of the binders at a single temperature. This limited scope constrained gaining a comprehensive understanding of the aged binder's behavior. While some data points on resilient modulus were collected, there were gaps and inconsistencies in the information available regarding the aging behavior of the binder within the mixture (Bell, 1989a; Bell, AbWahab, M.E., & Sosnovske, 1994).

In a more recent study conducted by Morian et al. (2011), the research examined the impact of various aggregate sources and mixture characteristics on the rate of binder oxidation and the stiffness of the mixture, all while maintaining constant air voids. This investigation revealed that mixture properties played a role in the oxidation process. However, it was noted that the precise mix of factors responsible for influencing oxidation and the underlying causes of these factors

affecting oxidation remained incompletely understood (Morian, Hajj, Glover, & Sebaaly, 2011). This knowledge gap highlights the challenge of establishing a clear link between the behavior of a known binder and its behavior when subjected to the influence of mixture characteristics. Consequently, the study concluded that a dependable aging analysis of mixtures could only be reliably determined by directly testing the mix and assessing its properties' changes after aging processes (Morian et al., 2011).

The protocols commonly used for simulating long-term aging can be categorized based on the state of the materials during the aging process, which can either involve loose mix or compacted specimens. However, these protocols come with challenges, primarily related to the slow oxidation rate, increased stiffness in aged loose mix compaction, and radiation oxidation gradients when aging compacted specimens (Jing et al., 2021). The current standard procedure for simulating long-term aging in asphalt mixtures is specified in AASHTO R30, which involves placing compacted specimens of the asphalt mixture in an oven at 85°C for five days (AASHTO, 2022).

Nevertheless, limitations in this procedure have prompted researchers to explore alternative methods that could better replicate long-term aging in asphalt mixtures and more accurately assess its effects on the properties of the asphalt mixture (Newcomb et al., 2019). These efforts aim to develop testing protocols that provide a more comprehensive understanding of the aging process and its impact on asphalt mixtures under various conditions.

The limitations associated with the AASHTO R30 aging methodology for compacted specimens are significant and include distortions in the geometry of the specimens, uneven air void distribution, and the presence of oxidation gradients (Michael D. Elwardany, Yousefi Rad, Castorena, & Kim, 2017). Although the use of metal wire mesh, as recommended in NCHRP 9-

23, can partially mitigate some of these issues, it doesn't provide a definitive solution to the challenges related to aging compacted specimens (Reed, 2010). Moreover, the oxidation gradients present both radially and vertically in the compacted specimens compromise the homogeneity of the samples, which can impact the validity of performance testing results obtained from specimens aged using this procedure (Houston, Mirza, Zapata, & Raghavendra, 2005).

One effective solution to these limitations is to age loose asphalt mixtures, where compaction is performed after the mixture has undergone aging. Aging loose mixtures offer several advantages, including a larger contact area for the asphalt binder, which accelerates oxidation more effectively than compacted specimens (Y. R. Kim et al., 2017). A summary comparing the two possible methodologies for asphalt mixture aging is provided in Table 1, which can help choose the most appropriate method for specific research or testing purposes.

Table 1. Comparison between loose mix and compacted specimens in the aging procedure (Y. R. Kim et al., 2017).

Loose Mix	Pros	• Homogenous aging in the mixture • Higher oxidation rate than compacted mix • Maintaining specimen integrity a non-issue
	Cons	• Difficulties associated with the compaction of aged loose mix limit its use for producing specimens for performance testing. • A limited amount of materials can be aged in a standard pressure aging vessel (PAV) chamber.
Compacted Specimen	Pros	• Can produce aged samples for performance tests if slumping is minimized through the use of wire mesh
	Cons	• Slower oxidation rate than loose mix • The integrity of the specimens is compromised at high temperatures and pressures due to slump, cracking upon pressure release, and differences in the coefficient of thermal expansion between binder and aggregate. • Oxidation gradients exist radially and throughout the height of the specimen.

Reports from NCHRP 09-54 have indicated that aging loose asphalt mixtures in an oven at 95°C is the preferred approach for simulating long-term aging in asphalt mixes while mitigating the limitations associated with the AASHTO R30 methodology (Y. R. Kim et al., 2017; Nooralhuda, 2022). Rad et al. (2017) conducted a study to assess the properties of asphalt binders

and the performance of mixtures aged at temperatures ranging from 70°C to 135°C and varying durations. Their findings indicated no significant differences in the relationship between the rheological properties of asphalt binders (e.g., log G*) and their chemical composition when aged below 95°C. However, as illustrated in Figure 10, distinct chemical differences were observed for mixtures aged at 135°C. Rad et al. (2017) suggested that this chemical modification of binders could harm the performance of mixtures aged at 135°C.

Based on their research, Rad et al. (2017) defined the optimal aging temperature as 95°C, as no adverse effects were observed in the relationship between binder chemistry and rheology for binders aged at this temperature or below. In contrast, a negative performance effect was noted for higher aging temperatures (Yousefi Rad, Elwardany, Castorena, & Kim, 2017). This highlights the importance of selecting an appropriate aging temperature to ensure aging simulations' accuracy and relevance to actual field conditions.

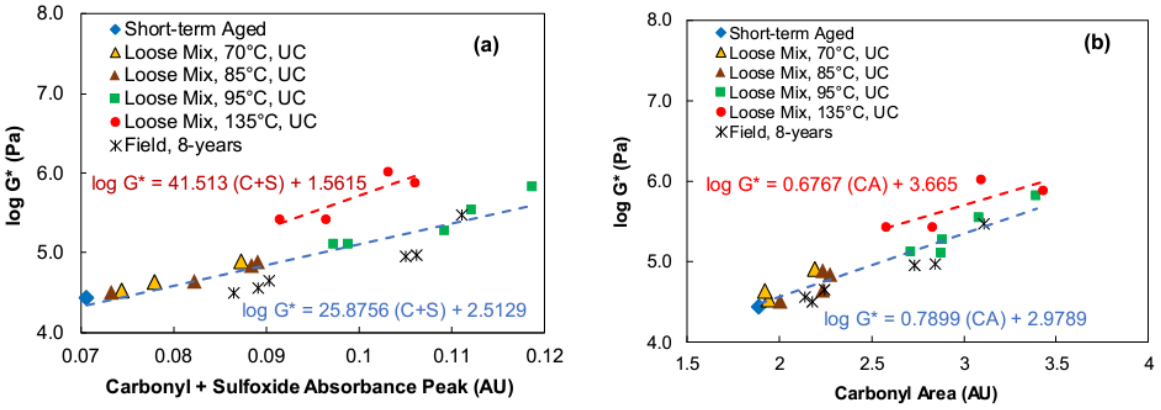

Figure 10. Relationship between rheological and chemical indicators for asphalt binders recovered from loose asphalt mixtures aged at different temperatures and binders extracted and recovered from different depths of asphalt pavement aged eight years in the field (Yousefi Rad et al., 2017).

2.4. Fatigue performance characterization

Researchers have employed various techniques to address the characterization of fatigue cracking performance, including advanced numerical simulations and experience-based knowledge (Sudarsanan & Kim, 2022; Y. D. Wang, Underwood, & Kim, 2020; Zhou et al., 2016). Additionally, index values play a crucial role in independently characterizing the fatigue performance of asphalt mixtures, irrespective of the pavement structure. These index values enable quicker decisions regarding mix design, quality assurance, and acceptance (Y. D. Wang et al., 2020). However, it's important to note that climate, pavement structure, and traffic loads significantly influence pavement fatigue cracking performance. (Rahbar-Rastegar, Sias Daniel, & Reinke, 2017). Therefore, in cases where full-scale testing is not feasible, it becomes essential to define model predictions that incorporate all these variables to characterize pavements' fatigue cracking performance effectively.

2.4.1 Glover-Rowe mix (G-R_m) Parameter

The Glover-Rowe index parameter was initially developed to assess the cracking performance of asphalt binders by considering their ductility properties. Rowe further simplified this parameter using the AASHTO M30 parameters G* and δ and proposed Equation 1 for its calculation, with measurements taken at 15°C and 0.005 rad/s (R. M. Anderson, G. N. King, D. I. Hanson, & P. B. Blankenship, 2011).

$$G - R = G^* \times \frac{(\cos \delta)^2}{\sin \delta} \qquad \text{Equation 1}$$

The Glover-Rowe binder parameter was adapted for assessing the cracking performance of asphalt mixtures by taking into account the material's ability to relax stresses through the parameters δ and $|E^*|$, as outlined in Equation 2 (Mensching, Rowe, & Sias Daniel, 2017).

$$G - R_m = |E^*| \times \frac{(\cos \delta)^2}{\sin \delta} \qquad \text{Equation 2}$$

In their study, Oshone et al. (2019) discovered that the *G-R*$_m$ parameter exhibited sensitivity to various factors, including aging, recycled material content, rejuvenator dosage and type, low-temperature PG, and production type of the asphalt mixes. Figure 11 illustrates the correlations observed among the significant combination of variables studied (Oshone et al., 2019).

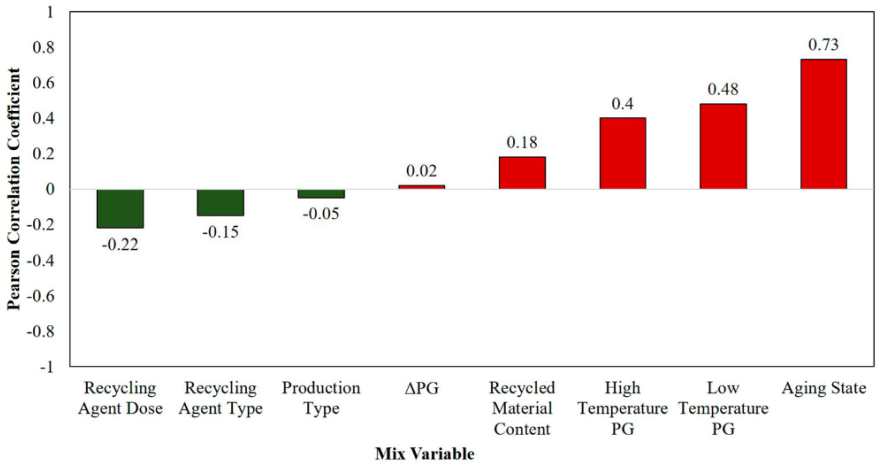

Figure 11. Pearson correlation coefficient between mixture variables and *G-R*$_m$ parameter (Oshone et al., 2019)

Zhang et al. (2021) conducted research that revealed strong correlations between the *G-R*$_m$ parameter and key mixture performance indices, including the flexibility index (FI) and the fracture strain tolerance (FST) value. Additionally, moderate correlations were observed with fracture energy (Gf) from DCT and the average reduction in pseudo stiffness up to failure (D^R), as depicted in Figure 12. These comparative analyses were conducted under various aging conditions, indicating the potential utility of the *G-R*$_m$ parameter as a simplified indicator for assessing the cracking performance of asphalt mixtures while accounting for aging effects in the analysis (Zhang, Sias, & Dave, 2021).

	G–R_m	G_f SCB	FI	G_f DCT	FST	D^R
G–R_m	***1.000***					
G_f SCB	–0.141	***1.000***				
FI	***–0.720***	0.227	***1.000***			
G_f DCT	*0.527*	0.194	*–0.618*	***1.000***		
FST	*–0.530*	0.301	***0.851***	–0.172	***1.000***	
D^R	*–0.523*	–0.216	*0.495*	*–0.582*	0.211	***1.000***

Figure 12. Comparisons and correlations between the *G-R*$_m$ Parameter with other Mixture Performance Indices (Zhang et al., 2021).

2.4.2 S_{app} Parameter

The S_{app} index parameter serves as a valuable indicator for assessing the fatigue resistance properties of asphalt mixtures. It takes into account the material's modulus, represented by $|E^*|$, and considers the mixture's toughness, which is its capacity to absorb energy without fracturing, as expressed in Equation 3 (Y. D. Wang, Underwood, & Kim, 2022).

$$S_{app} = 1000^{\frac{\alpha}{2}-1} \frac{a_T^{\frac{1}{\alpha+1}} \left(\frac{D^R}{C_{11}}\right)^{1/C_{12}}}{|E^*|^{\alpha/4}} \qquad \text{Equation 3}$$

Wang et al. (2022) conducted a comprehensive study that demonstrated the sensitivity of the S_{app} parameter to various factors known to influence the fatigue performance of asphalt mixtures. These factors included aggregate gradation, binder content, air void content, RAP content, binder grade, type of binder modifier, and laboratory oven-aging time. As depicted in Figure 14, their findings revealed that better fatigue cracking resistance was associated with finer gradation, increased binder content, lower air void content, and reduced RAP content. Additionally, specific additive modifiers like crumb rubber, thermopolymers, and SBS polymers improved fatigue performance.

Habbouche and Nair (2023) conducted an evaluation of the performance of plant-produced Hybrid rubber-modified asphalt (HRMA) mixtures compared to typical styrene-butadiene-styrene (SBS) modified asphalt mixtures using various tests and parameters, including the S_{app} index.

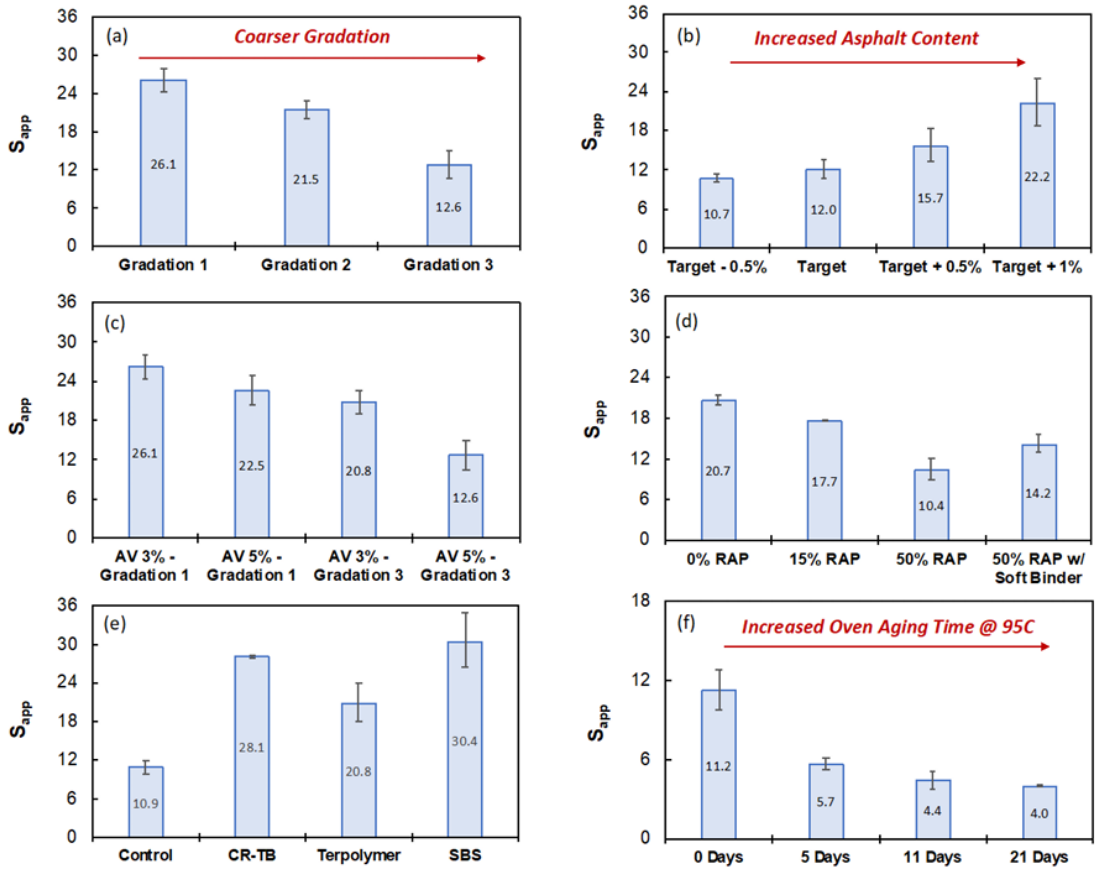

Figure 13. S_{app} values vs. (a) aggregate gradation, (b) binder content, (c) air void content, (d) RAP content, (e) binder modifier, and (f) laboratory oven-aging time (Y. D. Wang et al., 2022).

CHAPTER 3 - MATERIALS AND METHODS

The experimental plan is presented in Figure 14, with detailed explanations in the following four sections. The first section comprehensively describes the component materials and their respective proportions in the mixture. The second section discusses the laboratory aging protocols for asphalt mixtures' short-term, long-term, and accelerated weathering system aging. The third section provides more details on cracking performance tests, which include Dynamic Modulus ($|E^*|$) and cyclic fatigue tests conducted using the AMPT equipment to determine the mechanical properties needed to characterize the cracking performance of the mixtures. Lastly, the final section of this chapter outlines the analysis parameters and indexes derived from the test results.

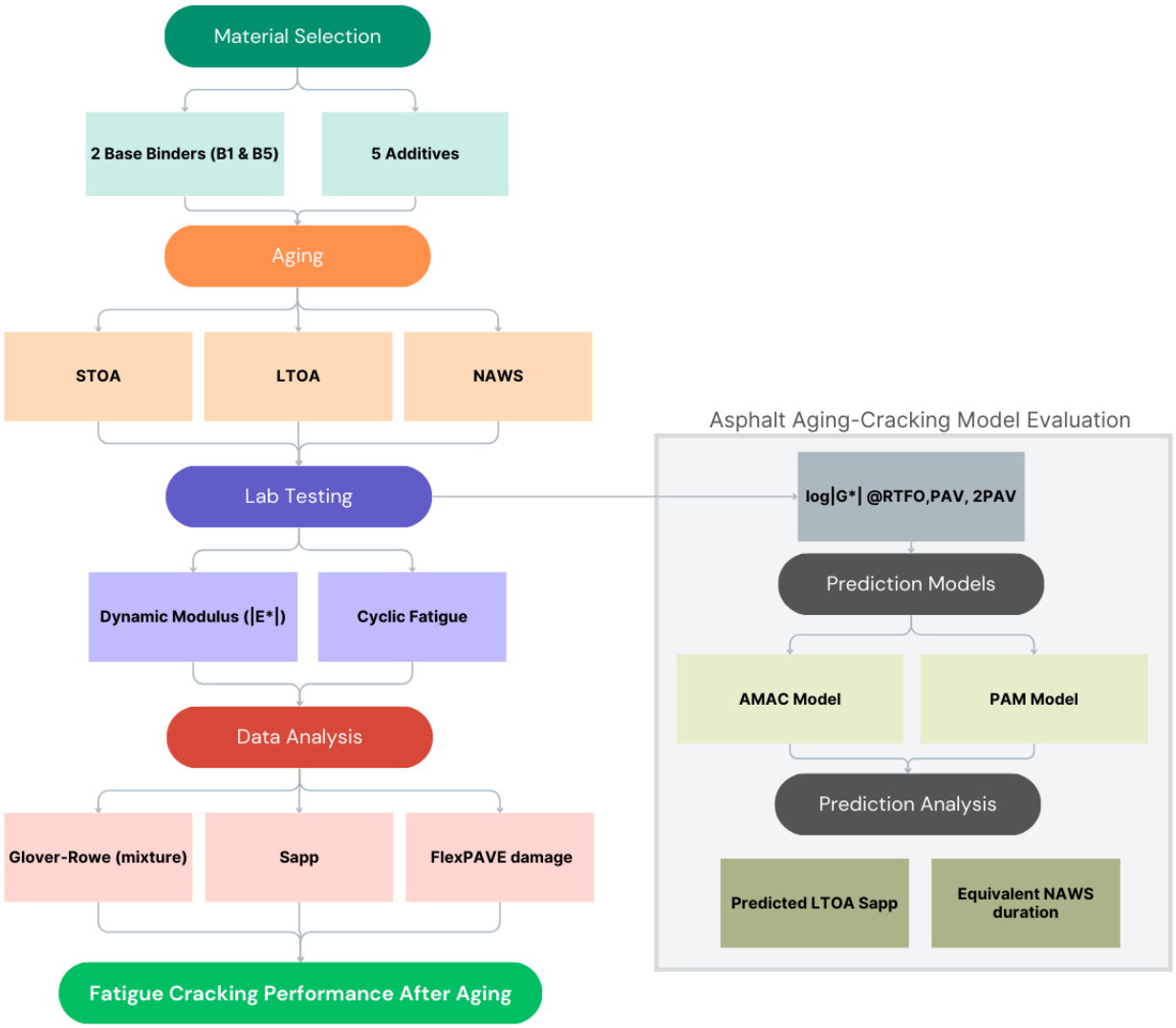

Figure 14. Experimental Plan

3.1. Materials

3.1.1 Aging-Resistant Technologies

Five aging-resistant technologies were selected for evaluation in this study. A short description of each additive technology is as follows:

- Additive 1: Thermosetting two-phase (i.e., Phase A, Phase B) chemical system with phase A composed of epoxy resin and phase B of base asphalt binder with epoxy cross-linker.
- Additive 2: Hybrid ground tire rubber (GTR) powder and a polymeric compound system.
- Additive 3: Hybrid anti-aging technology system composed of a high polymer content continuous phase styrenic block copolymer and a pine-based chemical recycling agent
- Additive 4: bio-derived polymer from epoxidized soybean oil.
- Additive 5: proprietary biosynthetic, petroleum-based, and rheology modifiers blend.

3.1.2 Asphalt Binders

Two base binders, Binder 1 and Binder 5, were previously selected to evaluate the selected aging-resistant technologies. Binder 1 is a PG 64-16 binder sourced from South Central United States, while Binder 5 is a PG 64-22 binder from Western Canada. These binders were chosen from six potential alternatives, as detailed by (Keuliyan, 2022). The Performance Grade (PG), particularly low critical temperatures, and the ΔTc parameter of both aged and unaged samples were analyzed to assess their aging susceptibility, as these parameters have shown good correlations with age-induced cracks in asphalt mixtures (R. Anderson, G. King, D. Hanson, & P. Blankenship, 2011).

For each base binder, five blends were prepared by mixing the base binder with each of the five aging-resistant technologies and tested to compare with the control (unmodified) base binder. Four aging-resistant technologies (i.e., Additives 2 to 5) were blended with the base binder with the assistance of respective manufacturers. In contrast, Additive 1 was blended with the base binder just before mixing as this additive is known to have thermosetting properties upon cooling

after blending, especially at dosages over 30% (Youtchef et al., 2006). Even though the dosages of Additive 1 were below this limit, they were combined with the base binders just before mixing to avoid these effects. A three-hour cure time was then allowed before mixing, ensuring no cooling of the blend occurred. Additive dosages were based on the manufacturer's recommendations and testing results from the prior binder experiment (Keuliyan, 2022).

3.1.3 Mix Gradation and Binder Content.

A 9.5mm nominal maximum aggregate size (NMAS) dense-graded mix design was selected for this study. Table 2 shows the aggregate proportions, including Granite 89s, Shorter Sand, Granite M10s, Baghouse fines, and 20% recycled asphalt pavement (RAP) material from Alabama. Table 3 presents the design aggregate gradation of the mixture. The design binder content remained constant at 5.5% without any adjustments for any of the evaluated technologies.

Table 2. Mix component proportions

Component	Percent (%)
Granite 89's	47.0
Granite M10's	10.0
Shorter Sand	22.0
Baghouse fines	1.0
RAP	20.0
Binder content	5.5

Table 3. Mix gradation.

Sieve Size (mm)	Sieve Size (in)	Percent Passing (%)
19.0	3/4"	100.0
12.5	1/2"	99.9
9.5	3/8"	98.1
4.75	# 4	69.5
2.36	# 8	48.9
1.18	# 16	39.8

0.600	# 30	30.0
0.300	# 50	16.8
0.150	#100	8.6
0.075	#200	5.41

3.2. Laboratory Aging

Three laboratory aging protocols were utilized in this study to condition loose mix samples and AMPT test specimens. Each simulates an aging stage in the life cycle of the asphalt mixture: during production and later in service. These protocols were employed to assess the effectiveness of additives in mitigating aging effects.

3.2.1 Short-term Oven Aging

The first protocol consisted of short-term oven aging (STOA) of a loose mix for 4 hours at 135°C, as outlined in AASHTO R30-19, *Standard Practice for Mixture Conditioning of Hot Mix Asphalt (HMA) (AASHTO, 2019c).* This method simulates the aging of the asphalt mixture during production and the early stage of pavement service life.

3.2.2 Long-Term Oven Aging

For the long-term oven aging (LTOA) protocol, the loose mix was placed in an oven for five days at 95°C after STOA to simulate the in-service oxidative aging of the mix, as recommended in NCHRP 09-54.

3.2.3 NCAT Accelerated Weathering System (NAWS)

The third aging protocol involved placing small Asphalt Mixture Performance Tester (AMPT) test specimens in the NCAT Accelerated Weathering System (NAWS). The samples were subjected to 3,000 hours of simultaneous cyclic actions in the system, including thermal oxidation, ultraviolet radiation, and moisture infiltration and diffusion, to simulate the long-term field aging of asphalt pavements.

3.3. Mixture Cracking Resistance Characterization

Dynamic Modulus ($|E^*|$) and Cyclic Fatigue tests were conducted on small AMPT specimens post-conditioning using the three protocols to determine their mechanistic and mechanical properties. Variations in these properties after distinct aging stages were then analyzed to evaluate the effectiveness of the aging-resistant technologies.

3.3.1 Dynamic Modulus ($|E^*|$) Test

The Dynamic Modulus for the asphalt mixture was determined following AASHTO TP-132, *Determining the Dynamic Modulus for Asphalt Mixtures Using Small Specimens in the Asphalt Mixture Performance Tester (AMPT) (AASHTO, 2019a)*. This protocol utilizes small specimens fabricated in the laboratory following the procedure outlined in AASHTO PP-99, *Standard Practice for Preparation of Small Cylindrical Performance Test Specimens Using the Superpave Gyratory Compactor (SGC) or Field Cores (AASHTO, 2019d).* The small cylindrical specimens are 38 mm (1.50 in) in diameter by 110 mm (4.33 in) in height. Four small specimens can be extracted around the center of gyratory compacted specimens, as illustrated in Figure 15.

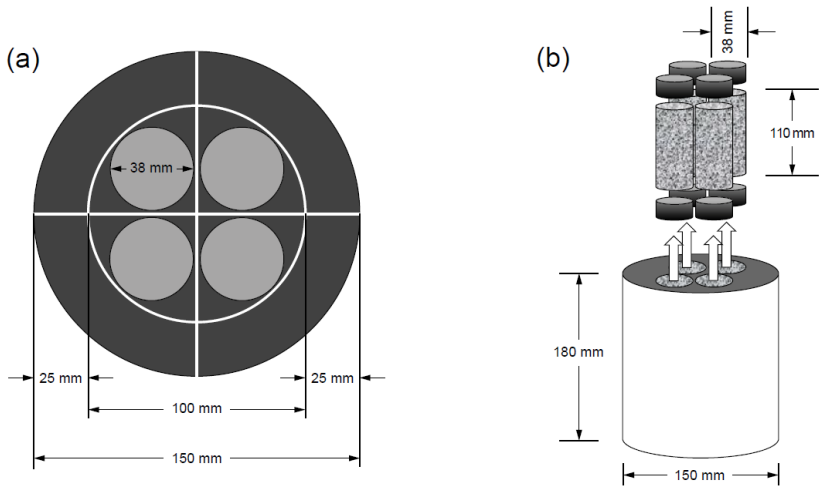

Figure 15. Graphics of coring from an SGC specimen (AASHTO, 2019d).

The Dynamic Modulus test requires triplicate specimens per mixture prepared to a target air void level of 7.0 ± 0.5 percent. Testing is conducted at three temperatures selected based on the PG of the binder in the mixture and at three frequencies for developing the $|E^*|$ master curve. Given the PG of the base binders used in this study (i.e., PG 64-16 and PG 64-22), the $|E^*|$ testing was conducted at 4°C, 20°C, and 40°C with frequencies of 10Hz, 1Hz, and 0.1 Hz. This testing plan resulted in nine unique test conditions, starting with the lowest temperature and highest frequency, then progressing through decreasing frequencies before changing to the higher temperature. The setup for the $|E^*|$ test and the AMPT equipment are shown in Figure 16.

Figure 16. Photo of Small Specimen |E^*| Sample (left) and Photo of AMPT (right)

Upon completion of the AMPT testing, data were reviewed, and the |E^*| master curve for each mixture was then developed following Equation 4 through Equation 6, as outlined in AASHTO R84-17 *Developing Dynamic Modulus Master Curves for Asphalt Mixtures Using the Asphalt Mixture Performance Tester (AMPT)*. This procedure differs slightly from the procedure presented in the Mechanistic-Empirical Pavement Design Guide (MEPDG) (AASHTO, 2021).

$$log|E^*| = \delta + \frac{(E_{max} - \delta)}{1 + e^{\beta + \gamma \log(f_r)}} \quad \text{Equation 4}$$

Where,

|E^*| = Dynamic modulus, ksi;

E_{max}=limiting maximum modulus, ksi;

δ, β, and ϒ = fitting coefficient

f_r= reduced frequency, Hz.

The reduced frequency calculation uses the Arrhenius equation presented in Equation 5,

$$\log f_r = \log f + a(T) \quad \text{Equation 5}$$

Where,

f_r = the reduced frequency at the reference temperature, Hz;

f = the loading frequency at the test temperature, Hz, and

a(T) = the shift factor at temperature T.

The shift factor at temperature T can be calculated following Equation 6,

$$\log[a(T)] = \frac{\Delta E_a}{19.14714}\left(\frac{1}{T} - \frac{1}{T_R}\right) \quad \text{Equation 6}$$

Where,

ΔE_a = the fitting parameter related to the activation energy;

T = the test temperature, K, and

T_r = the reference temperature, K.

This study's reference temperature for developing the dynamic modulus master curve was 20°C. For calculating the limiting maximum modulus $|E^*_{max}|$, AASHTO R84 specifies the Hirsch estimation model based on the VMA and VFA volumetric properties (AASHTO, 2021; Christensen, Pellinen, & Bonaquist, 2003). An example of a dynamic modulus master curve for a typical asphalt mixture material is shown in Figure 17.

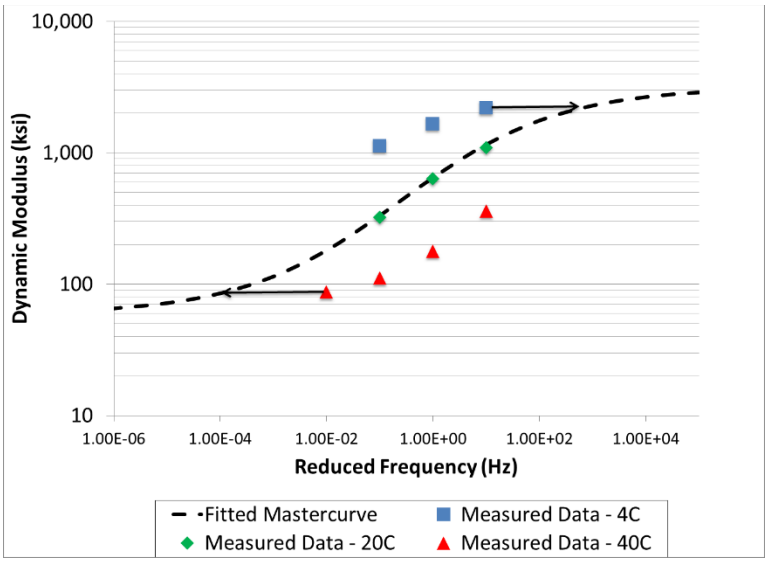

Figure 17. Example Dynamic Modulus Master curve.

3.3.2 AMPT Cyclic Fatigue

The AMPT Cyclic Fatigue test was employed in this study to evaluate the fatigue cracking resistance of the mixtures. Specimens for this test were prepared in the laboratory using the same methodology as for the Dynamic Modulus test specimens, as described in AASHTO PP 99-19 (AASHTO, 2019d). For each mixture at a given aging level, at least three replicates were tested following AASHTO TP 133-19, *Standard Method of Test for Determining the Damage Characteristic Curve and Failure Criterion Using Small Specimens in the Asphalt Mixture Performance Tester (AMPT) Cyclic Fatigue Test* (AASHTO, 2019b).

For this test, each small cylindrical specimen is glued to end platens at the top and bottom, and the plates are then bolted to the AMPT, through which a controlled actuator displacement cyclic load can be applied to the specimen. For this study, the test was performed at 21°C and 10 Hz, and an appropriate strain level was selected based on the mixture's stiffness. During testing, the phase angle should increase until it peaks and falls from the peak. The number of cycles at which the phase angle peaks represents the cycles to failure for the test. An example of individual

specimen AMPT cyclic fatigue data is shown in Figure 18. This failure should occur between 2,000 and 80,000 cycles on a typical test, per AASHTO TP133-19. Failures outside this range would necessitate adjusting the strain levels used for the test.

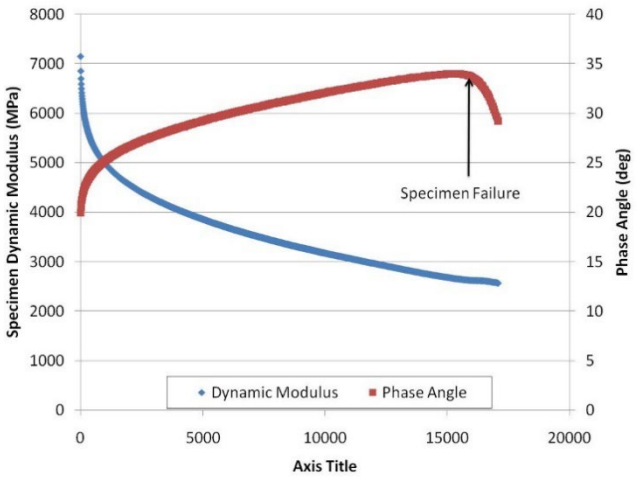

Figure 18. Example AMPT Fatigue Test Data – Individual Specimen.

During the AMPT Cyclic Fatigue test, the specimen is expected to crack or fail between the gauge points used to hold the on-specimen LVDTs, as shown in Figure 19, defined as a "middle" failure. Failures outside this range, termed "end-failures," are generally deemed non-acceptable, warranting the testing of an additional specimen. A minimum of three middle failures were obtained for each mixture tested in the AMPT Cyclic Fatigue test.

Figure 19. Example of 'Middle' Failure in AMPT Cyclic Fatigue Test.

3.4. Mixture Cracking Indexes

3.4.1 Mixture Glover-Rowe Parameter

Results obtained from the $|E^*|$ testing were used to calculate the Glover-Rowe mix parameter for characterizing the fatigue cracking performance of the mixes. Dynamic modulus measurements and their corresponding phase angles were also used to create black space diagrams for each material at different aging levels and determine the effectiveness of additive technologies in improving stress-relaxation properties.

Glover-Rowe parameter as a rheological index for hot mix asphalt mixtures was calculated according to Equation 7, combining the effect of stiffness ($|E^*|$) and embrittlement phase angle (δ) at 20°C and 5Hz.

$$G - R_m = |E^*| cos^2\delta / sin\delta \quad \text{Equation 7}$$

Where,

$|E^*|$ = Dynamic modulus at target temperature and specified frequency, ksi; and

δ = phase angle at target temperature and specified frequency, degrees.

An index ratio was calculated according to Equation 8 to determine the aging susceptibility of each mix. Equation 9 Glover-Rowe effectiveness index was calculated for each mixture to determine the effectiveness of the additives at a specific aging condition by comparing the parameter for the modified mix to the control mix.

$$G - R_m \text{ Aging Index} = \frac{(\text{G} - \text{R}_{\text{aged condition}})}{(\text{G} - \text{R}_{\text{STOA}})} \quad \text{Equation 8}$$

$$G - R_m \text{ Effectiveness Index} = \frac{(\text{G} - \text{R}_{\text{aged condition}})_{\text{Additive mix}}}{(\text{G} - \text{R}_{\text{aged condition}})_{\text{Control mix}}} \quad \text{Equation 9}$$

3.4.2 Cyclic Fatigue Testing

The FlexMAT v2.1.3 analysis spreadsheet was employed to determine each mixture's damage characteristic curve (C vs. S) and D^R failure criterion parameter based on the AMPT cyclic fatigue and $|E^*|$ test data. The $|E^*|$ master curves were developed based on both the 2S2P1D model (a generalization of the Huet-Sayegh model) (Olard & Di Benedetto, 2003) in the FlexMAT software and the sigmoidal model, as shown in Equation 4. The $|E^*|$ data were then used with AMPT cyclic fatigue test data to generate a unique damage characteristic curve for each mixture, relating material integrity (C) with the asphalt mix's accumulated damage (S). The S_{app} index parameter was determined to evaluate the mix's cracking performance. This parameter combines the asphalt mixture's modulus and toughness to represent the mix's damage capacity following the

viscoelastic continuum damage (VECD) theory (Y. D. Wang et al., 2020). The S_{app} index was calculated using the FlexMAT spreadsheet, following Equation 10.

$$S_{app} = \frac{1}{1000} \frac{\left(\frac{a_T^{\frac{C_{12}}{\alpha+1}}}{C_{11}} D^R \right)^{\frac{1}{C_{12}}}}{|E^*|^{\frac{\alpha}{4}}} \quad \text{Equation 10}$$

Where,

a_T = time-temperature shift factor value at the target temperature;

$|E^*|$ = dynamic modulus at the target temperature and 10 Hz, ksi;

D^R = Failure criterion (Equation 11);

α = damage accumulation parameter;

C_{11} = damage fitting parameter; and

C_{12} = damage fitting parameter.

$$D^R = \frac{sum\ (1 - C)}{N_f} \quad \text{Equation 11}$$

Where,

sum (1-C) = area below the curve of the damage characteristic curve; and

N_f = number of cycles to failure.

The target temperature for S_{app} calculation is based on the average climate reference temperature (i.e., average high and low PG minus 3°C) (Y. D. Wang et al., 2020). Therefore, S_{app} index values are location-specific; in this study, the location was Lee County (Auburn), Alabama.

An index ratio was later computed according to Equation 12, based on the S_{app} parameters determined after STOA and long-term aging, to assess the aging susceptibility of each mix. The

S_{app} effectiveness index, calculated using Equation 13, evaluates the effectiveness of additives by comparing the S_{app} parameters of a modified mix to the control mix determined under the same aging condition.

$$S_{app}\ Aging\ Index = \frac{S_{app_{aged}}}{S_{app_{STOA}}} \quad \text{Equation 12}$$

$$S_{app}\ Effectiveness\ Index = \frac{S_{app_{aged_{(Additive\ mix)}}}}{S_{app_{aged_{(Control\ mix)}}}} \quad \text{Equation 13}$$

3.5. FlexPave™ Analysis

FlexPave™, developed by the North Carolina State University research team, is a pavement design and analysis tool capable of predicting pavement structures' rutting and cracking performance. The software's first version consisted of a three-dimensional Fourier transform-based finite element analysis tool with moving loads. Its simulations consider the effects of temperature using temperature-time history data obtained from the Enhanced Climatic Model. Both fatigue damage and rutting can be determined, but this research focuses on fatigue damage calculations. Fatigue damage is computed through the simplified viscoelastic continuum damage (S-VECD) model embedded in the software.

AMPT $|E^*|$ and cyclic fatigue data were used as input to the FlexPave™ structural model to predict the fatigue performance of a given pavement structure. Other inputs required for the analysis were selected to simulate a pavement structure at the NCAT Test Track and are briefly summarized as follows:

- Pavement type: New Pavement;

- Analysis option: pavement performance analysis (fatigue cracking only);
- Pavement design life: 20 years;
- Pavement structure: three-layer pavement
    - Asphalt layer: 5 in, using the $|E^*|$ and cyclic fatigue test results as material inputs.
    - Aggregate base: 6 in, elastic modulus = 10,000 psi, Poisson's ratio = 0.40.
    - Subgrade: infinite layer, elastic modulus = 30,000 psi, Poisson's ratio = 0.45.
- Climate data: EICM temperature profile for Troy, AL (closest location to Auburn, AL in FlexPave); and
- Traffic data: single axle, dual tires, 18-kip axle load, design speed=45mph, daily equivalent single axle loads (ESALs) = 2,740 (to simulate 20 million ESALs over 20 years), 0,4% traffic growth.

After the simulation, the predicted percentage of damage (% damage) at the end of the 20 years of pavement design life was used as the primary parameter to compare the fatigue cracking performance of the modified asphalt mixtures with that of the control mixtures.

CHAPTER 4 - RESULTS AND DISCUSSION

This chapter presents the results obtained from asphalt mixture performance testing. The test results are subsequently analyzed to assess the efficacy of additive technologies in enhancing asphalt mixture properties, specifically those concerning fatigue cracking performance, across various aging levels.

4.1. Dynamic Modulus |*E**|

The |*E**| master curves were calculated following the sigmoidal model shown in Equation 4. Figure 20 and Figure 21 compare the master curves of the mixtures made with Base Binders 1 and 5, respectively, at various aging conditions. Variations in stiffness are most notable at lower and intermediate frequencies across all aging conditions.

Base Binder 1 mixtures containing additives 4 and 5 exhibit lower stiffness than the control mixture across all three aging conditions, as observed in Figure 20. Conversely, Additives 1 and 2 mixtures show similar stiffness to the control mixture after LTOA. Under the NAWS conditioning protocol, the dynamic modulus curves exhibit greater variations. Still, the trends align closely with those observed for STOA—mixtures with additives 1, 2, and 3 exhibit higher stiffness compared to the control mixture, while those with additives 4 and 5 display lower stiffness.

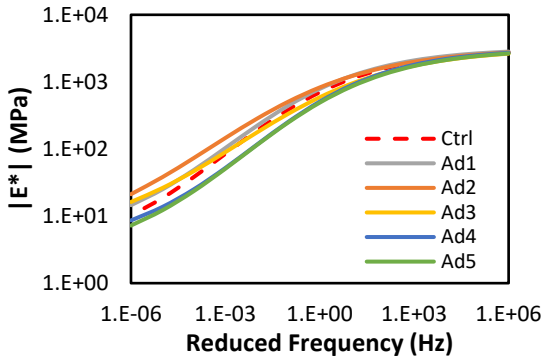

(a) STOA

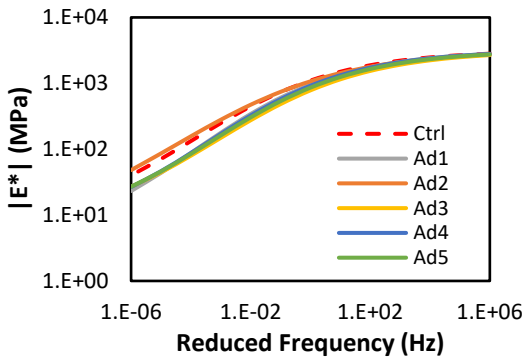

(b) LTOA

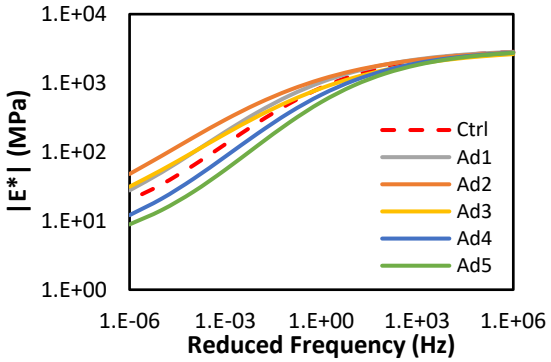

(c) NAWS

Figure 20. |*E**| master curves for control and additive-modified binder 1 mixes at (a) STOA, (b) LTOA, and (c) NAWS conditions.

Figure 21 compares the master curves for mixtures prepared with Base Binder 5. In Figure 21a, mixtures with additives 1 and 2 exhibit higher stiffness than the control mix, while those with additives 3, 4, and 5 show lower stiffness after STOA. Similar trends are observed in Figure 21b for mixtures after LTOA and Figure 21c for those after NAWS. Notably, the curves in Figure 21b show less scatter. In addition, the mixture with additive 4 shows much lower stiffness compared to other mixtures after NAWS, as shown in Figure 21c.

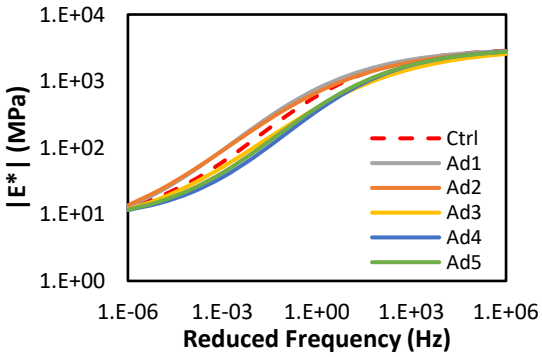

(a) STOA

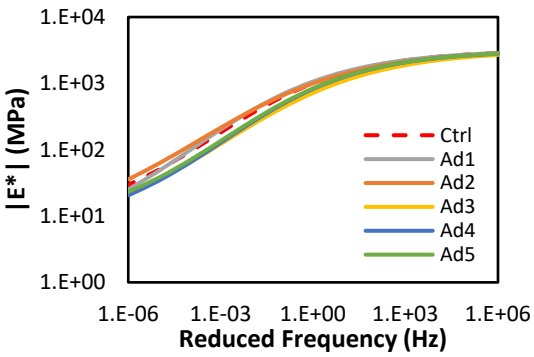

(b) LTOA

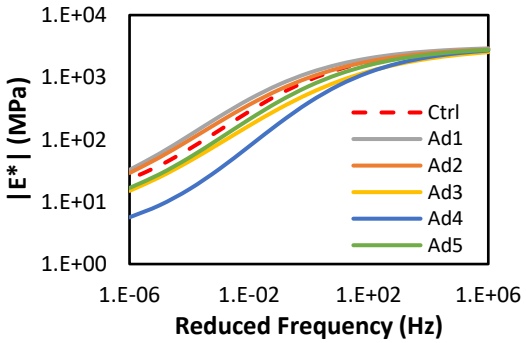

(c) NAWS

Figure 21. |*E**| master curves for control and additive-modified binder 5 mixes at (a) STOA, (b) LTOA, and (c) NAWS conditions.

Figure 22 and Figure 23 compare the dynamic modulus master curves for each mixture under the three distinct aging protocols. A progressive shift in the master curves toward higher positions is anticipated as aging advances from STOA to LTOA, indicating increased stiffness. The expected stiffening effect is evident in both figures, where the |*E**| values consistently increase in relation to the severity of aging from STOA to LTOA. However, the impact of the NAWS protocol varies depending on the specific Base Binder and additive used in the mixture.

For mixtures using Base Binder 1, shown in Figure 22, Additives 1, 2, and 3 after NAWS and LTOA master curves are closely aligned, as shown in Figure 22b, Figure 22c, and Figure 22d. This trend suggests that these aging protocols have a similar effect on the stiffness of these mixtures. However, in the case of the control mixture and the mixture with Additive 4, their NAWS |*E**| curves fall between the LTOA and STOA curves, as seen in Figure 22a and Figure 22e, suggesting that the NAWS aging protocol is not as severe as the LTOA protocol for these specific mixes. Furthermore, as shown in Figure 22f, the STOA |*E**| curve is close to the NAWS |*E**| curve for the mixture containing Additive 5, indicating the insensitivity of this particular mixture to the NAWS aging protocol.

For mixtures with Base Binder 5, shown in Figure 23, the LTOA and NAWS aging protocols have a similar effect on the $|E^*|$ of the mixtures containing Additives 1 and 2. For the control mixture and those with Additives 3 and 5, the NAWS $|E^*|$ curves fall between the STOA and LTOA| E*| curves. Furthermore, the $|E^*|$ of the mixture with Additive 4 is insensitive to the NAWS aging protocol, as evidenced in Figure 23e.

.

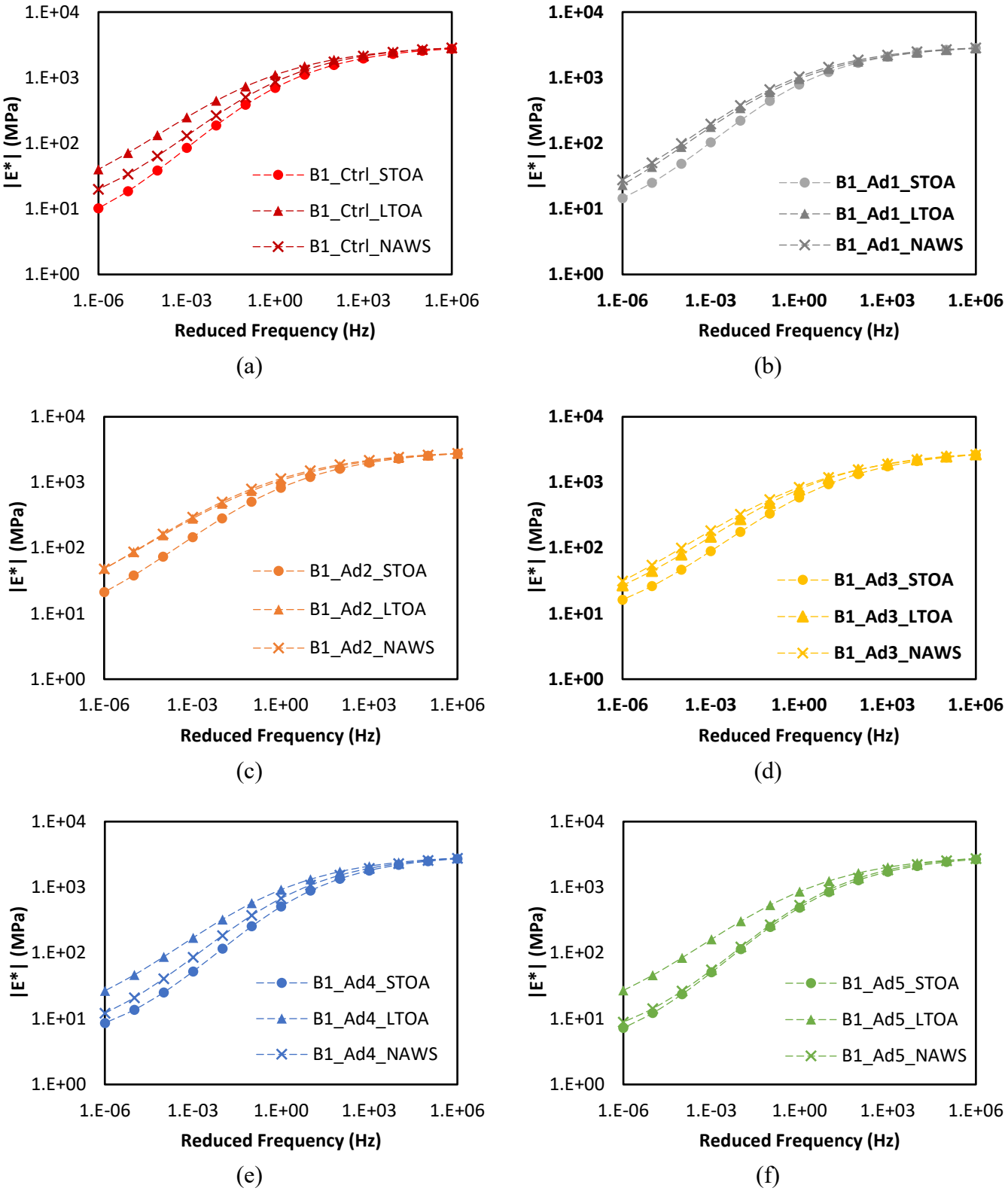

Figure 22. $|E^*|$ master curve for base binder 1 asphalt mixtures at different aging levels. (a) Control mix, (b) Additive 1, (c) Additive 2, (d) Additive 3, (e) Additive 4, and (f) Additive 5.

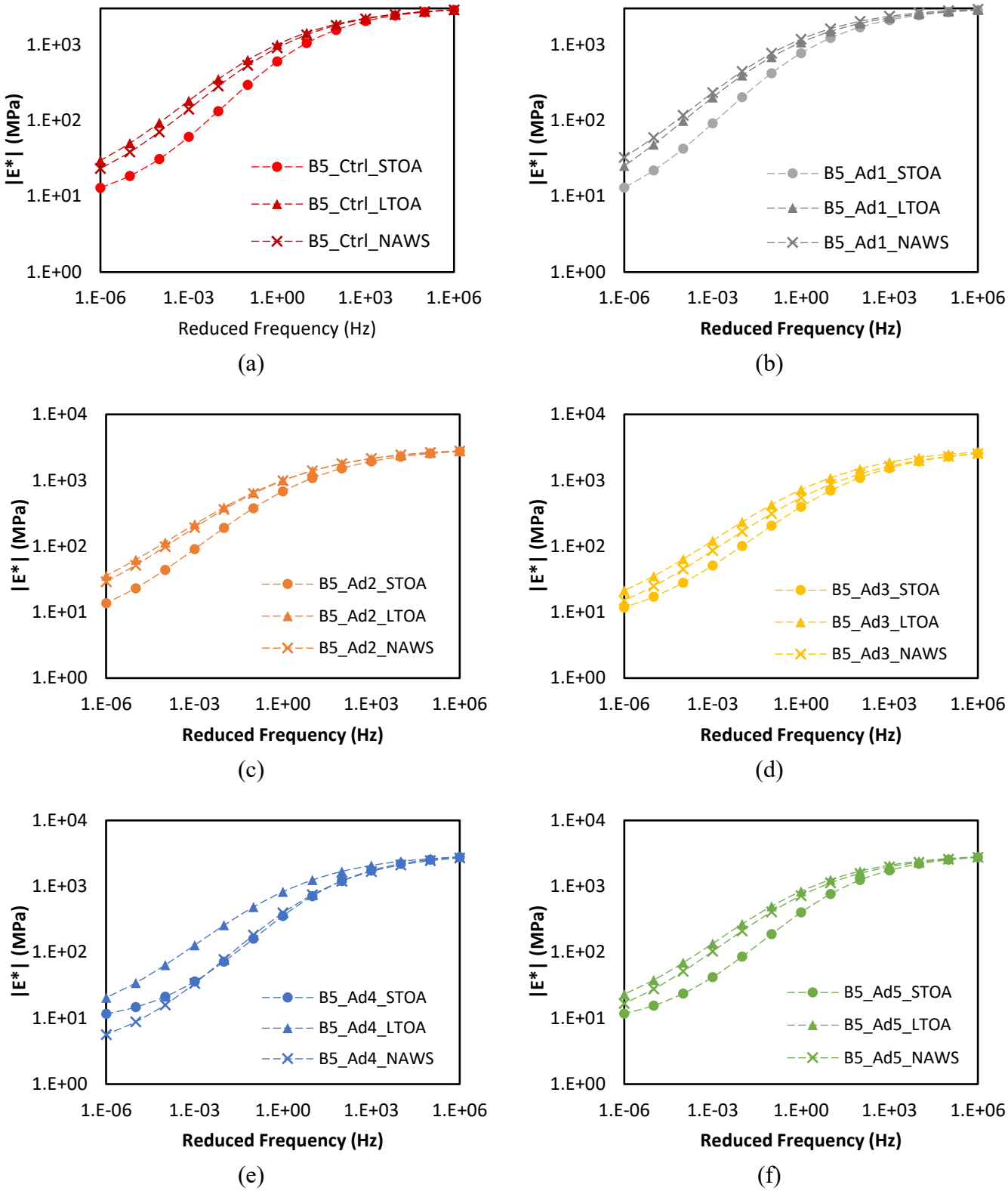

Figure 23. $|E^*|$ master curve for base binder 5 asphalt mixtures at different aging levels. (a) Control mix, (b) Additive 1, (c) Additive 2, (d) Additive 3, (e) Additive 4, and (f) Additive 5.

An aging ratio was calculated to assess the $|E^*|$ variation in each mix following LTOA or NAWS compared to its STOA. A ratio of 1 indicates no stiffness difference at a given reduced frequency. In contrast, higher aging ratios indicate a more pronounced increase in stiffness due to aging, suggesting greater susceptibility to aging.

Figure 24 shows the $|E^*|$ aging ratios for mixtures with Binders 1 and 5 across reduced frequencies. Notably, the most significant increases in stiffness are observed at low and intermediate frequencies (i.e., high and intermediate test temperatures), suggesting that aging predominantly impacts the mix's stiffness within this range. Also evident are more substantial changes in $|E^*|$ values for Binder 1 and Binder 5 mixtures when subjected to LTOA compared to NAWS. In Figure 24d, mixtures containing Additive 4 with Binder 5 under NAWS aging conditions are softer than those aged under STOA at low frequencies, indicating that this mix exhibited reduced susceptibility to hardening following NAWS aging.

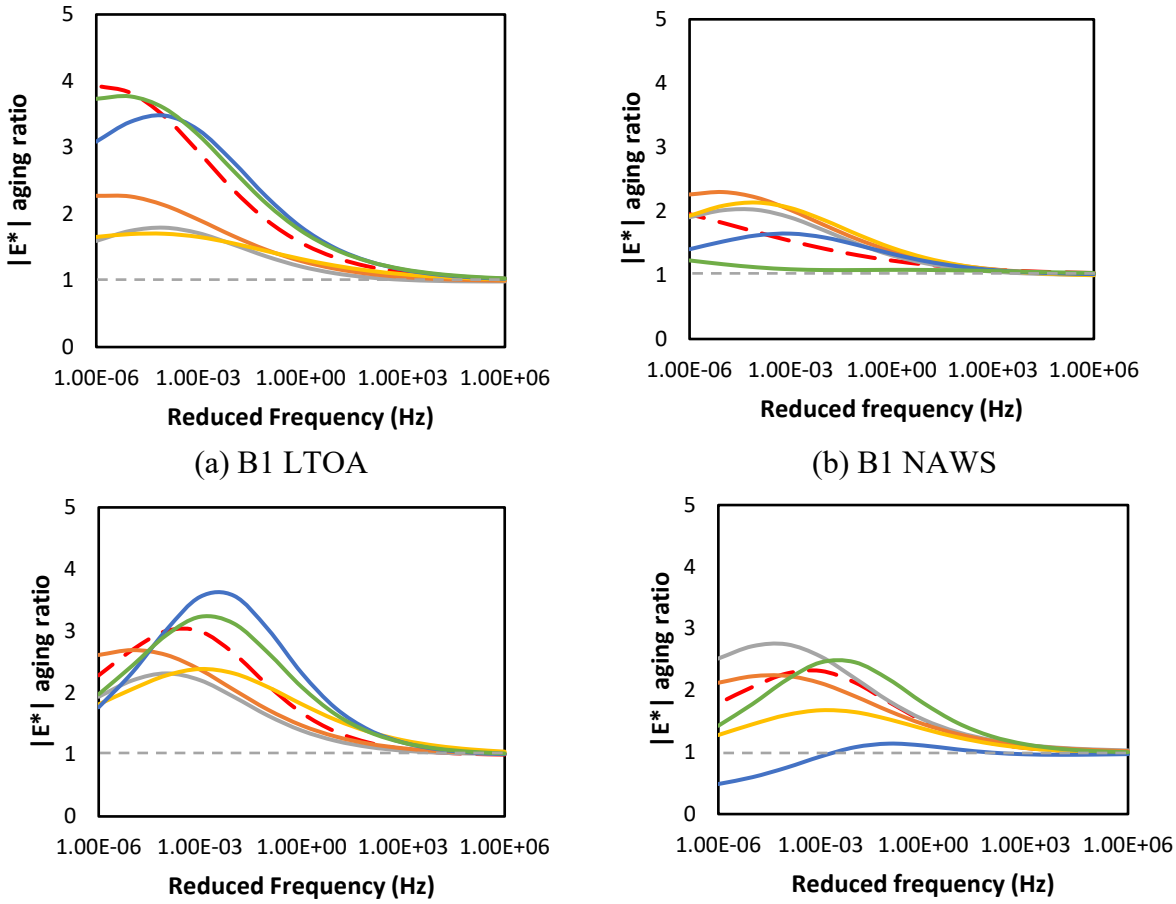

Figure 24. |*E**| aging ratio for binder 1 and binder 5 mixes for LTOA and NAWS aging conditions.

Figure 25 shows the average |*E**| aging ratio for mixtures with Binders 1 and 5 under LTOA and NAWS conditions. The average |*E**| aging ratio represents the average change in |*E**| across reduced frequencies when transitioning from STOA to LTOA or NAWS. Under LTOA, mixtures containing Additives 4 and 5 for both base binders exhibit similar or slightly higher increases in |*E**| values compared to the control mixture. A higher |*E**| aging ratio suggests that while mixtures with Additives 4 and 5 were softer than the control mix at STOA and LTOA, they experienced greater stiffness increases after LTOA than the control mix. However, these increases in |*E**| after aging were not significant enough to result in stiffer modified mixes after aging than

the control mix. Conversely, mixtures with Additives 1, 2, and 3 yield lower |E^*| aging ratios than the control mix for both base binders, indicating that these mixes were less prone to stiffening after LTOA than the control mix.

The trends in dynamic modulus change exhibit variations between NAWS and LTOA conditions. Figure 25a shows that for Binder 1 mixtures, Additives 1, 2, 3, and 4 result in similar or higher stiffness increases after aging, with only Additive 5 yielding a lower |E^*| aging ratio. In contrast, for Binder 5 mixtures, as shown in Figure 23b, Additives 3 and 4 exhibit lower stiffness increases than the control mix. Conversely, Additives 1, 2, and 5 demonstrate similar or higher stiffness increases after NAWS aging, as depicted in Figure 25b. The stiffness change after NAWS is similar or higher for most additives during NAWS conditioning. These stiffness changes after aging explain the similar or increased scatter observed in the |E^*| curves between STOA and post-NAWS conditions, as illustrated in Figure 20 and Figure 21.

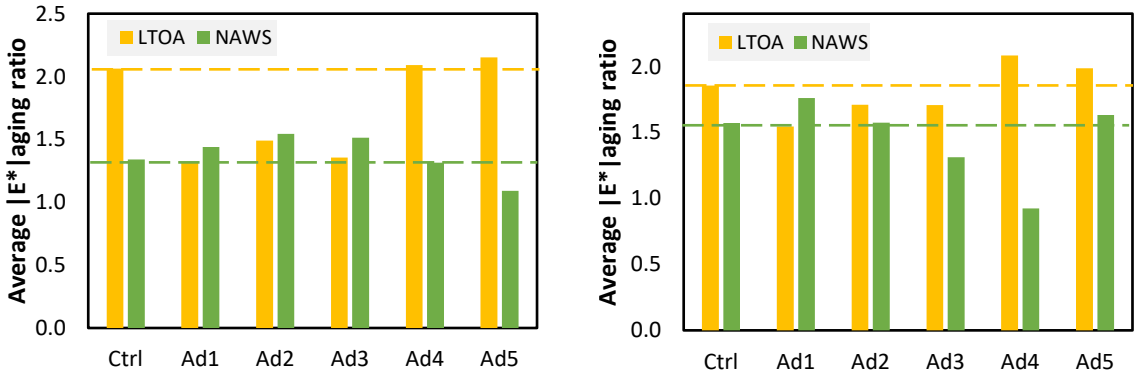

Figure 25. |E^*| average aging ratio for (a) binder 1 and (b) binder 5 mixes for LTOA and NAWS aging conditions

4.2. Glover-Rowe mix (G-R_m) and Black Space Diagrams

An analysis focused solely on dynamic modulus information was conducted in the previous section. In contrast, this section combines dynamic modulus and the phase angle into a single

parameter known as Glover-Rowe ($G\text{-}R_m$) for asphalt mixtures. Although the Glover-Rowe parameter was initially developed for asphalt binder evaluation, this section adapts a similar concept for asphalt mixture evaluation. Data for $|E^*|$ and phase angle (δ) at 20°C and 5 Hz obtained from dynamic modulus testing were used to create black space diagrams and calculate the $G\text{-}R_m$ parameter. Figure 26 and Figure 27 show the black space diagrams for Binders 1 and 5, respectively, after STOA, LTOA, and NAWS aging.

In these diagrams, observations characterized by low stiffness ($|E^*|$) and high δ are associated with better cracking performance. $|E^*|$ reflects the mix's ability to accumulate stresses, while the phase angle (δ) in the black space diagram signifies the mix's capacity to dissipate these stresses (Mensching et al., 2017). As aging progresses, stiffness increases, and the mix's relaxation properties (δ) decrease, causing observations to shift from the bottom-right area (lower $|E^*|$ - higher δ) to the top-left area (higher $|E^*|$ - lower δ) of the black space diagram. These trends are apparent in both Figure 26 and Figure 27, where STOA observations tend to be located in the bottom-right area of the black space diagrams and shift towards the top-left area with aging. The $G\text{-}R_m$ parameter captures this relationship between stiffness and δ, as demonstrated in Equation 14.

$$G - R_m = |E^*| cos^2\delta / sin\delta \qquad \text{Equation 14}$$

Lower values of $|E^*|$ and higher values of δ are indicative of improved cracking performance, resulting in lower $G\text{-}R_m$ parameters. The extent to which an observation shifts within the black space diagram is directly related to the mixture's susceptibility to aging, and this can be quantified by comparing $G\text{-}R_m$ parameters at two different aging conditions. The shift of $G\text{-}R_m$ parameters in Figure 26 and Figure 27 reflects the impact of aging on each mixture. Therefore, the

properties observed at STOA and LTOA, along with the change in position within the black space diagram, serve as a means to evaluate the effectiveness of an additive in enhancing aging resistance.

For instance, in Figure 26a, the mix with Additive 4 (represented by a red circle) at STOA is positioned more towards the bottom-right area of the diagram compared to the mix with Additive 3 (represented by a yellow circle). However, after LTOA, the mix with Additive 4 shifted further towards the top-left area than the mix with Additive 3, indicating that the mix with Additive 4 experienced a more significant shift in the diagram and was consequently more affected by aging.

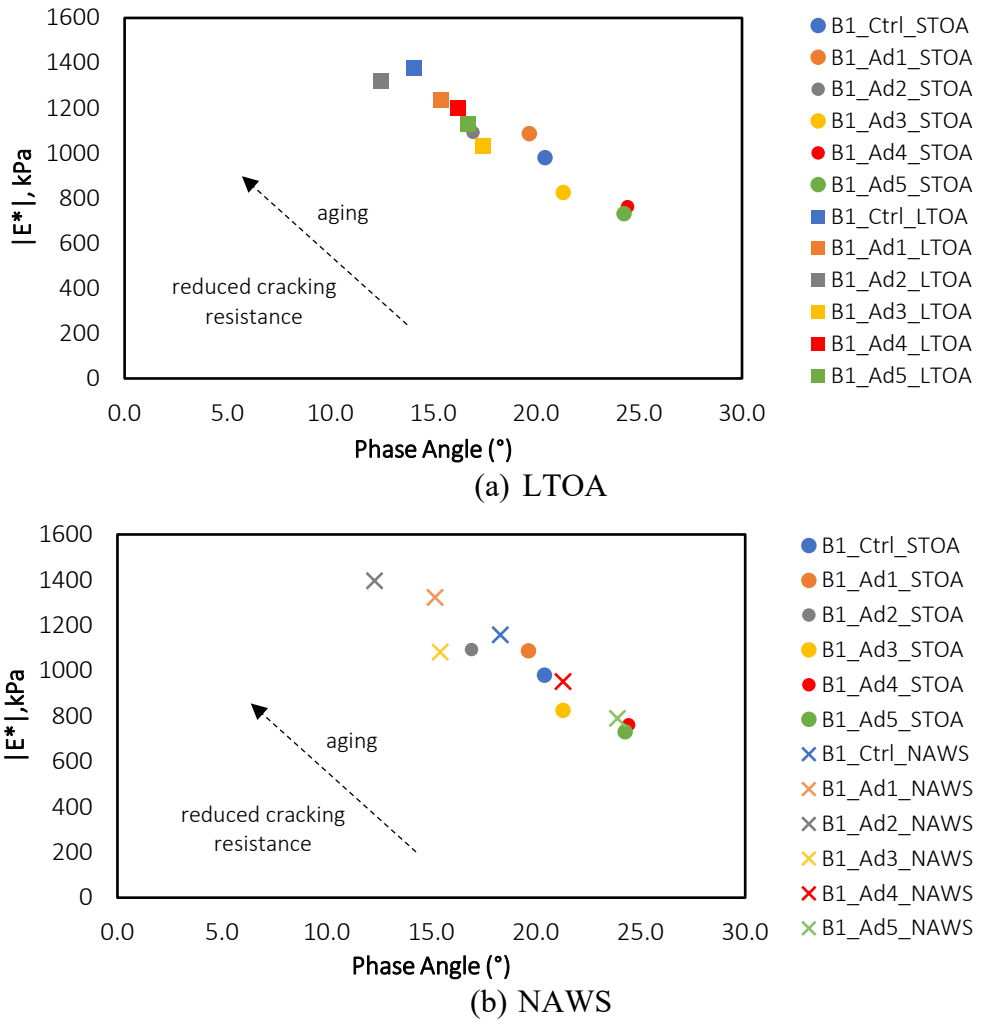

Figure 26. Black space diagram for binder 1 mixes at (a) LTOA and (b) NAWS aging protocols.

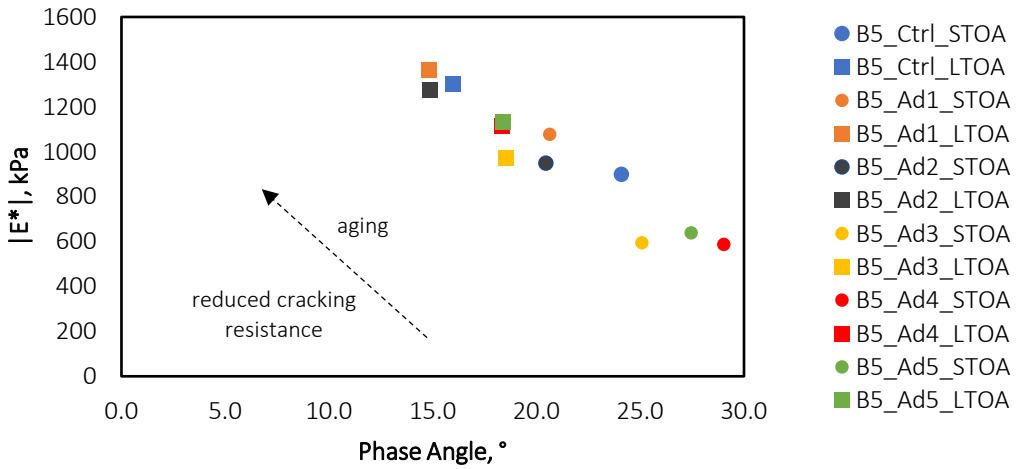

(a) LTOA

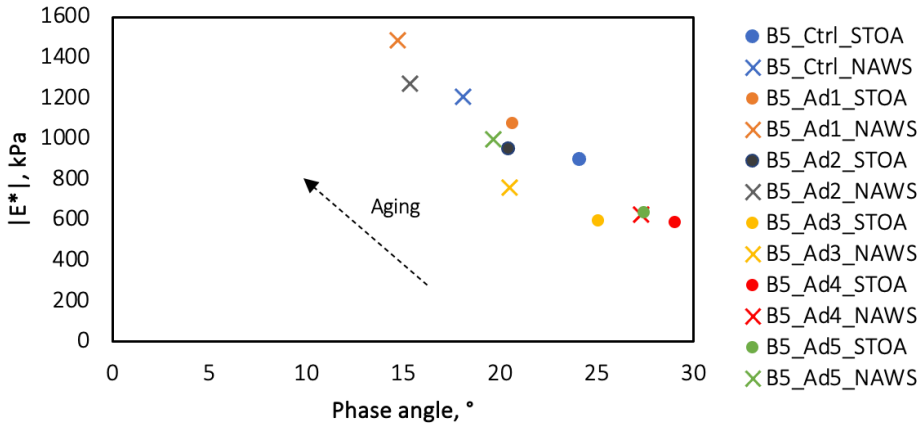

(b) NAWS

Figure 27. Black space diagram for binder 5 mixes at (a) LTOA and (b) NAWS aging protocols.

The *G-R*$_m$ parameter was calculated for mixtures prepared with two base binders at three different aging conditions to quantify the properties observed in the black space diagrams. As the *G-R*$_m$ parameter is derived from the representative $|E^*|$ master curve and is not an average value of the individual experimental master curves, comparing each mixture's results involves observing differences in the charts, and no statistical testing could be performed to determine these differences.

The results of *G-R*$_m$ for all the evaluated mixtures are presented in Figure 28. As the data shows, the LTOA and NAWS aged mixtures produced higher *G-R*$_m$ values than the corresponding STOA mixes, indicating reduced cracking resistance for the more heavily aged mixtures, as expected.

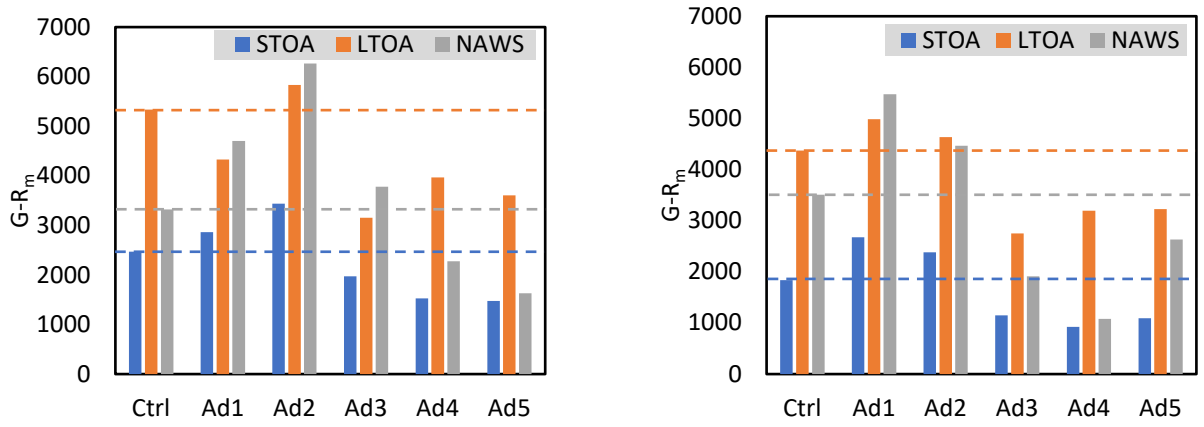

Figure 28. Glover-Rowe parameter for mixes at three different aging conditions for (a) B1 and (b) B5-based asphalt mixtures.

Furthermore, Figure 29 and Figure 30 illustrate the *G-R*$_m$ parameters at STOA, LTOA, and NAWS, providing insight into the effect of including the additive technology at specific aging conditions. Figure 29a shows that mixtures with Binder 1 and Additives 3, 4, and 5 exhibit lower *G-R*$_m$ values than the corresponding control mix at the STOA condition, suggesting improved cracking resistance. However, Additives 1 and 2 showed higher *G-R*$_m$ values than the control mix at STOA. Figure 29b shows a similar trend for mixtures after LTOA, except for Additive 1, which reduced the *G-R*$_m$ value compared to the control mix. Regarding the NAWS mixes, only mixtures containing Additives 4 and 5 yielded lower *G-R*$_m$ values than the control mix, indicating that these additives could maintain properties associated with good cracking performance after NAWS aging.

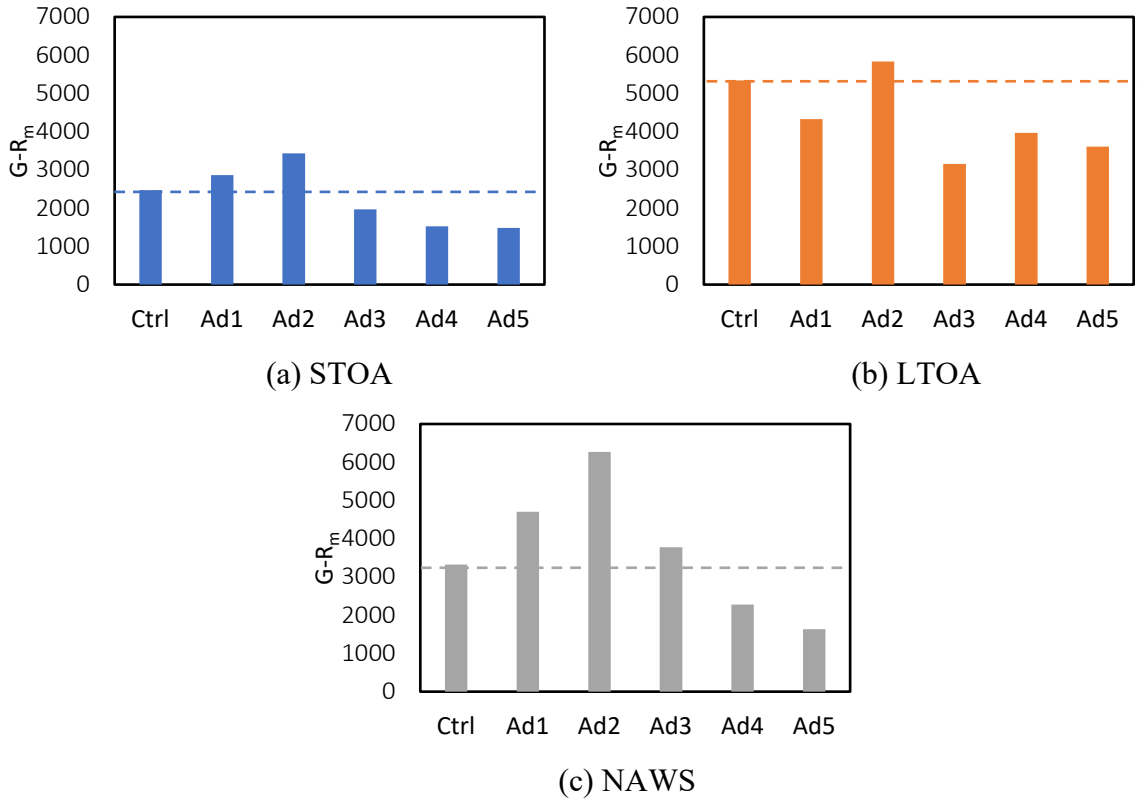

(a) STOA (b) LTOA

(c) NAWS

Figure 29. Glover-Rowe parameter for binder 1 mixes at (a) STOA, (b) LTOA, and (c) NAWS.

Figure 30 displays the *G-R*$_m$ parameters for Binder 5 mixtures subjected to STOA, LTOA, and NAWS aging protocols. Figure 30a, corresponding to Binder 5 at STOA, shows similar trends to those of Binder 1 mixtures. Notably, mixtures containing Additives 3, 4, and 5 showed lower *G-R*$_m$ values than the control mix, indicative of improved cracking performance-related properties. Interestingly, despite the expected increase in *G-R*$_m$ with aging, these same mixtures maintained lower *G-R*$_m$ values than the control mix at STOA and after LTOA and NAWS, as evident in Figure 30b and Figure 30c. This trend indicates that while the stiffness properties of Binder 5 mixtures evolved and were adversely impacted by aging, Additives 3, 4, and 5 enhanced the mix's properties at STOA, and this enhancement persisted after aging, irrespective of LTOA or NAWS protocols.

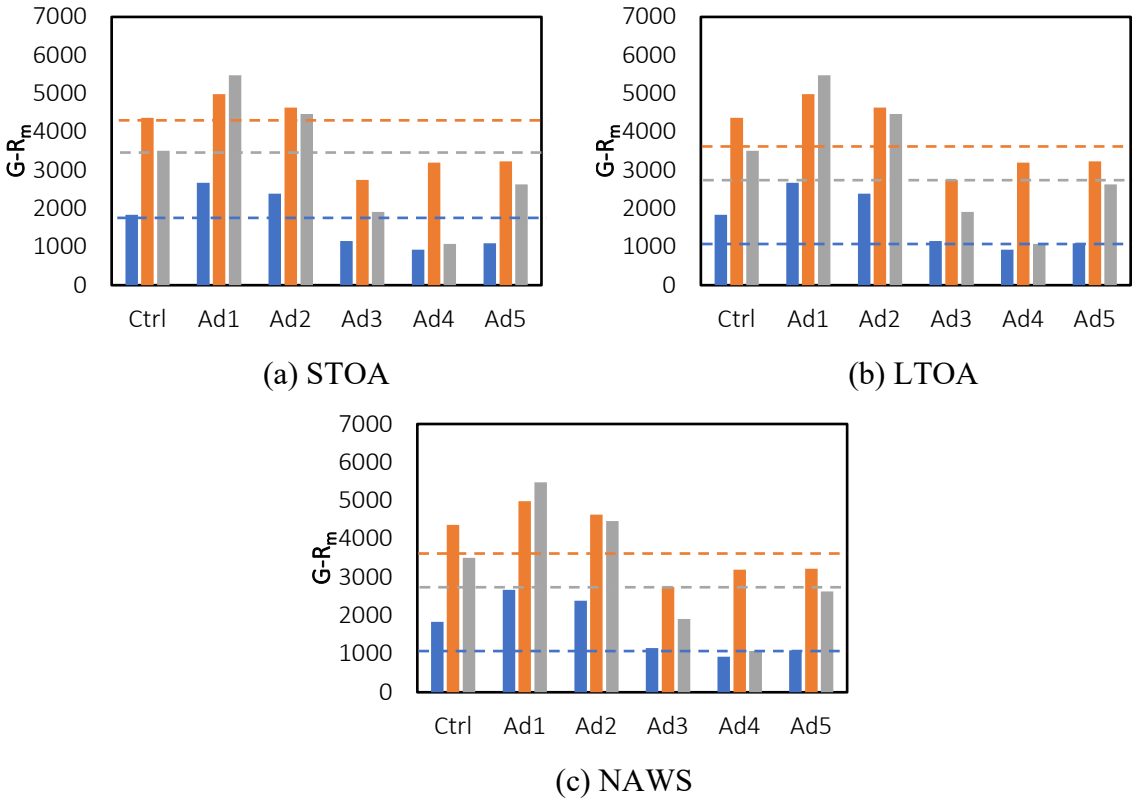

(a) STOA

(b) LTOA

(c) NAWS

Figure 30. Glover-Rowe mix parameter for binder 5 mixes at (a) STOA, (b) LTOA, and (c) NAWS.

The *G-R*$_m$ effectiveness index was calculated to assess the extent to which an additive improved cracking resistance compared to the control mix under the same aging conditions. Figure 31 presents the results of the *G-R*$_m$ effectiveness index for each mixture at STOA, LTOA, and NAWS. Indexes equal to 1 suggest no change in *G-R*$_m$ when the mixture is modified, while values above 1 indicate an increase in *G-R*$_m$ for modified mixtures at the same aging conditions. Consequently, an index value lower than one is indicative of better cracking resistance than the control mix, as observed for Additives 3, 4, and 5 at STOA, LTOA, and NAWS. The results were generally consistent for both Base Binders 1 and 5, except for Additive 3 with Binder 1 after NAWS aging, where the effectiveness index exceeded one. Notably, Additives 1 and 2 were

largely ineffective in reducing *G-R*$_m$ compared to the control mixture, except for the Binder 1 mixture containing Additive 1 after LTOA, as shown in Figure 31b.

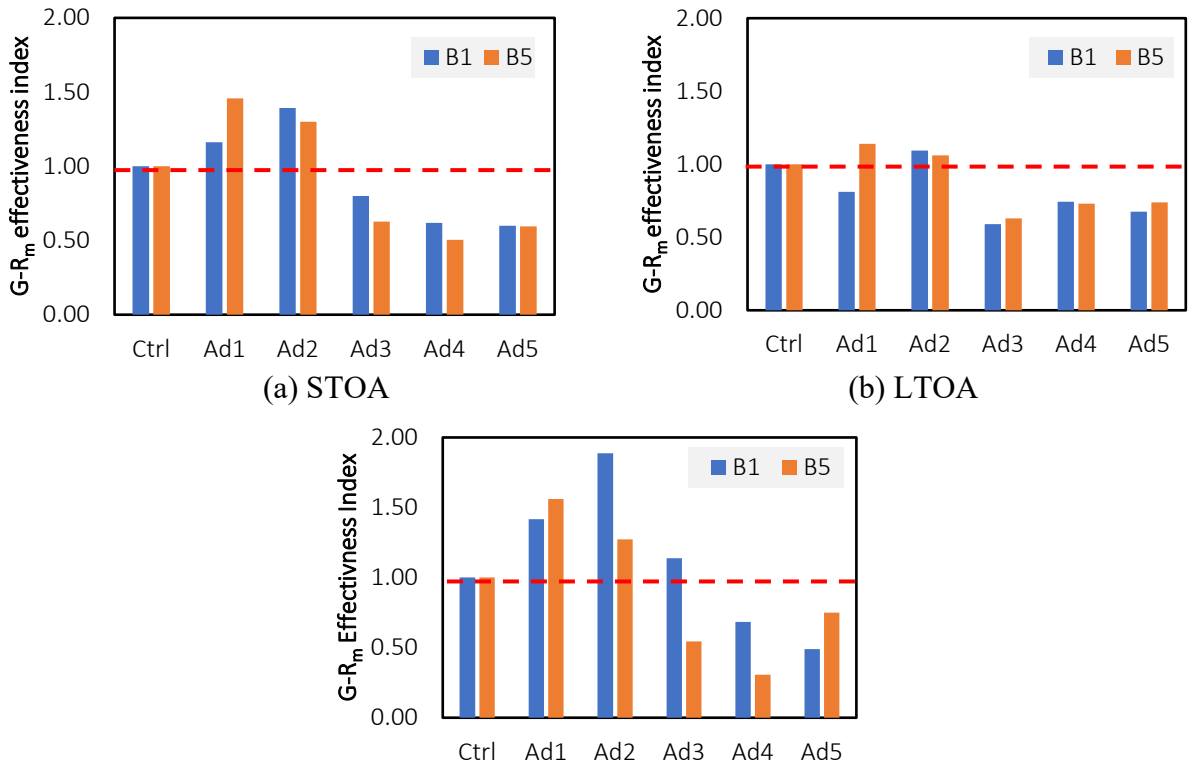

Figure 31. Glover-Rowe mix effectiveness index for mixes at (a) STOA, (b) LTOA, and (c) NAWS

The increase in *G-R*$_m$ observed after aging was quantified by calculating an aging index, which is presented in Figure 32, or all the mixtures at LTOA and NAWS. This index indicates the change in the position of the observations in the black space diagram, where lower values of the aging index suggest greater resistance to the stiffening effects of aging.

For the LTOA condition, mixes modified with Additives 1, 2, and 3 exhibited the same or lower aging indexes than their respective control mixes, as depicted in Figure 32a. Notably, Binder 1 mixture with Additive 1 at LTOA yielded the lowest aging index for this condition. This value reflects the mix's ability to achieve a higher *G-R*$_m$ at STOA but a lower value than the control mix after LTOA, indicating superior aging resistance.

Conversely, Additives 4 and 5 increased the aging susceptibility of the mix to LTOA by amplifying the change in the $G\text{-}R_m$ parameter after aging. Although this heightened aging susceptibility did not significantly elevate the $G\text{-}R_m$ parameter after LTOA—remaining lower than that of the control mix after aging—it could pose potential issues for longer aging periods if these mixes continue to age at a faster rate than the control mix.

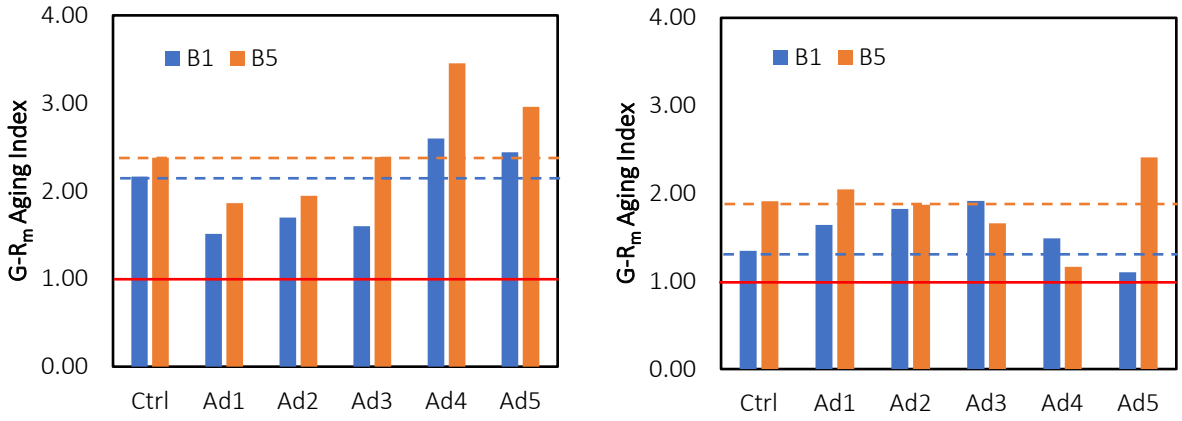

Figure 32. Glover-Rowe mix aging index for mixes at (a) LTOA and (b) NAWS.

4.3. Fatigue Cracking Damage Characterization.

Cyclic fatigue testing assessed the damage accumulation by determining each mixture's damage characteristic curves (C vs. S). Figure 33 and Figure 34 present the C vs. S curves for mixtures using Base Binders 1 and 5 under the three aging conditions. These curves offer insights into the deterioration of the mixtures. Shorter and higher-located curves indicate greater damage accumulation (Y. R. Kim et al., 2021). Consequently, the curves for LTOA and NAWS conditions are expected to be shorter and above those for STOA due to the stiffening effect of further aging. However, as depicted in Figure 33 and Figure 34, not all studied mixtures show LTOA and NAWS curves that are consistently shorter and above those of STOA.

In Figure 33, which pertains to Binder 1 mixtures, the C vs. S curves for Additives 1, 2, and 3 show minimal shifts from STOA to LTOA conditions. However, longer curves are observed for these mixes under STOA conditions. For the other mixtures (i.e., the control mixture and mixtures with Additives 4 and 5), there are larger shifts in the C vs. S curves from STOA to LTOA, suggesting these mixtures are more sensitive to LTOA. In addition, the NAWS curves for the control mixture and mixtures with Additives 1, 2, and 4 fall above the STOA curves, suggesting these mixtures are more sensitive to NAWS aging. Conversely, the NAWS curves for Additives 3 and 5 are overlaying but shorter than the STOA curves.

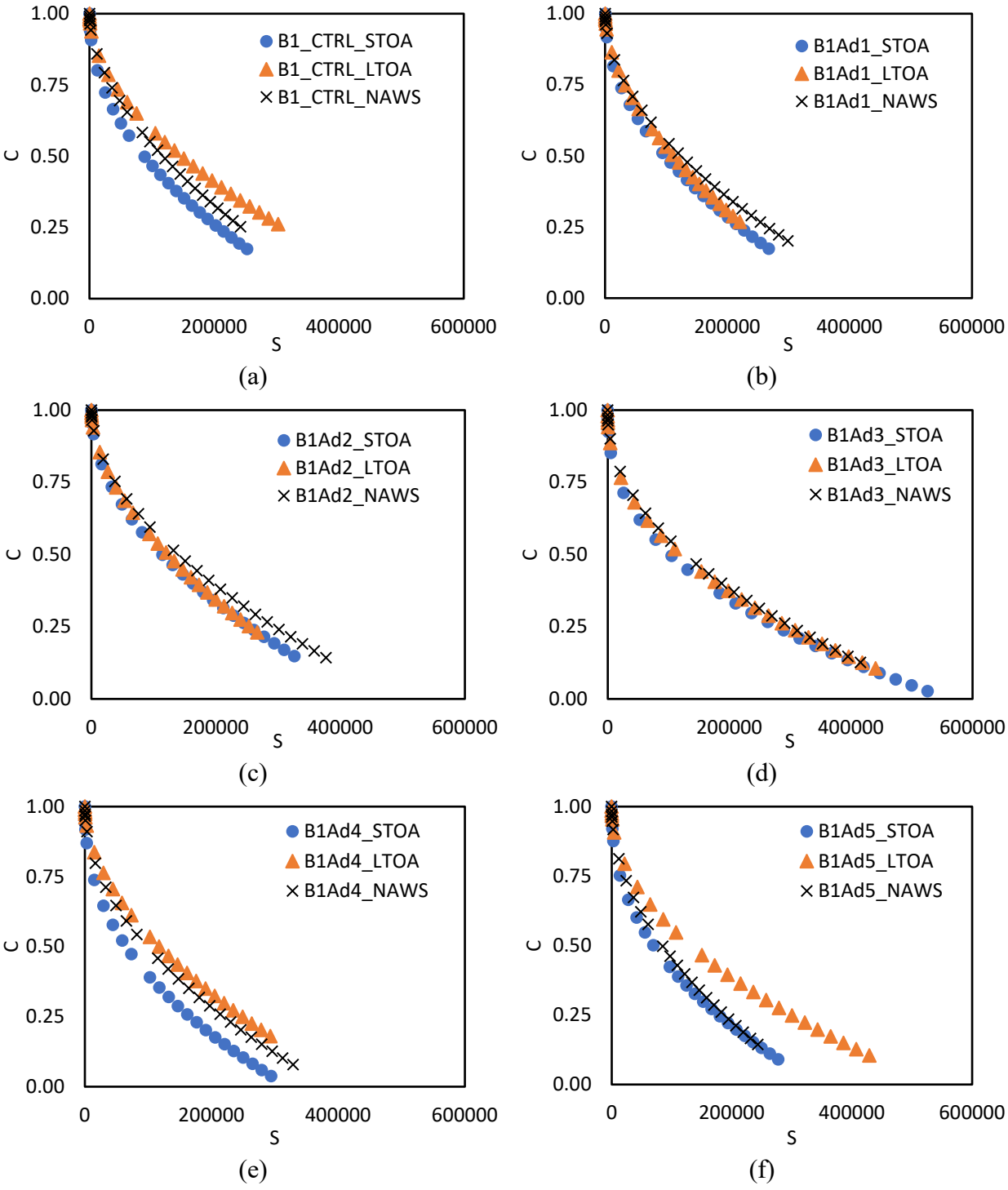

Figure 33. Damage characteristic curves (C vs. S) for (a) control, (b) additive 1, (c) additive 2, (d) additive 3, (e) additive 4, and (f) additive 5 B1-based mixes at STOA, LTOA, and NAWS conditions.

In Figure 34, which illustrates the damage characteristic curves for Binder 5 mixtures, all LTOA curves fall above the STOA curves, except for the LTOA curve of Additive 1. The Additive 1 damage characteristic curve is similar but shorter to the corresponding STOA curve. This similarity indicates comparable damage accumulation characteristics but less cracking resistance due to the length of the curve. Notably, the LTOA curves for the control and mixtures with Additives 3, 4, and 5 are longer than the corresponding STOA curves. These trends are also evident for the NAWS curves, where the NAWS curves for the control and mixtures with Additives 1, 2, and 5 fall above their STOA counterparts. In contrast, the C vs. S curves for Additives 3 and 4 were located close to the STOA curves, suggesting a similar behavior to the STOA mixtures until failure.

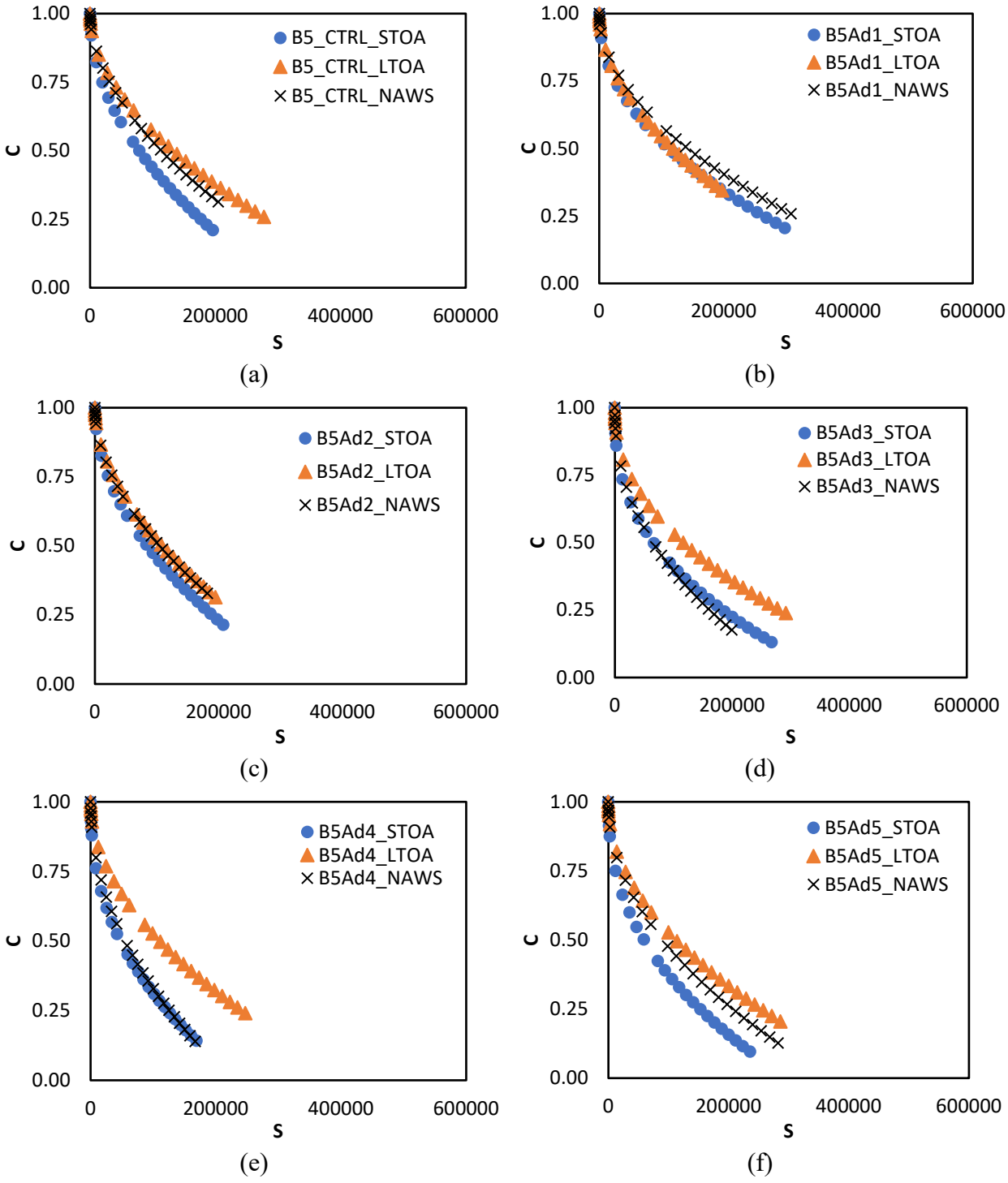

Figure 34. Damage characteristic curves (C vs. S) for (a) control, (b) additive 1, (c) additive 2, (d) additive 3, (e) additive 4, and (f) additive 5 B5-based mixes at STOA, LTOA, and NAWS conditions.

In addition to the damage characteristic curves discussed above, the D^R failure values were determined for each mixture, as shown in Figure 35 and Figure 36. Higher D^R values indicate better cracking resistance. Hardening due to aging typically leads to reduced D^R values.

Figure 35 shows D^R failure values for mixtures with Base Binder 1. Mixtures with Additives 1 and 2 yield D^R values similar to the control mix, indicating no improvement in cracking resistance under the three aging protocols. However, mixtures with Additives 3, 4, and 5 show improved cracking resistance, as evidenced by higher D^R values than the control mix under the three aging conditions.

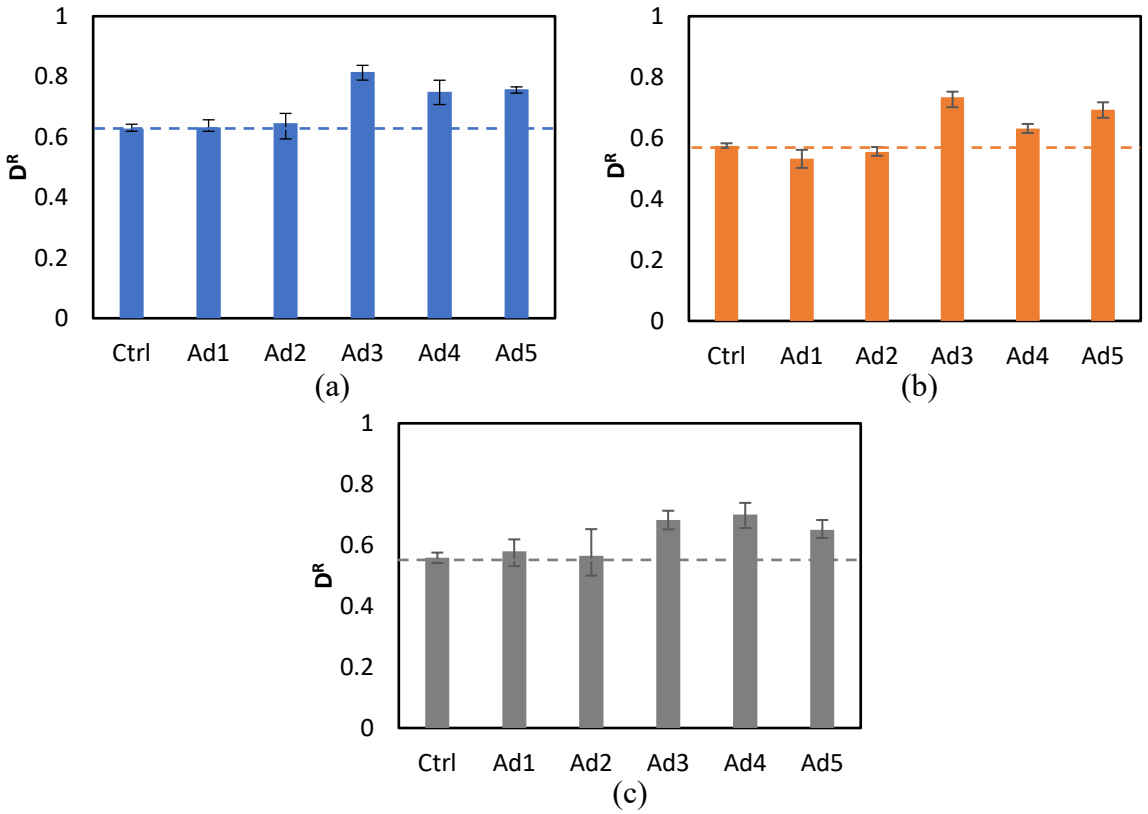

Figure 35. D^R failure criterion for Binder 1 mixtures at (a) STOA, (b) LTOA, and (c) NAWS.

Figure 36 presents the D^R results for mixtures prepared with Base Binder 5, showing similar trends to those for Base Binder 1 mixtures. Under STOA conditions, mixtures with Additives 1 and 2 yield D^R values comparable to the control mix, suggesting no improvement in cracking

resistance. Mixtures with Additives 3, 4, and 5 show higher D^R values, indicative of improved cracking resistance.

Aging had a greater impact on the D^R values of Base Binder 5 mixtures. After LTOA and NAWS, mixtures with Additives 3, 4, and 5 exhibit D^R values closer to those of the control mix. Conversely, mixtures with Additives 1 and 2 yield lower D^R values than the control mixtures, indicating higher susceptibility to aging than the control mix.

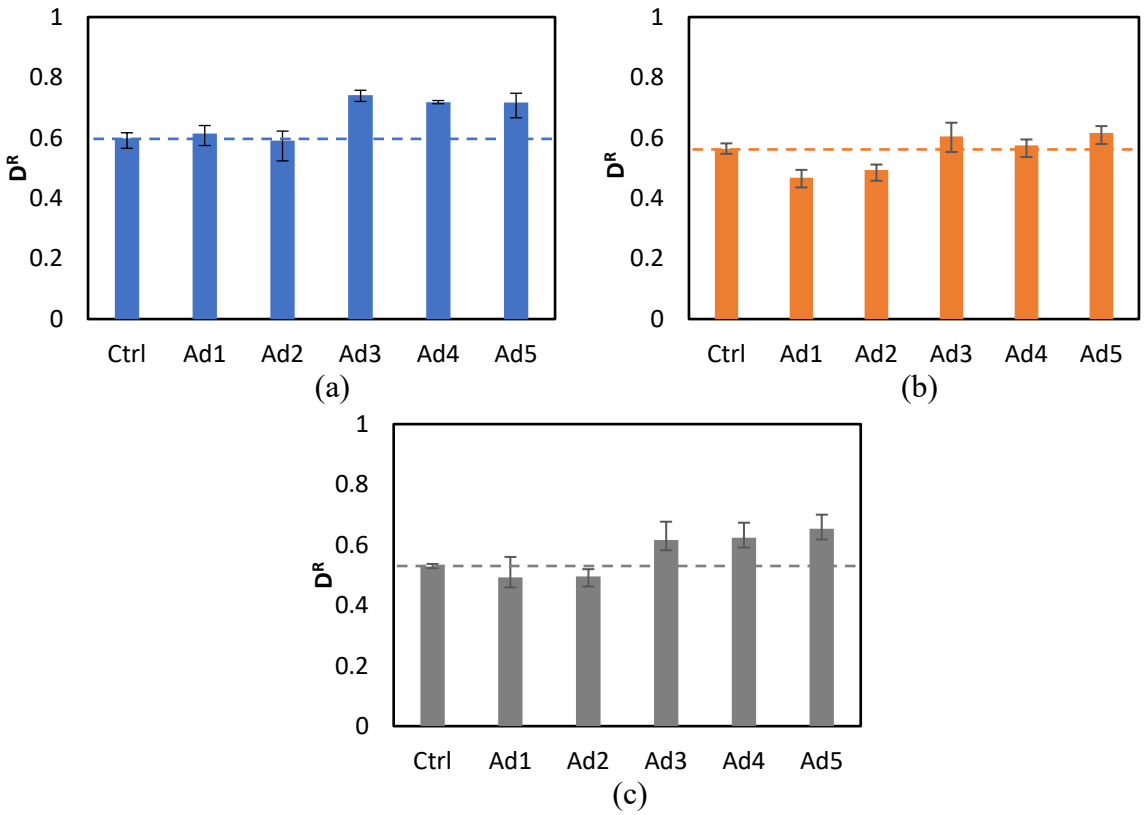

Figure 36. D^R failure criterion for Binder 5 mixtures at (a) STOA, (b) LTOA, and (c) NAWS.

Although the D^R parameter provides a good indication of the cracking resistance of asphalt mixtures, it cannot be used alone itself to compare mixture cracking performance. An analysis considering stiffness and fatigue resistance or a structural analysis considering pavement structure,

traffic level, climate, and other material properties should be done for a reliable comparison (Wuang, 2019).

A D^R aging index was calculated to determine the mixtures' aging susceptibility by quantifying the change of D^R after aging. This index refers to the ratio between the aged D^R and the unaged D^R. The D^R parameter is expected to decrease with aging. However, lower decreases or higher aging index values are desired and would indicate higher aging resistance. Figure 37 shows the D^R aging index results for all the studied mixtures. It is observed in Figure 37a that both control mixtures yielded the highest aging resistance, and only Additive 5 with base Binder 1 mixture yielded a similar result to the control mixture. For the NAWS condition, Additives 1 and 4 with base Binder 1 yielded higher aging resistance than the control. Only Additive 5 with base Binder 5 yielded higher NAWS aging resistance than the control mixture.

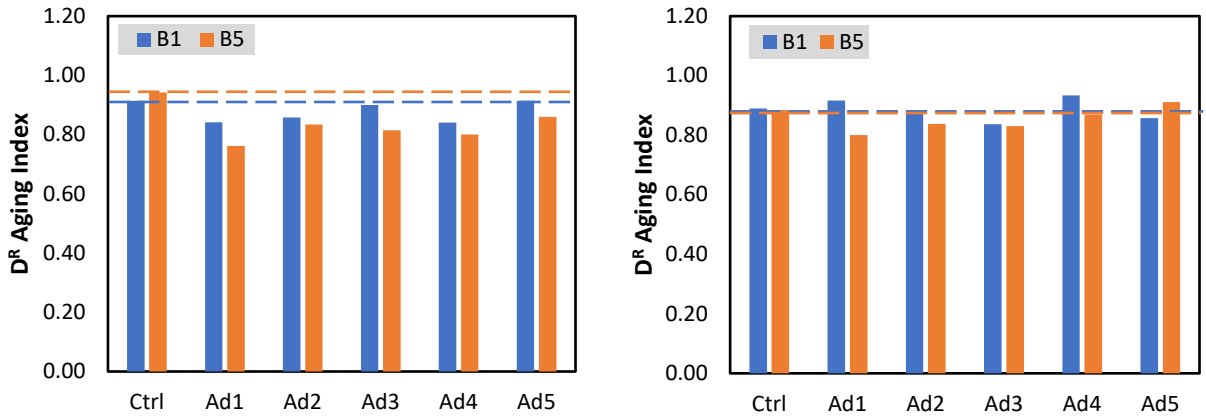

Figure 37. D^R aging index for (a) Binder 1 and (b) Binder 5 mixtures.

4.4. S_{app} Parameter

The S_{app} parameter was calculated based on dynamic modulus and cyclic fatigue test results to evaluate the cracking resistance of the mixtures at three aging levels. Unlike D^R, the S_{app} parameter takes into account both the stiffness and fatigue resistance of the mixture (Y. D. Wang

et al., 2020). A higher S_{app} parameter indicates better cracking resistance. As the S_{app} parameter is calculated from the representative damage characteristic curve and representative $|E^*|$ master curve and is not an average value of the individual experimental master curves, comparing each mixture's S_{app} involves observing differences in the charts, and no statistical testing could be performed to determine these differences.

Figure 38 illustrates the S_{app} results under both base binders' STOA, LTOA, and NAWS aging conditions. The LTOA and NAWS aged mixtures exhibit lower S_{app} values than the corresponding STOA mixtures, indicating decreased cracking resistance with aging.

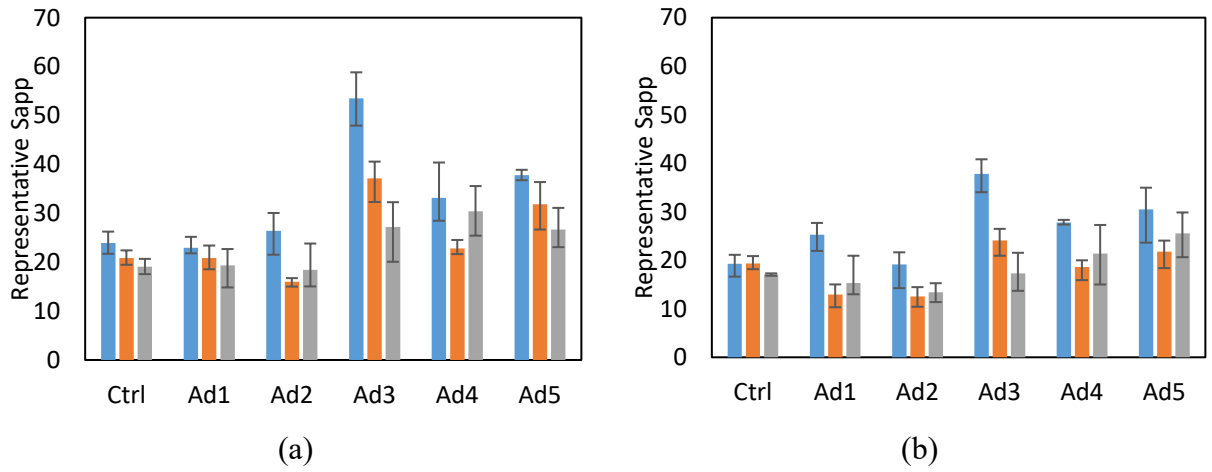

Figure 38. S_{app} Parameter for (a) binder 1 and (b) binder 5 mixes at different aging conditions.

In Figure 39, the S_{app} parameters for mixtures with Base Binder 1 shown in Figure 38a are presented in three separate graphs, each for an aging condition. Figure 39a shows the S_{app} parameters of the STOA mixtures. The mixtures with Additives 1 and 2 show similar S_{app} parameters to the control mixture, while the mixtures with Additives 3, 4, and 5 exhibit higher S_{app} parameters, suggesting better resistance to cracking. These trends are also observed in Figure 39c for the mixtures under NAWS aging conditions. However, different trends are shown in Figure

39b for the LTOA mixtures. Compared to the control mixture, the mixture with Additive 2 shows a lower S_{app} parameter, while the mixtures with Additives 1 and 4 have similar S_{app} values. Moreover, the mixtures with Additives 3 and 5 have higher S_{app} values.

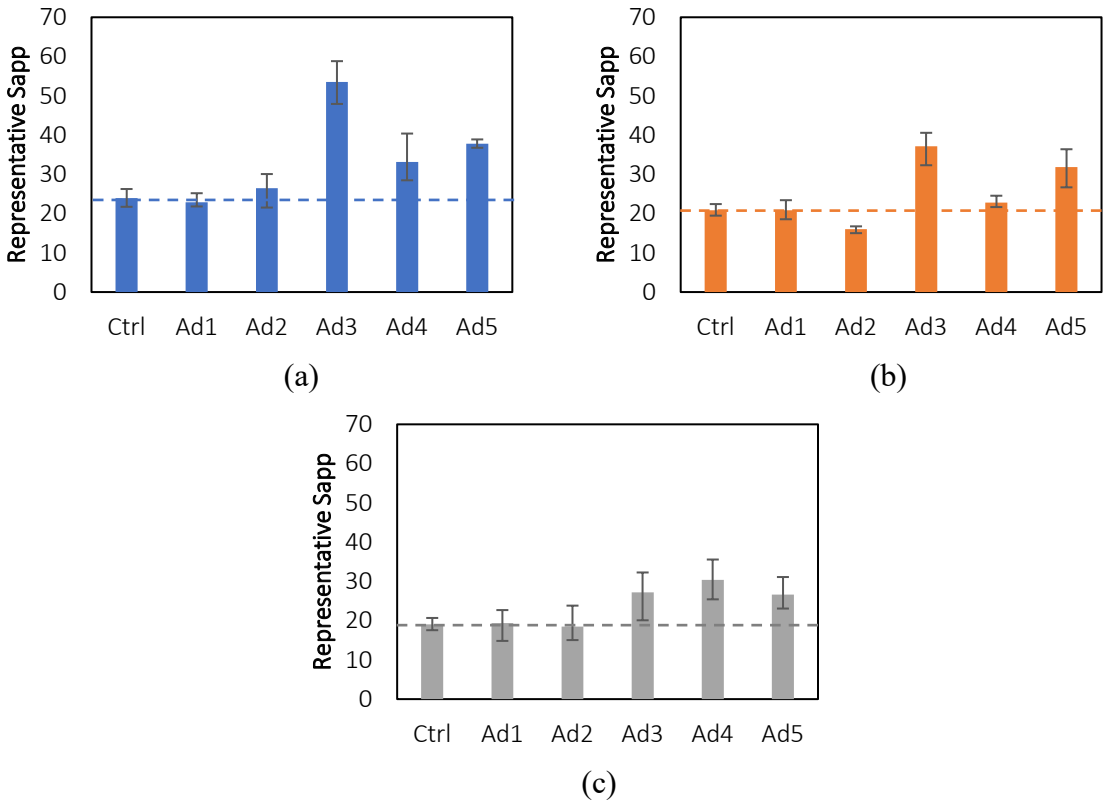

Figure 39. S_{app} Parameter at (a) STOA, (b) LTOA, and (c) NAWS aged conditions for B1-based mixes.

As for mixtures with Base Binder 1, the S_{app} parameters for mixtures with Base Binder 5 shown in Figure 38b are presented in three graphs in Figure 40, each for an aging condition. The mixtures with Additives 1 and 2 show similar and slightly higher S_{app} parameters than the control mixture under STOA conditions. However, they exhibit lower S_{app} values under LTOA and NAWS aging

conditions. In contrast, the mixtures with Additives 3, 4, and 5 exhibit similar or higher S_{app} values than the control mixtures under all three aging conditions.

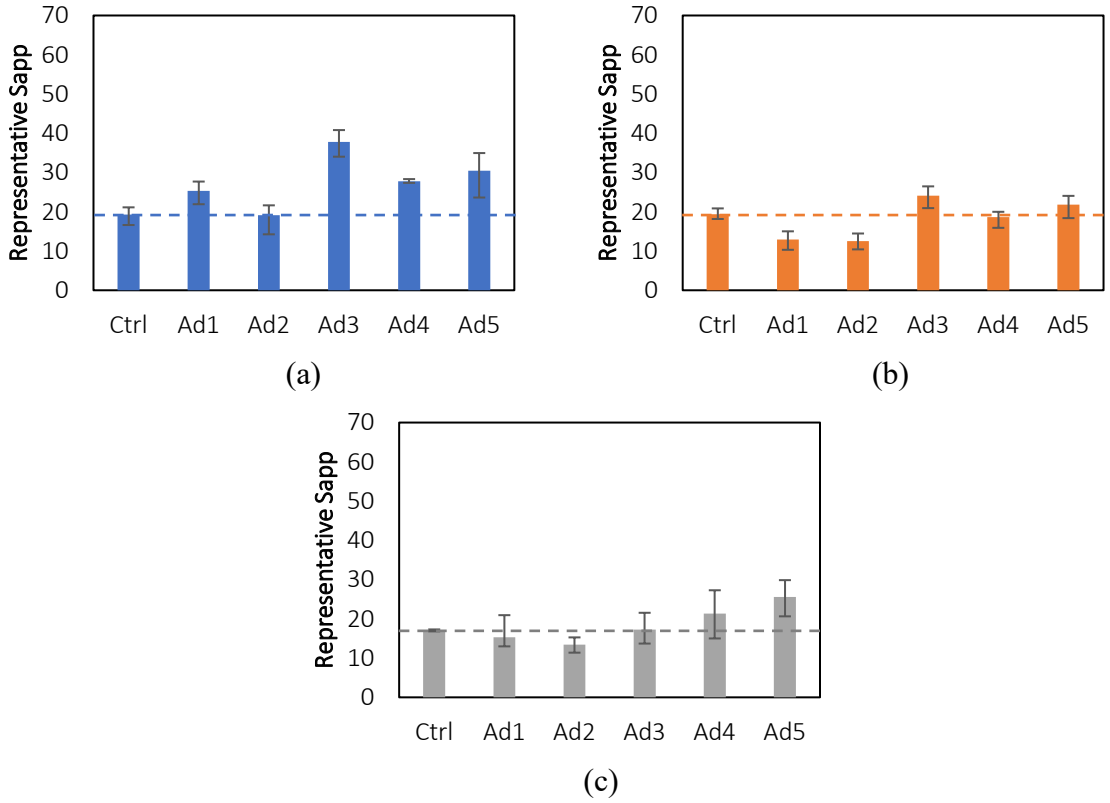

Figure 40. S_{app} Parameter at (a) STOA, (b) LTOA, and (c) NAWS aged conditions for B5-based mixes.

The S_{app} effectiveness index was determined to facilitate a comparison of the effect of the aging-resistant additive technologies on the S_{app} parameter compared to the control mixture. An effectiveness index of 1 indicates no impact on the S_{app} parameter when using an additive. In contrast, an index greater than 1 indicates an improvement in the S_{app} parameter, suggesting enhanced cracking resistance, while an index less than 1 suggests an unfavorable effect. Figure 41 displays the effectiveness index for both base binders under the three different aging conditions. Additives 3, 4, and 5 favorably impact the S_{app} parameter in all aging conditions. In contrast,

Additives 1 and 2 have minimal effects under the STOA and NAWS conditions and unfavorable impacts under the LTOA conditions.

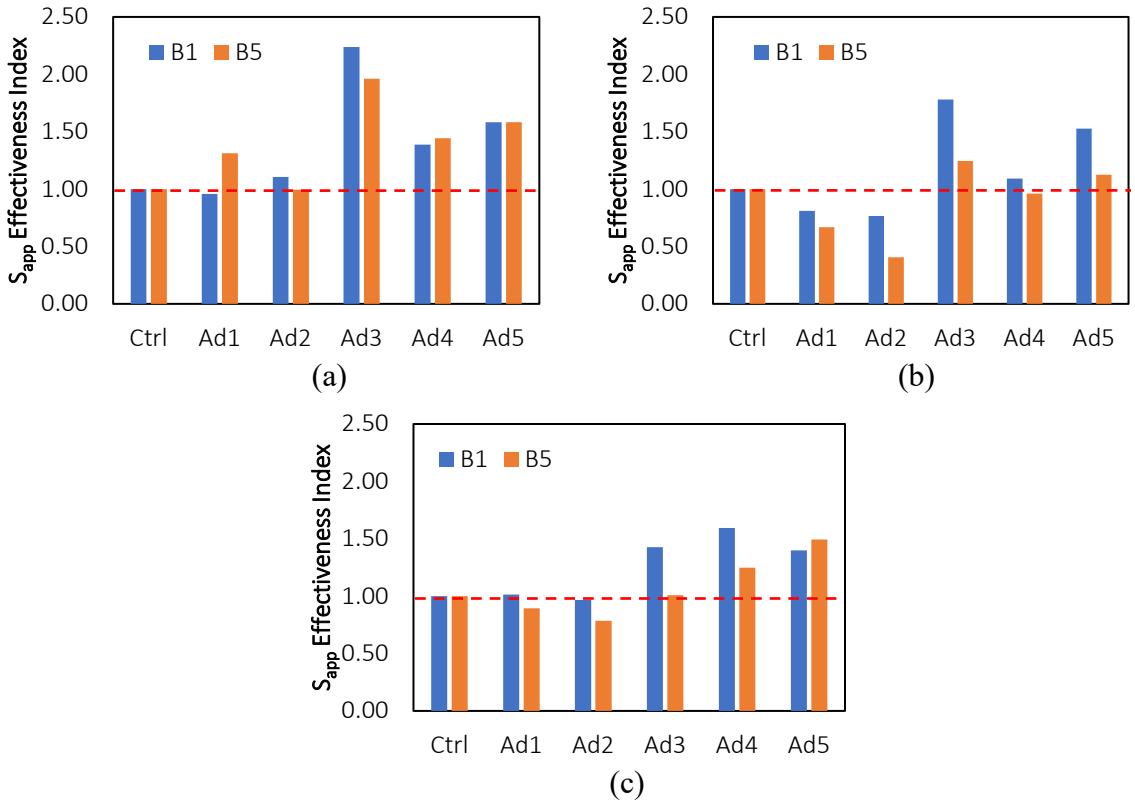

Figure 41. S_{app} effectiveness index for B1 and B5 mixes at (a) STOA, (b) LTOA, and (c) NAWS aging conditions.

In addition, the S_{app} aging index was calculated to evaluate the sensitivity of asphalt mixtures to LTOA and NAWS aging conditions in relation to STOA. Since the S_{app} parameter of an asphalt mixture decreases with aging, an aging index of 1 suggests a mixture's S_{app} parameter is less affected by LTOA or NAWS aging compared to STOA, which can be a desirable characteristic for an additive. Figure 42 presents the S_{app} aging indexes for the mixtures evaluated in this study, comparing the effects of LTOA and NAWS aging with those of STOA.

Under LTOA conditions shown in Figure 42a, all mixtures with additives show lower S_{app} aging indexes, meaning greater decreases in S_{app} parameters from STOA to LTOA than the control

mix. Among mixtures with Base Binder 1, the control mix has the highest S_{app} aging index, closely followed by the mixture with Additive 5, and the mixture with Additive 2 has the lowest S_{app} aging index. For mixtures with Base Binder 5, the control mixture shows no change after LTOA compared to STOA, followed by the mixture with Aadditive 5. The mixture with Additive 1 has the lowest S_{app} aging index.

Figure 42b presents the S_{app} aging indexes for mixtures aged in the NAWS. For mixtures with Base Binder 1, only mixtures with Additives 1 and 4 show higher S_{app} aging indexes than the control mixture. Among mixtures with Base Binder 5, the control mixture has the highest S_{app} aging index.

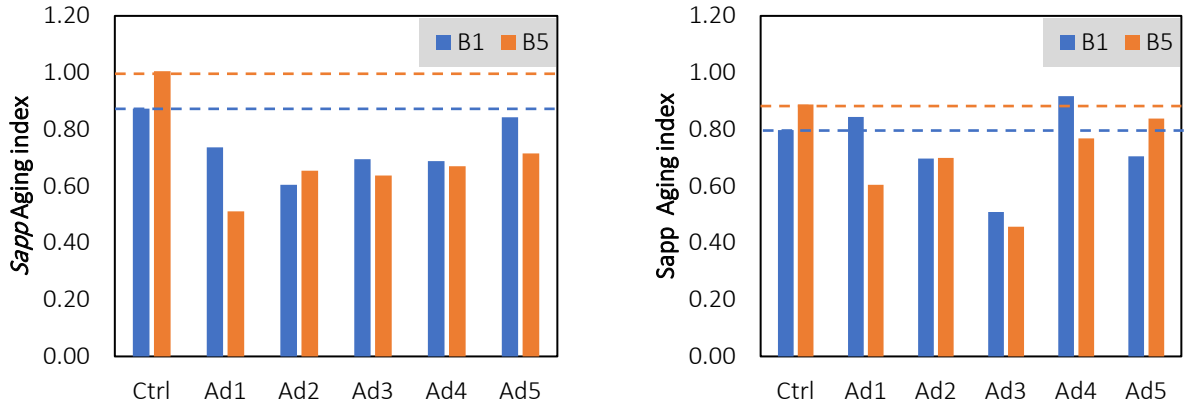

Figure 42. S_{app} aging index for (a) LTOA and (b) NAWS aged mixtures.

In summary, the S_{app} parameter was determined to evaluate the cracking resistance of mixtures across three aging levels. Higher S_{app} values indicate better resistance. Mixtures with Additives 3, 4, and 5 show higher S_{app} values and S_{app} effectiveness indexes than the control mixtures across all three aging levels. However, based on the S_{app} aging index, mixtures with additives tend to show a greater reduction in the S_{app} parameter from STOA to LTOA/NAWS than the control mixtures.

4.5. FlexPAVE™ Damage Prediction

Dynamic modulus and cyclic fatigue testing results served as input for the FlexPave software, which assessed the cracking resistance of the mixtures examined in this study. Beyond considering mixture properties, FlexPave simulations can incorporate pavement structure, weather, and traffic conditions. Three methods were performed under identical pavement structure, climate, and traffic conditions.

4.5.1 Method A. FlexPAVE 1.0 (STOA-No aging)

FlexPave software version 1.0 was used to evaluate fatigue damage in the surface layer of the pavement after 20 years of service life. The predicted percent damage at the end of the analysis period is presented in Table 4. It is observed that the modified mixtures, except B5 with Addiitve 5, exhibit lower predicted percent damage, indicating enhanced resistance to cracking.

Table 4. Predicted Percent Damage after 20 years from FlexPAVE 1.0 simulation.

Mix ID	Base Binder 1	Base Binder 5
Ctrl	9.77	11.36
Ad1	9.11	8.96
Ad2	7.61	10.57
Ad3	5.11	8.25
Ad4	9.62	12.56
Ad5	8.68	10.29

Figure 43 presents the evolution of damage for mixtures containing Base Binder 1. The 5% fatigue damage threshold was used to assess the life extension benefits of using each additive. This 5% threshold was selected due to its proximity to the fatigue damage observed for the mixture with Additive 3 after 20 years of service. Results of life extension benefit at this damage level for Binder 1 mixtures are presented in Table 5. Although the control mixture exhibits the greatest percent fatigue damage after the 20-year analysis period, the Additive 4 mixture reaches 5%

fatigue damage sooner than the control mixture during its early service life. Nonetheless, its rate of fatigue damage accumulation is slower, ending in lower percent fatigue damage after 20 years of service. This earlier attainment of the 5% fatigue damage results in the negative life extension shown in Table 5 for the Additive 4 mixture.

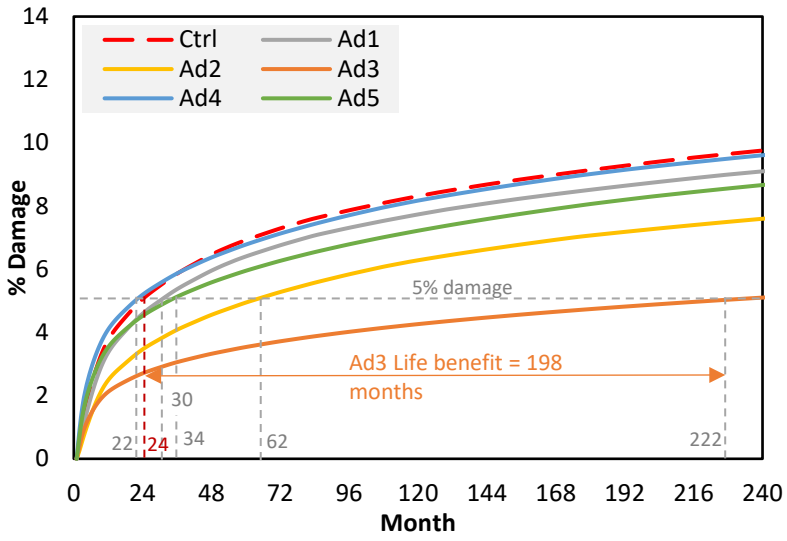

Figure 43. Damage evolution for Base Binder 1 asphalt mixtures obtained from FlexPAVE 1.1 simulation.

Table 5. Life extension calculated at 5% damage for Base Binder 1 asphalt mixtures.

Mix ID	Months to reach 5% damage	Life extension compared to Control, months
Ctrl	24	0
Ad1	30	6
Ad2	62	38
Ad3	222	198
Ad4	22	-2
Ad5	34	10

Figure 44 shows the damage evolution for mixtures with Base Binder 5. An 8% fatigue damage was selected in this case to assess the life extension benefits of using each additive compared to the control mixture. This 8% threshold was selected due to its proximity to the fatigue damage observed for the mixture with Additive 3 after 20 years of service. The life extension benefit results at this damage level are summarized in Table 6. Mixtures with additives exhibit lower percent fatigue damage than the control mix, except for the mixture with Additive 4. The softening effect of Additive 4 in Binder 5 is translated into reduced cracking performance by the FlexPAVE model. In contrast, according to the software model, Additive 3, a high polymer content additive, is expected to have considerably lower damage percentages.

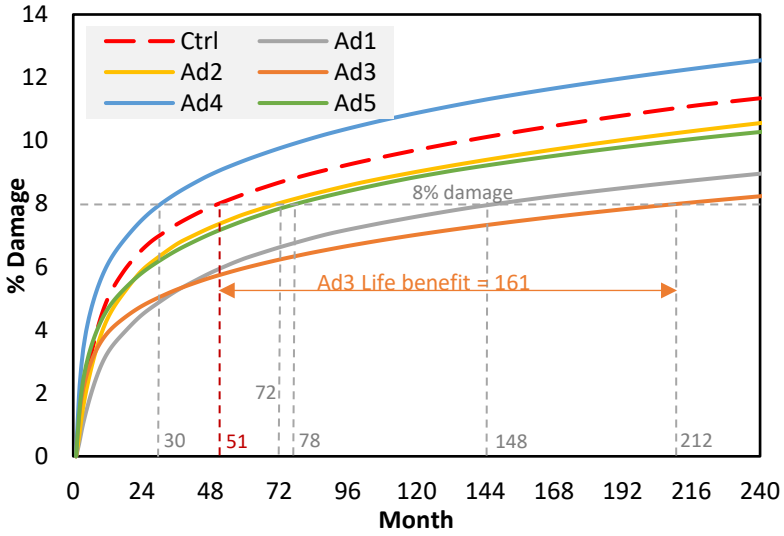

Figure 44. Damage evolution for Base Binder 5, asphalt mixtures using FlexPAVE 1.1.

Table 6. Life extension calculated at 8% damage for Base Binder 5 asphalt mixtures.

Mix ID	Months to reach 8% damage	Life extension compared to Control, months
Ctrl	51	0
Ad1	148	97
Ad2	72	21
Ad3	212	161
Ad4	30	-21
Ad5	78	27

4.5.2 Method B. FlexPAVE 2.0 (STOA-Aging)

The FlexPAVE 1.1 described in Method A does not consider the aging effect during the simulated service life. Therefore, this simulation only affects the mixture's properties by loading, climate, and pavement structure. Aging is not considered in every simulation cycle on FlexPAVE 1.1. Therefore, the initial and damage accumulation properties at the STOA condition are the simulation's starting point, and the mix's aging resistance characteristics were not considered.

FlexPAVE 2.0 simulations were performed in Method B to include the detrimental aging effect in the simulation. In this method, the aging resistance of the mix also influences the damage evolution in the asphalt layer during the analysis period.

Figure 45 presents the results of the damage evolution of Binder 1-based asphalt mixtures considering the aging effect. Different trends compared to FlexPAVE 1.0 were obtained in this case. Additives 1, 2, and 3 yielded lower damages than the control mix at the end of the analysis period. In contrast, the obtained damage curves of mixes with additives 4 and 5 were located above the control mix, indicating a detrimental effect on cracking performance by including the additives.

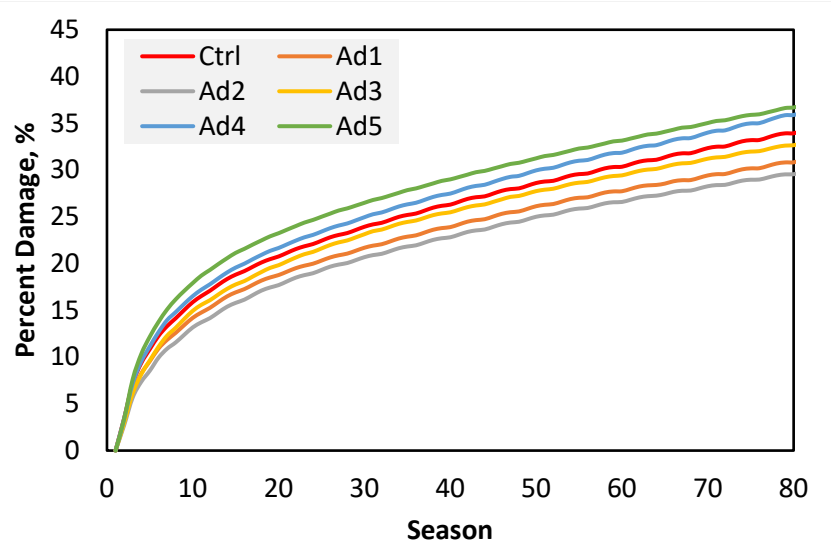

Figure 45. Total damage evolution with aging effect for binder 1 asphalt mixtures using FlexPAVE 2.0.

Figure 46 shows the damage evolution curves for binder 5 mixtures. As observed in this figure, the results indicate that none of the additives improved the mix resistance to cracking, which is inconsistent with all previous results. Mixtures with additive 4, consistently with FlexPAVE 1.0, yielded the highest damage percentage during the analysis period, while Additive 2 yielded the lowest damage.

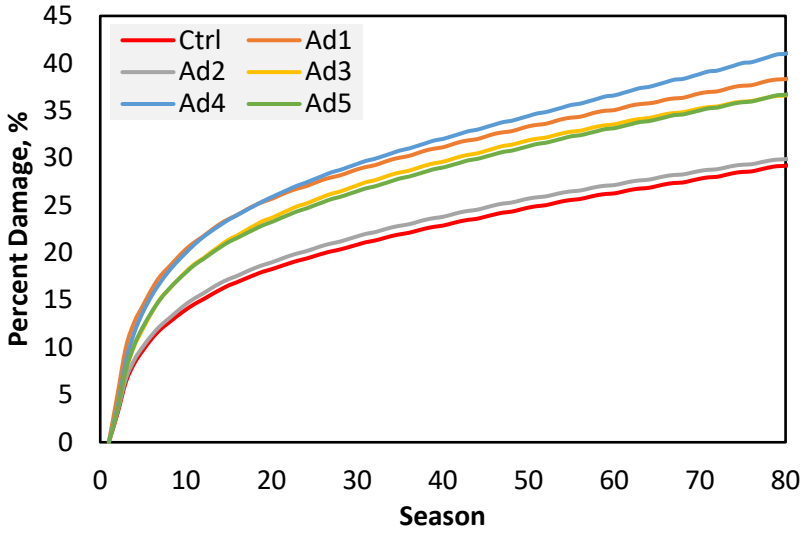

Figure 46. Total damage evolution with aging effect for binder 5 asphalt mixtures using FlexPAVE 2.0.

Although a simulation considering the aging effect is the most realistic approach to simulate the damage evolution and determine each additive's effectiveness, this software version is still in development, and results should not be considered definitive. Therefore, for this study's objective, results from Method A are considered more reliable.

4.5.3 Method C. FlexPAVE 1.1 (LTOA-No aging)

A third method was also performed, intending to consider aging into account using FlexPAVE 1.1. The LTOA $|E^*|$ and cyclic fatigue characteristics were input for the analysis in this method. Results of this simulation are presented in Figure 47 for Binder 1 and Figure 48 for Binder 5 mixtures.

The obtained trends differ from Method A and Method B. Binder 1 mixtures with additives 3 and 5 yielded lower percent damage at the end of the analysis period than the control mix, as observed in Figure 47. Additives 3 and 5, which contain high polymer content, are expected to result in better fatigue cracking performance in the simulation model. The softening effect, combined with the damage accumulation properties of Additives 1, 2, and 4, produced less resistance to cracking mixtures than the Binder 1 control mix, according to the model.

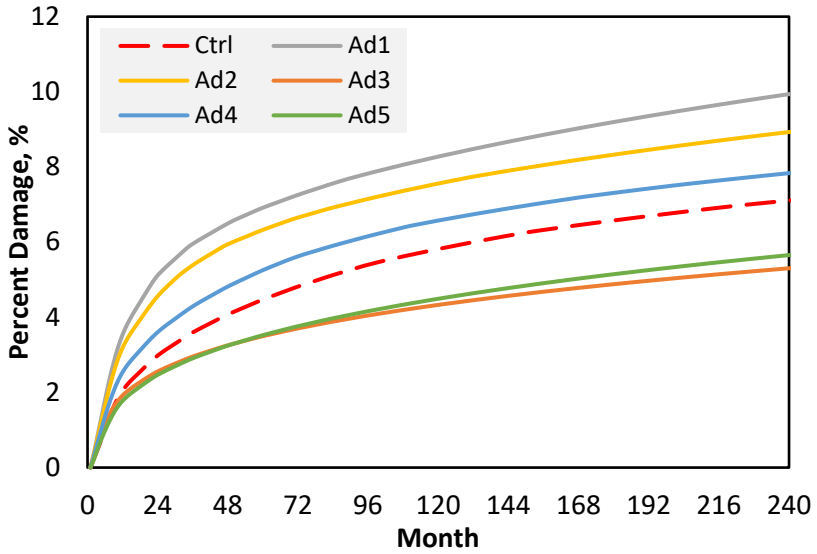

Figure 47. Damage evolution for LTOA binder 1 asphalt mixtures using FlexPAVE 1.0.

A similar effect was observed for mixtures with binder 5 in Figure 48. Only additive 3 yielded lower cracking damage than the control mix during the simulated service life. Additives 4 and 5 yielded higher but similar damages than the control mixture. In contrast, the FlexPAVE simulation predicted much higher damage percentages for mixtures with Additive 1 and 2.

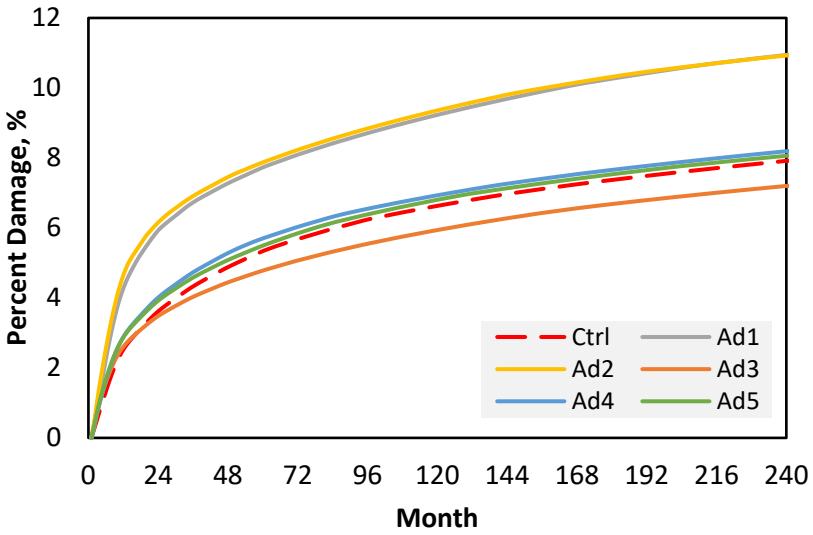

Figure 48. Damage evolution for LTOA binder 5 asphalt mixtures using FlexPAVE 1.0.

No consistency in results with previous simulations was found with this method. However, inputting parameters of the already-aged mix to consider aging with this software version represents a limitation and is inadequate for evaluating aging. Aged mixtures are stiffer, which relates to lower strains after stress from traffic loading. This hardening effect of aging results in lower damage percentages than STOA mixtures at the end of the analysis period in the FlexPAVE simulations. Aging occurs gradually, and the negative effects on the cracking resistance of the mixtures should be considered at each period of analysis. Although FlexPAVE 2.0 follows this methodology, the model must be fully developed. Due to this limitation, results from Method C are not considered as reliable as those from Method A.

4.6. Relative Ranking of Cracking-Related Parameters

Table 7 presents the relative ranking of each additive based on three parameters, including $G\text{-}R_m$ and $S_{app,}$ and percent fatigue damage determined by FlexPave. Compared to the control mixtures, an ideal additive would exhibit a lower $G\text{-}R_m$ effectiveness index, a higher S_{app} effectiveness index, and lower percent fatigue damage at the end of the FlexPave analysis period. Below are observations based on the results shown in Table 7.

- For mixtures with Additive 1, the ranking is either similar to or lower than that of the control mix based on the $G\text{-}R_m$ and S_{app} parameters under LTOA and NAWS aging conditions. However, FlexPave percent fatigue damage data indicate that mixtures with Additive 1 are more resistant to cracking than the control mixture.
- Mixtures incorporating Additive 2 are ranked lower than the control mix, according to the $G\text{-}R_m$ and S_{app} parameters under LTOA and NAWS aging conditions. However, FlexPave percent fatigue damage is lower for mixtures with Additive 2, suggesting a potential improvement in resistance to cracking.
- Mixtures modified with Additive 3 are ranked higher than the control mixture based on all three evaluation metrics. This superior performance is likely attributed to an effective synergy between a bio-based rejuvenator and a high polymer content in the additive formulation.
- Mixtures containing Additive 4 are ranked higher than the control mix based on all three evaluation metrics, except for the 20-year FlexPave simulation for this mixture with Base Binder 5. Since aging was not considered in the FlexPave simulation and better performance was noted in other indicators, it is suggested that Additive 4 improves the resistance of the asphalt mixtures to cracking.

- Mixtures with Additive 5 are ranked higher than the control mixture across all evaluation metrics, base binders, and aging protocols, suggesting better resistance to cracking than the control mixtures.

Table 7. Aging-cracking resistance relative ranking for asphalt mixtures after LTOA and NAWS.

LTOA					
Binder 1			**Binder 5**		
***G-R*$_m$**	***S*$_{app}$**	**FlexPAVE (Method A)**	***G-R*$_m$**	***S*$_{app}$**	**FlexPAVE (Method A)***
Ad3	Ad3	Ad3	Ad3	Ad3	Ad3
Ad5	Ad5	Ad2	Ad4	Ad5	Ad1
Ad4	Ad4	Ad5	Ad5	Ctrl	Ad5
Ad1	Ctrl	Ad1	Ctrl	Ad4	Ad2
Ctrl	Ad1	Ad4	Ad2	Ad1	Ctrl
Ad2	Ad2	Ctrl	Ad1	Ad2	Ad4
NAWS					
Binder 1			**Binder 5**		
***G-R*$_m$**	***S*$_{app}$**	**FlexPAVE (Method A)**	***G-R*$_m$**	***S*$_{app}$**	**FlexPAVE (Method A)**
Ad5	Ad4	Ad3	Ad4	Ad5	Ad3
Ad4	Ad3	Ad2	Ad3	Ad4	Ad1
Ctrl	Ad5	Ad5	Ad5	Ad3	Ad5
Ad3	Ad1	Ad1	Ctrl	Ctrl	Ad2
Ad1	Ctrl	Ad4	Ad2	Ad1	Ctrl
Ad2	Ad2	Ctrl	Ad1	Ad2	Ad4

CHAPTER 5 - PREDICTION MODELS

This chapter presents the findings from predicting fatigue performance parameters using the Asphalt Mixture Aging-Cracking (AMAC) model. The AMAC model, introduced in the NCHRP 09-54 report by Kim et al. (2021), was applied to forecast S_{app} values for longer aging durations than those tested in the laboratory. Additionally, the model was used to determine the equivalent days of aging in the oven at 95°C for the NAWS mixtures. The following sections detail these predictions, offering anticipated fatigue performance information for the mixtures under extended aging conditions.

5.1. AMAC Model Methodology

The AMAC model relies on input parameters derived from the mixture's short-term properties. Moreover, the model required determining the binder's log |G*|, both at short-term conditions and the aging level of interest, typically at 64°C and 10 rad/s. The log |G*| values were directly measured in the laboratory from the virgin binder after RTFO, PAV, and 2PAV aging conditions. The change in the log |G*| values was used to determine the equivalent log |G*| values of the mixtures aged at different days in an oven at 95°C, using the Pavement Aging Model (PAM), described in Equation 15 (Saleh et al.).

$$\log |G^*|_{kinetics} = \log |G^*|_0 + M\left[\left(1 - \frac{k_c}{k_f}\right)\left(1 - e^{-k_f t}\right) + k_c t\right] \quad \text{Equation 15}$$

Where,

$\log |G^*|_{kinetics}$: dynamic shear modulus at the target aging level

$\log |G^*|_0$: dynamic shear modulus at 64°C, 10 rad/sec at STOA;

k_c: rate of constant reaction;

k_f: rate of fast reaction; and,

M: fitting parameter related to fast reaction reactive material, representing aging susceptibility.

t: aging duration in the oven at 95°C in days.

The PAM model, developed by Kim et al. (2021) as part of the NCHRP 09-54 project Phase III, allows determining the log |G*| at different aging levels based on the STOA $log|G^*|$ and its aging susceptibility as observed in Figure 49. This determination of the |G*| enables the translation of the changes in |G*| to changes in the mixture's linear viscoelastic and fatigue properties (Y. R. Kim et al., 2021). For this study, the log |G*| was predicted for a 5-day-aging period in a 95°C oven. This $log|G^*|$ allowed to predict the mixture characteristics needed to calculate S_{app} at this aging level. The predicted and experimental data were then compared to evaluate the model.

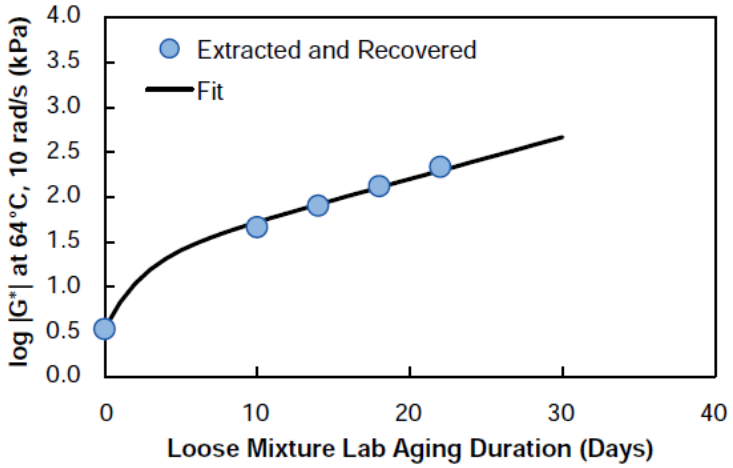

Figure 49. Example of $log|G^*|$ values obtained from testing at multiple aging durations and the PAM fitting curve (Y. R. Kim et al., 2021).

The model captures each aging susceptibility through the M parameter, where higher M values are related to higher aging susceptibility—the fitting parameter M was determined for each mixture following Equation 17. As observed in Equation 17, the model considers the effect of including RAP into the mixtures and calculates the M parameter as the combination of both virgin

and RAP binder. The M_{virgin} parameter is determined by optimizing the PAM model from Equation 15. This optimization finds the M_{virgin} value that minimizes the error between the model predictions and the experimental $log|G^*|$. Then, a mixture M_{blend} parameter is calculated considering the effect of the RAP binder included in the mixture, as observed in Equation 16 and Equation 17 (Y. R. Kim et al., 2021).

$$log|G^*|_{0,Blend} = (1 - ABR)\log|G^*|_{0,Virgin} + ABR \times log|G^*|_{0,RAP} \quad \text{Equation 16}$$

$$M_{Blend} = (1 - X_{RAP})M_{Virgin} + X_{RAP}M_{RAP} \quad \text{Equation 17}$$

Where,

$log|G^*|_{0,\text{Blend}}$: STOA dynamic shear modulus of the binder blend,

$log|G^*|_{0,\text{Blend}}$: STOA dynamic shear modulus of the virgin binder,

$log|G^*|_{0,\text{Blend}}$: STOA dynamic shear modulus of the RAP binder,

ABR: asphalt binder replacement and

X_{RAP}: mass fraction of RAP.

The PAM model considers a time-aging shift factor (*tAS)* to estimate the shifted $|E^*|$ curve of aged mixtures based on the $|E^*|$ curves obtained at the STOA. The *tAS* increases the STOA stiffness, predicting a stiffer material after aging. The calculation of the *tAS* considers the change in $log|G^*|$ between the target aging level and unaged level and a fitting parameter as observed in Equation 18 (Y. R. Kim et al., 2021). The fitting parameter *c* was defined as 1.71 for all mixtures, as indicated by Kim et al. (2011), for Level 2 calculations. Calibration of the *c* parameter could increase the model's effectiveness in predicting the aged $|E^*|$ curves.

$$\log(a_A) = c \times \left(\log|G^*| - \log|G^*|_{ref}\right) \quad \text{Equation 18}$$

where,

a_A: tAS factor at a given age level;

|G*|: dynamic shear modulus at a specific aging level;

$|G^*|_{ref}$: dynamic shear modulus measured at the reference age level and

c: fitting parameter (1.71)

The final predicted |*E**| master curve was obtained by shifting the STOA |*E**| master curve using the time-temperature shift factor (*tTS*) and the *tAS*. For this section, the |*E**| calculations were performed using the 2sP1d model, described in Equation 19, where all the fitting parameters were obtained from FlexMAT. The reduced frequencies for the aged |*E**| master curve were calculated following Equation 20, which includes both the time-temperature and time-aging effects.

$$|E*| = \frac{E_\infty - E_0}{1 + \delta(i\omega f_r)^{-k} + (i\omega f_r)^{-h} + (i\omega f_r)^{-1}} \quad \text{Equation 19}$$

$$f_r = f \times a_T \times a_A \quad \text{Equation 20}$$

where,

fr: time-temperature and aging reduced frequency;

f: testing frequency;

aT: Time-temperature shift factor (tTS); and

a_A: Time-aging shift factor (tAS) at a given age level.

An aging shift factor is also used to predict the asphalt mixes' fatigue damage properties. This procedure involved calculating predicted damage characteristic curves (C vs. S) and the failure criterion D^R for each mix at the LTOA condition. Regarding the *C vs. S* curves, aging

typically leads to shorter and higher curves due to the stiffening effect of aging in the mixture (Y. R. Kim et al., 2017). The AMAC model adjusts the STOA C_{11} parameter, as described in Equation 22, shifting up the STOA damage characteristic curve but keeping the same length as the STOA. This adjustment enables the prediction of the characteristics of the aged mixtures.

$$C = 1 - C_{11}S^{C_{12}} \quad \text{Equation 21}$$

$$C = 1 - \left(\frac{C_{11}}{{a_A}^{C_{12}}}\right)S^{C_{12}} \quad \text{Equation 22}$$

Finally, The D^R failure criterion was the third predicted parameter to characterize the mixtures' performance to fatigue cracking based on damage accumulation. The prediction of the D^R based on the STOA, affected by the changes in $log|G^*|$ due to aging, was calculated using Equation 23, Equation 24, and Equation 25.

$${D^R}_{LTA} = {D^R}_{STA} - ({D^R}_{STA} - 0.1)e^{\frac{1.44(\log\ |G^*|_{LTA,Tref,10rad/s} - 4.5)}{(max\Delta \log|G^*|)(\Delta \log|G^*|)}} \quad \text{Equation 23}$$

Where,

$$max\Delta \log|G^*| = 4.5 - \log\ |G^*|_{STA,Tref,10rad/s} \quad \text{Equation 24}$$

$$\Delta \log|G^*| = \log\ |G^*|_{LTA,Tref,10rad/s} - \log\ |G^*|_{STA,Tref,10rad/s} \quad \text{Equation 25}$$

The predicted S_{app} value was calculated by using the predicted parameters in the S_{app} calculation equation. A summary of the S_{app} prediction procedure is presented in

Figure 50.

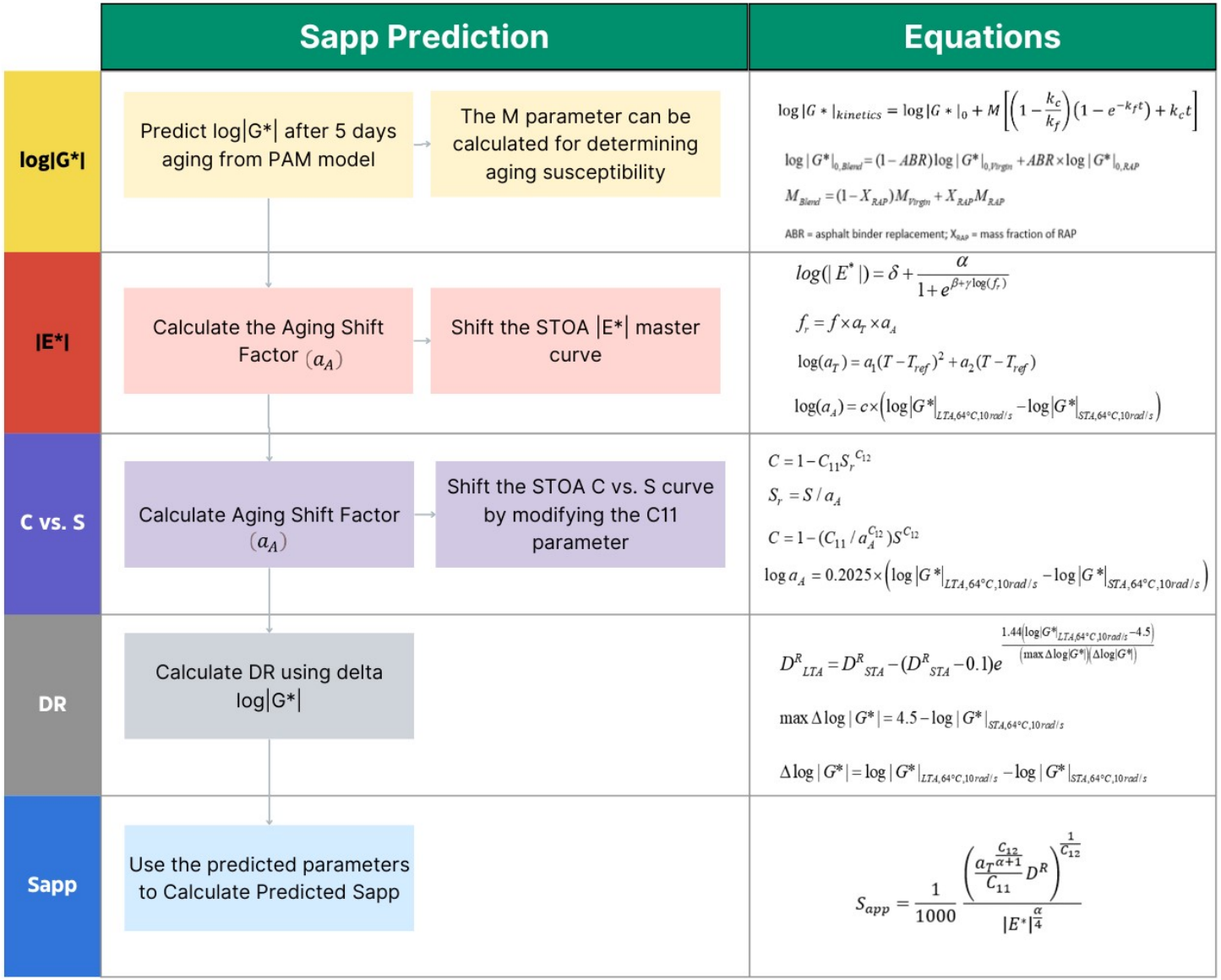

Figure 50. S_{app} prediction procedure diagram.

5.1.1 NAWS Equivalent Oven Aging Duration Methodology

The changes in the mix properties following NAWS were utilized with the AMAC model to assess the effect of this conditioning method in the binder's $log|G^*|$ and determine the equivalent aging duration in an oven at 95°C. To find this duration, a $log|G^*|$ value that resulted in the same S_{app} value after NAWS was calculated. After the $log|G^*|$ was determined, the PAM model was used to calculate the aging equivalent number of days in the oven for loose mixture at 95°C for each mixture, as illustrated in Figure 51.

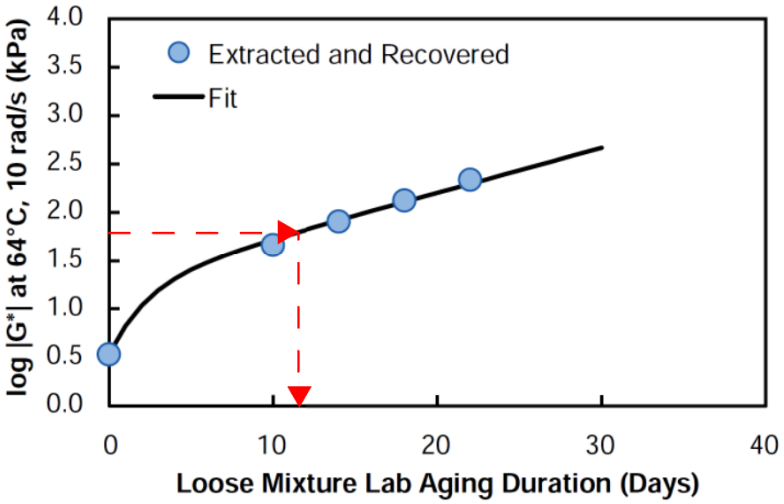

Figure 51. Equivalent aging duration determination diagram.

5.2. *Log|G*|* at LTOA Estimation

Table 8 summarizes the measured $log|G^*|$ values at STOA and the predicted $log|G^*|$ values for the 5-day aging period obtained from the PAM model. Results of $\Delta log|G^*|$ indicate how much the model predicted an increase in the binder stiffness based on the DSR experimental data at RTFO, PAV, and 2PAV. Similar $\Delta log|G^*|$ values were obtained among the additives, where the

control mixture yielded the highest increase for Binder 1, and Additive 4 was the only observation higher than the control Binder 5.

Table 8. PAM Kinetics model $log|G^*|$ prediction at different aging times.

Aging*	log |G*| (kPa)											
	Binder 1						Binder 5					
	Ctrl	**Ad1**	**Ad2**	**Ad3**	**Ad4**	**Ad5**	**Ctrl**	**Ad1**	**Ad2**	**Ad3**	**Ad4**	**Ad5**
STOA	0.53	0.73	1.10	0.91	0.08	0.08	0.51	0.91	1.16	1.03	0.04	0.42
LTOA**	1.60	1.61	1.78	1.67	1.00	1.00	1.42	1.69	1.79	1.66	0.98	1.28
$\Delta log\|G^*\|$	1.07	0.88	0.68	0.76	0.92	0.92	0.91	0.78	0.63	0.63	0.94	0.86

**Predicted using the PAM model.

Figure 52 presents the *M* parameters for each mixture. It is observed that the modified mixtures exhibited lower *M* values than the control mix for all Binder 1 mixtures. Specifically, among the Binder 5 mixtures, the mixture containing additive 4 yielded a slightly higher *M* value than the control, while the other modified mixtures yielded lower values than the control mixture. This expected trend is consistent with the $\Delta log|G^*|$ results observed in Table 8. The *M* parameter indicates aging susceptibility, with higher values related to increased aging susceptibility (Michael Dawoud Elwardany, 2017). Accordingly, based on the *M* parameter results, the modified mixtures exhibited similar or reduced aging susceptibility compared to their corresponding control mixtures.

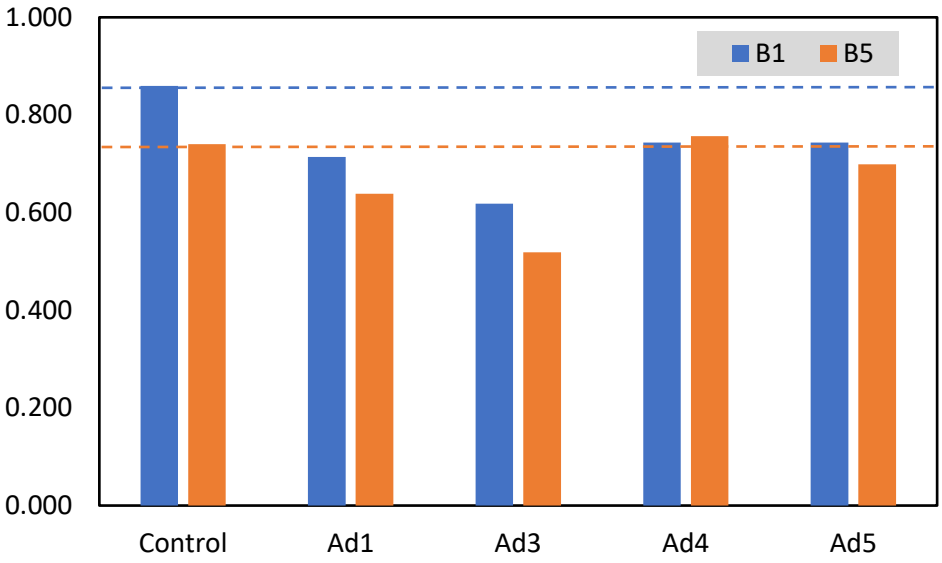

Figure 52. *M* parameter for B1 and B5 mixtures.

5.3. LTOA S_{app} Prediction

5.3.1 Estimated LTOA Dynamic Moduli

The results of the *tAS* calculations for each mixture after 5 oven aging are summarized in Table 9. Mixtures containing binders more susceptible to stiffening after aging are anticipated to yield higher *tAS* values, consequently leading to predicted stiffer mixes.

Table 9. Time-aging shift factor for 5-day oven aging at 95°C.

Mixture ID	Binder 1	Binder 5
Ctrl	1.82	1.56
Ad1	1.48	1.34
Ad2	1.16	1.06
Ad3	1.30	1.08
Ad4	1.57	1.60
Ad5	1.57	1.47

Figure 53 and Figure 54 depict the |E^*| curves, measured and predicted, for mixtures based on binders 1 and 5 at different aging conditions: short-term aging (STOA) and 5 days oven-aged (LTOA). Additionally, |E^*| values obtained after 5 days of aging in the oven at 95°C (LTOA) are included for comparison with the predicted data. It is observed that the predicted data exhibit a more pronounced shift in the |E^*| curve compared to the laboratory results obtained after LTOA. Lower *tAS* values would reduce the shift of the predicted curve and increase the model's accuracy. This reduction in *tAS* could be related to the constant value (1.71) used for the *c* parameter, as indicated by Kim et al. (2011) for level 2 approximations, based on the available data.

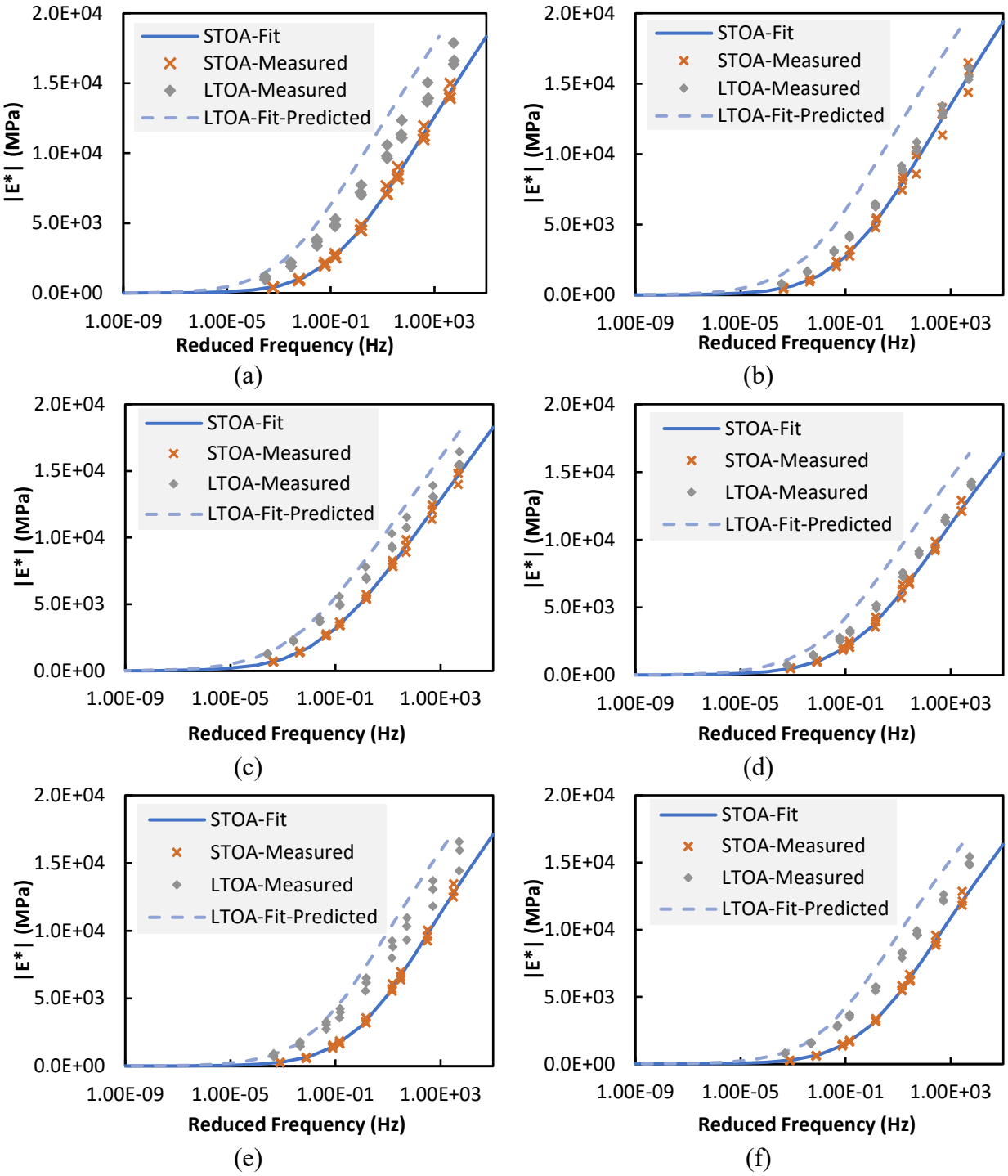

Figure 53. Measured and predicted |*E**| curves at STOA, LTOA, and 20 days oven aging for (a) Control, (b) additive 1, (c) additive 2, (d) additive 3, (e) additive 4, and (f) additive 5 binder 1-based mixtures.

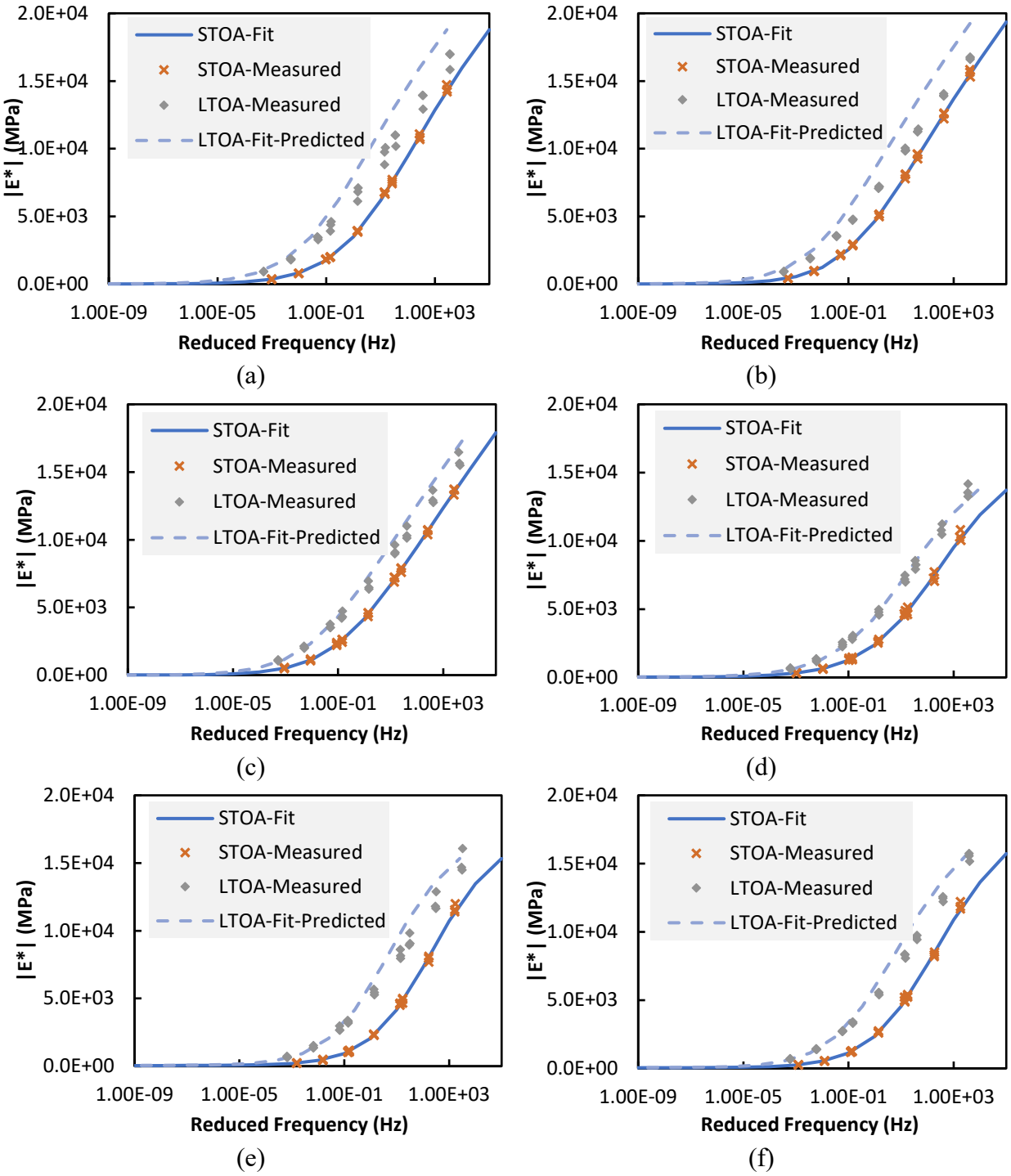

Figure 54. Measured and predicted |*E**| curves at STOA, LTOA, and 20 days oven aging for (a) Control, (b) additive 1, (c) additive 2, (d) additive 3, (e) additive 4, and (f) additive 5 binder 1-based mixtures.

Figure 55 compares the measured and predicted dynamic modulus values after 5 days of aging in the oven at 95°C (LTOA). The performance of the AMAC model in predicting $|E^*|$ trends is notably satisfactory, as indicated by the obtained R^2 value of 0.98. However, it's important to note that the model tends to overestimate the effect of aging on stiffness. This overestimation is evident in the scatterplot, where most data points are positioned above the line of equality (LOE), signifying that the model predicts higher $|E^*|$ values than those observed in the laboratory. Increased variability in the predictions, particularly at higher $|E^*|$ values, is observed.

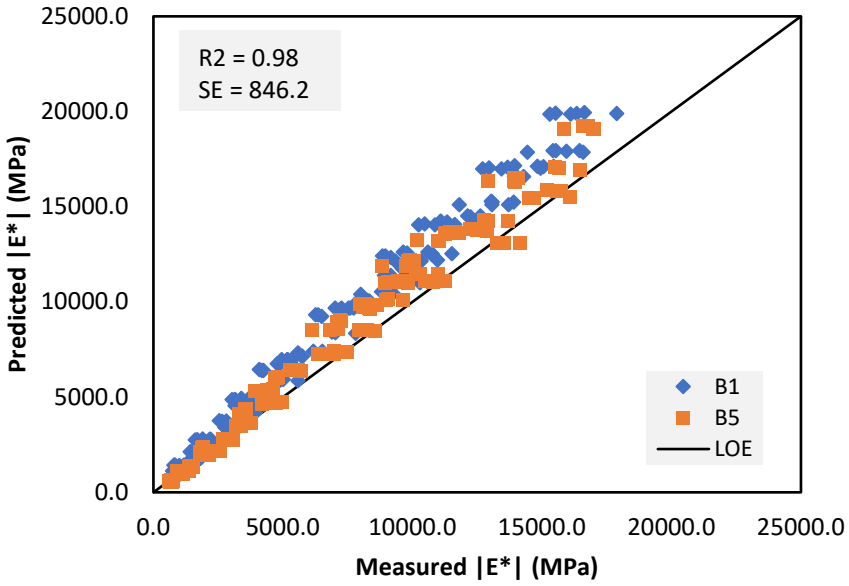

Figure 55. Comparison of measured and predicted LTOA dynamic modulus ($|E^*|$).

Figure 56 and Figure 57 provide a breakdown of the comparison between measured and predicted dynamic modulus values after 5 days of aging in the oven at 95°C (LTOA) based on the base binder type. The model demonstrates a strong correlation between the predicted and measured $|E^*|$ values, as evidenced by the high R^2 value of 0.98 for both base binders. Notably, when the base binder separates observations, the variability in the model predictions is reduced. This

separation results in a lower standard error of 738.0 for binder 1 mixes and 753.4 for binder 5 mixes, further enhancing the accuracy of the model's predictions.

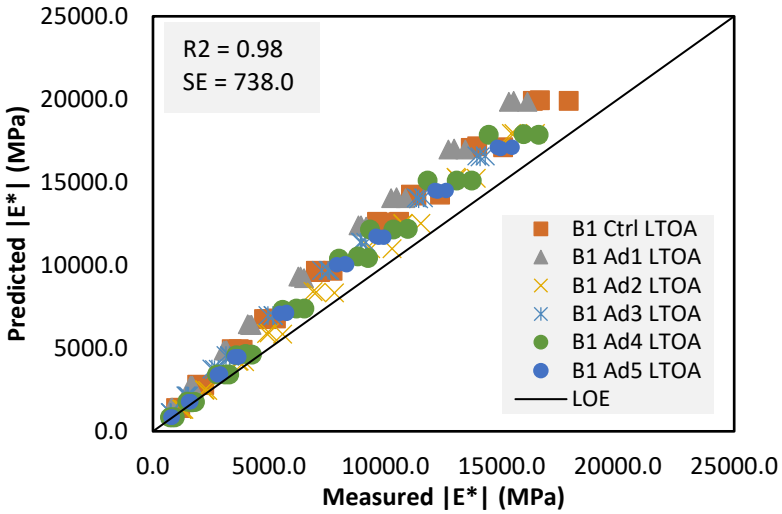

Figure 56. Comparison of measured and predicted LTOA dynamic modulus ($|E^*|$) for B1-based asphalt mixtures.

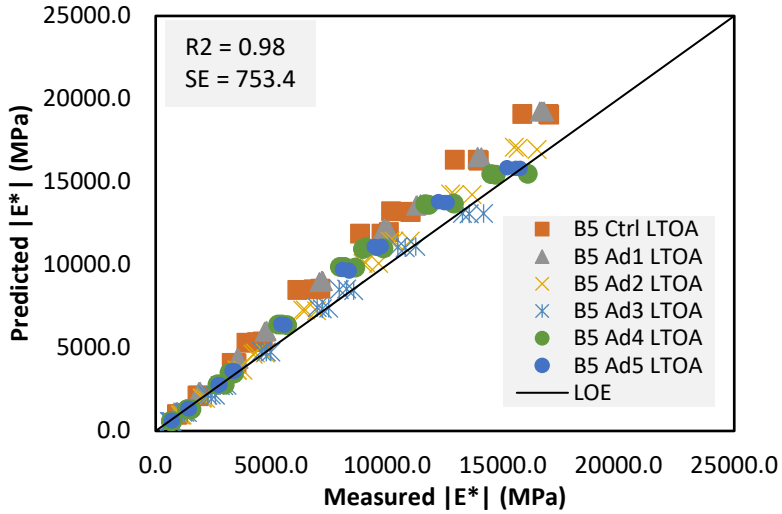

Figure 57. Comparison of measured and predicted LTOA dynamic modulus ($|E^*|$) for B5-based asphalt mixtures.

Although the model can predict the complete master curve by adjusting and shifting the STOA curve using the aging shift factor, the $|E^*|$ at 10 rad/s and the reference temperature are the only parameters needed for the S_{app} calculation. Figure 58 compares the predicted and measured $|E^*|$ at this frequency and temperature. It is observed that consistently with the previous results, the model predicts stiffer mixes for all the observations, affecting the final predicted S_{app} calculation.

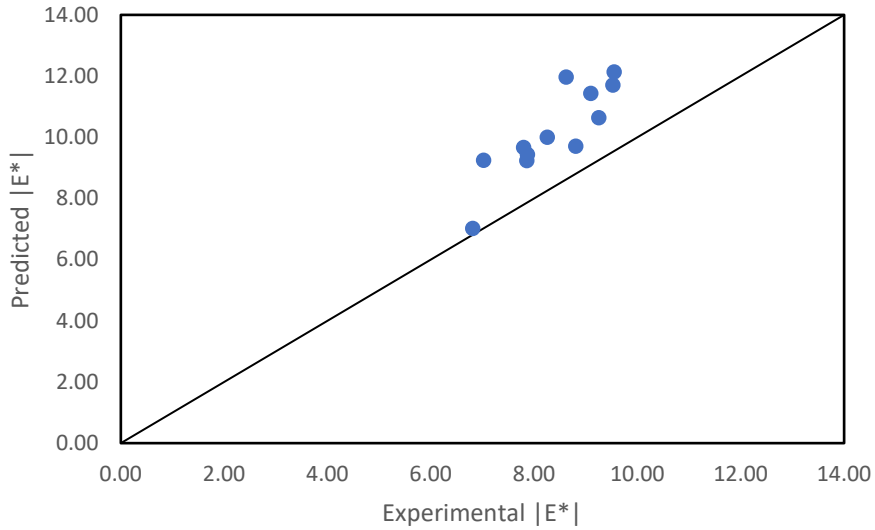

Figure 58. Predicted $|E^*|$ vs. Experimental $|E^*|$ at 10 rad and 20°C.

5.3.2 Estimated LTOA C vs. S Curves

Figure 59 and Figure 60 show the damage characteristic curves for the measured STOA mixtures, long-term aged mixtures, and the predicted curves for LTOA mixtures. As observed in Figure 59a and Figure 59e, good predictions of the damage characteristic curves were observed for the binder 1 control and additive 4 mixes. The rest of the Binder 1 mixture didn't yield measured results as close to the results predicted by the model.

Higher or flatter *C vs. S* curves were predicted, while similar to the STOA curves were obtained. These unexpectedly longer and closer to the STOA curves could be attributed to a

positive effect of the additives in the mix on the damage accumulation after aging that the model cannot predict adequately.

Figure 60 presents the measured and predicted damage characteristic curves for the base Binder 5 mixtures. The control and additive 2 mixtures yielded the best LTOA damage characteristic curve predictions, as observed in Figure 60a and Figure 60c. Higher predictions than the measured curves were obtained for the B5-additive 1 mix. In contrast, additives 3, 4, and 5 yielded shorter and lower predictions than the measured curves.

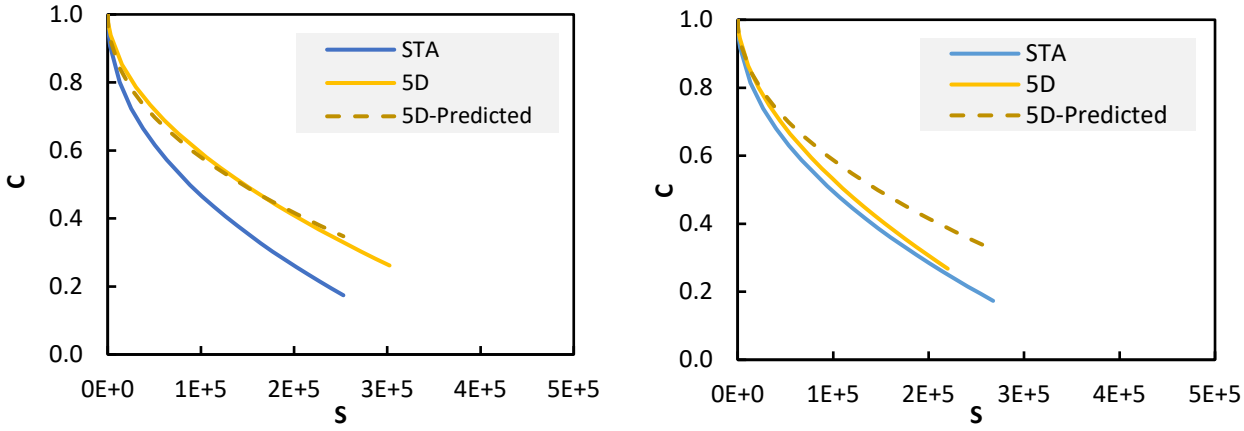

(a)

(b)

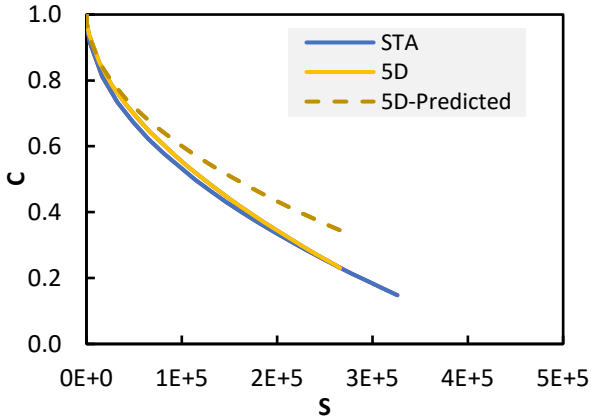

(c)

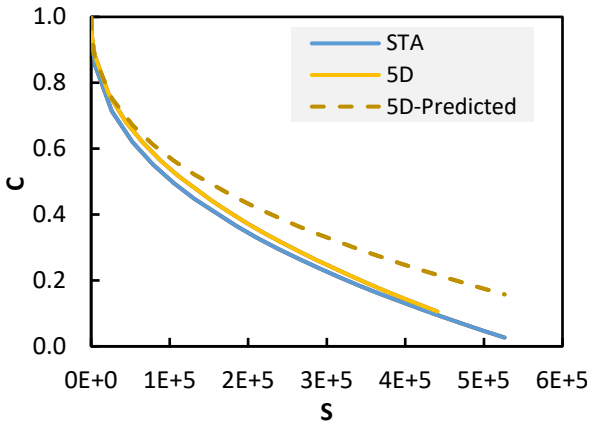

(d)

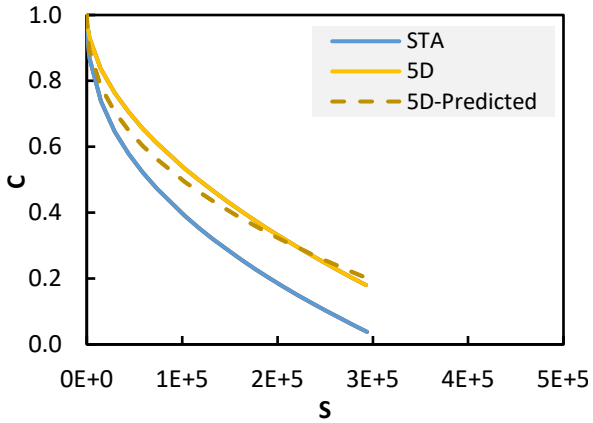

(e)

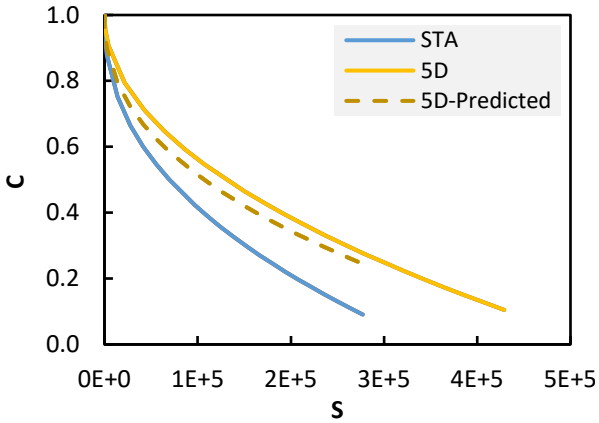

(f)

Figure 59. Damage characteristic curves for (a) control, (b) additive 1, (b) additive 2, (c) additive 3, (d) additive 4, (e) additive 5, for B1-based mixtures.

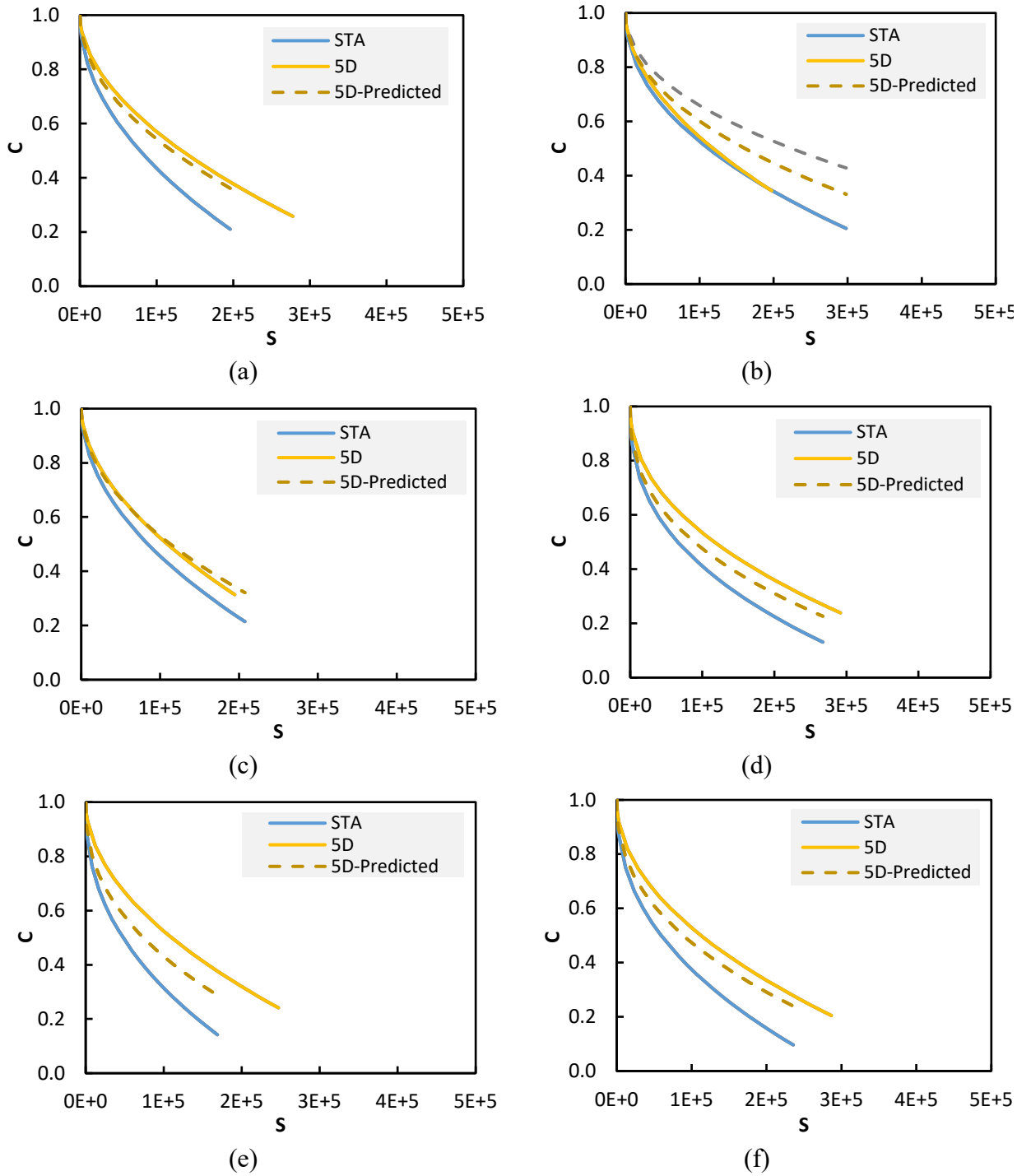

Figure 60. Damage characteristic curves for (a) control, (b) additive 1, (b) additive 2, (c) additive 3, (d) additive 4, and (e) additive 5 for B5-based mixtures.

A comparison between the measured and predicted pseudo-stiffness (C) for the LTOA-conditioned mixes is presented in Figure 61. Although some mixes yielded better predictions, as analyzed previously, a strong correlation between the predicted and measured observations were found by obtaining an R^2 of 0.984 and a low standard error of 0.05. Variability of the predictions is observed with data points deviating from the LOE at intermediate and lower C values. The length of the C *vs.* S curve was assumed to be the same for the predicted and measured C values and was not predicted by the model.

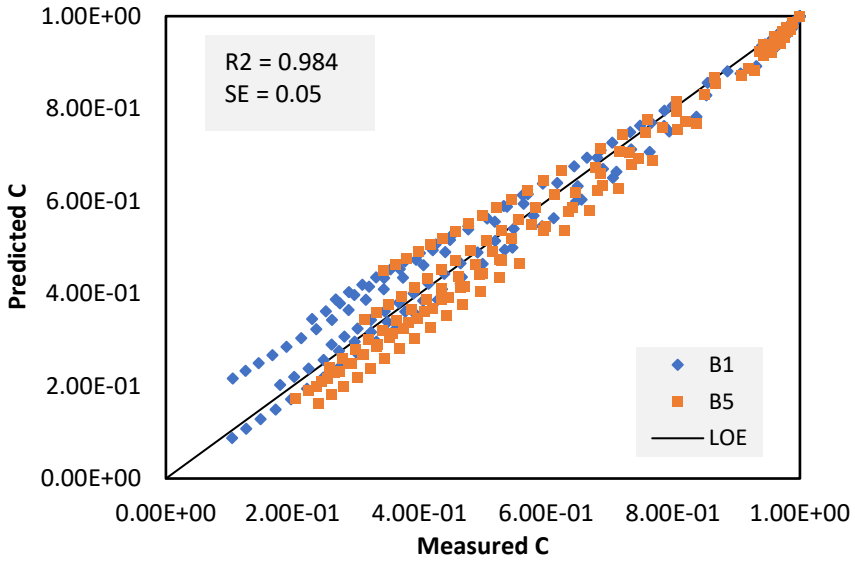

Figure 61. Comparison of predicted and measured pseudo-stiffness (C).

As observed in Equation 17, C_{11} is the only parameter modified by the aging factor. Therefore, the errors between the predicted and measured C come mainly from the error in the model predicting the C_{11} fitting parameter. Figure 62 presents the comparison between the C_{11} predicted and measured parameters. It is observed that the model estimates lower C_{11} values than the experimentally obtained.

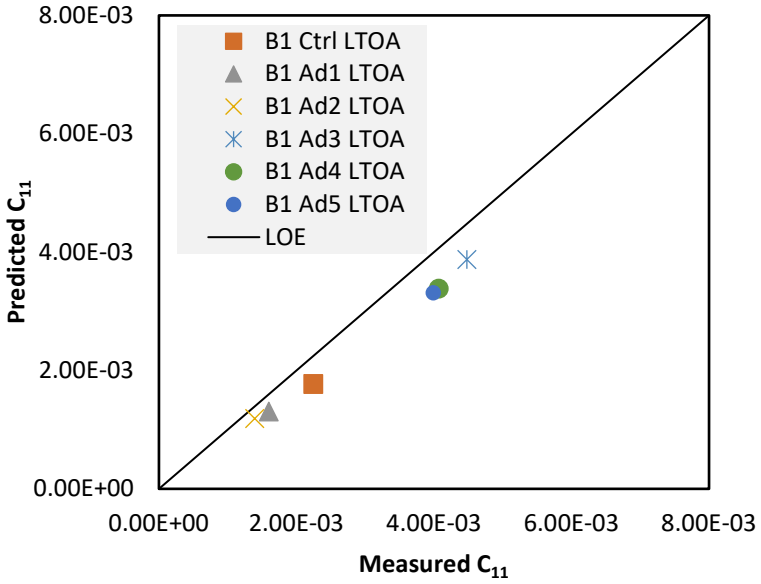

(a)

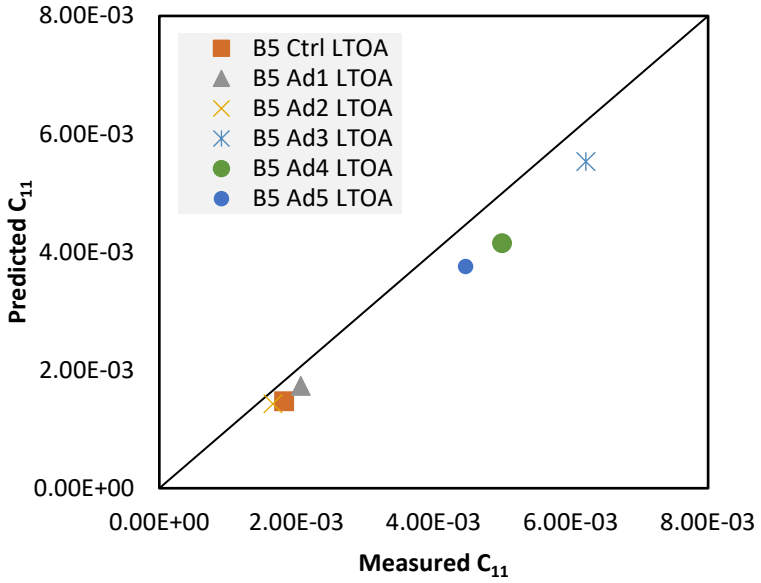

(b)

Figure 62. Predicted C_{11} vs. Measured C_{11} parameter for (a) Binder 1 mixtures and (b) Binder 5 mixtures.

5.3.3 Estimated LTOA D^R Parameter

The predicted D^R values were obtained from the measured STOA D^R, modified considering the $log|G^*|$ changes due to aging, as described in Equation 23. Lower D^R values are expected as aging increases and $log|G^*|$ increases (Y. R. Kim et al., 2021). Table 10 presents the predicted and calculated LTOA D^R values for the studied mixes from measured data. Predicted D^R values were the same or lower than the experimentally obtained for all the Binder 1 mixtures. The same trend was observed for Binder 5 mixtures, excluding mixtures containing additives 1, 2, and 3, which yielded higher D^R values.

Table 10. Predicted and calculated D^R for LTOA asphalt mixtures.

Mix	**Binder 1**		**Binder 5**	
	D^R	**Predicted D^R**	**D^R**	**D^R Predicted**
Ctrl	0.57	0.43	0.56	0.45
Ad1	0.53	0.49	0.47	0.49
Ad2	0.55	0.55	0.49	0.52
Ad3	0.73	0.66	0.60	0.64
Ad4	0.63	0.56	0.57	0.54
Ad5	0.69	0.56	0.62	0.55

A comparison between the predicted and calculated LTOA D^R parameters is presented in Figure 63. An adequate correlation between the predicted and calculated D^R parameters can be observed, determined by the R^2 of 0.42. Although the model made a good prediction of the previous parameters, lower accuracy is observed in the prediction of the D^R parameter.

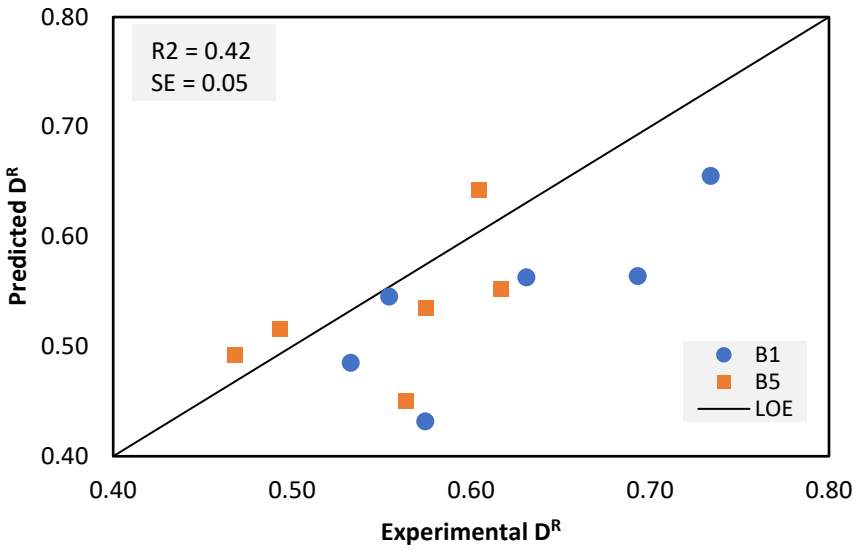

Figure 63. Comparison of predicted and experimental D^R parameters

5.3.4 Estimated LTOA S_{app}

Finally, using the three predicted parameters (i.e., $|E^*|$, damage characteristic curves, and D^R values), the predicted S_{app} value was calculated for the LTOA condition according to Equation 10. The results of predicted and calculated S_{app} values are presented in Table 11, indicating the ranking with a number between parenthesis. It is observed in Table 11 that most of the predicted S_{app} values were lower than the experimental representative S_{app} values. However, the B1-Additive 2, B5-Additive 1, and B5-Additive 2 mixtures yielded higher predicted S_{app} values than the experimentally determined. Both predicted and experimental rankings indicate that additive 3 is the mixture with higher cracking resistance, independently of the base binder. The ranking of the other additives varies from the predicted and experimental methods and depends on the base

binder. The model indicated that the control mixtures yielded the worst cracking resistance for both base binders. However, the experimental data indicates that the mixtures with additives 1 and 2 yielded lower cracking resistance than the control mixture for both base binders.

Table 11. Predicted and representative LTOA S_{app} parameters for binder 1 and 5-based asphalt mixtures.

Mix	Binder 1		Binder 5	
	Predicted S_{app}	**Experimental S_{app}**	**Predicted S_{app}**	**Experimental S_{app}**
Ctrl	10.4 (6)	20.9 (4)	9.3 (6)	19.4 (3)
Ad1	12.9 (5)	16.9 (5)	13.7 (3)	12.9 (5)
Ad2	18.6 (2)	16.0 (6)	18.7 (2)	12.6 (6)
Ad3	27.4 (1)	37.2 (1)	20.7 (1)	24.1 (1)
Ad4	14.3 (4)	22.8 (3)	9.8 (5)	18.6 (4)
Ad5	16.2 (3)	31.9 (2)	12.4 (4)	21.8 (2)

A comparison of predicted and determined representative S_{app} values is presented in **Error! Reference source not found.**. Only three observations were located over the LOE, indicating a S_{app} underestimation of the model for most mixtures. The model resulted in an R^2 of 0.27 and an *SE* of 4.73, which doesn't indicate an adequate prediction of the parameters by the model. A combination of predictions of stiffer mixes and lower D^R than the experimentally determined ones produced much lower values of S_{app} obtained from the model than from laboratory testing.

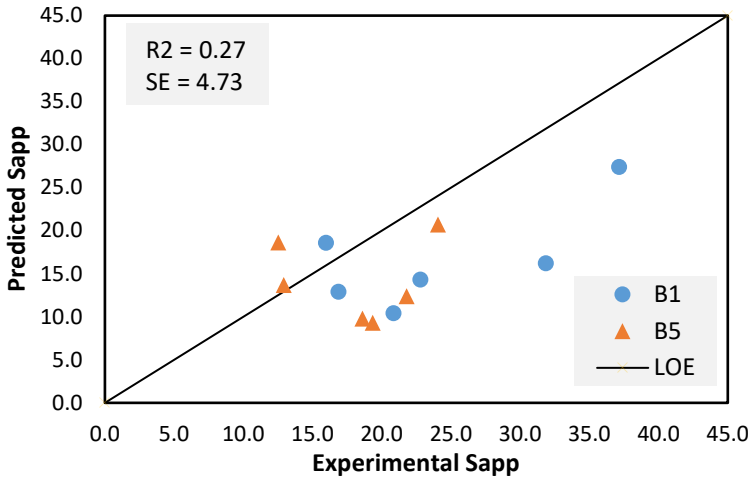

Figure 64. Comparison of the predicted and experimental S_{app} parameters.

Figure 65 summarizes the predicted and experimental parameters calculated to determine the S_{app}. It is observed how overestimating the $|E^*|$ and C_{11} parameters combined with underestimating the D^R parameter led to lower S_{app} values predicted by the model than the ones obtained in the laboratory.

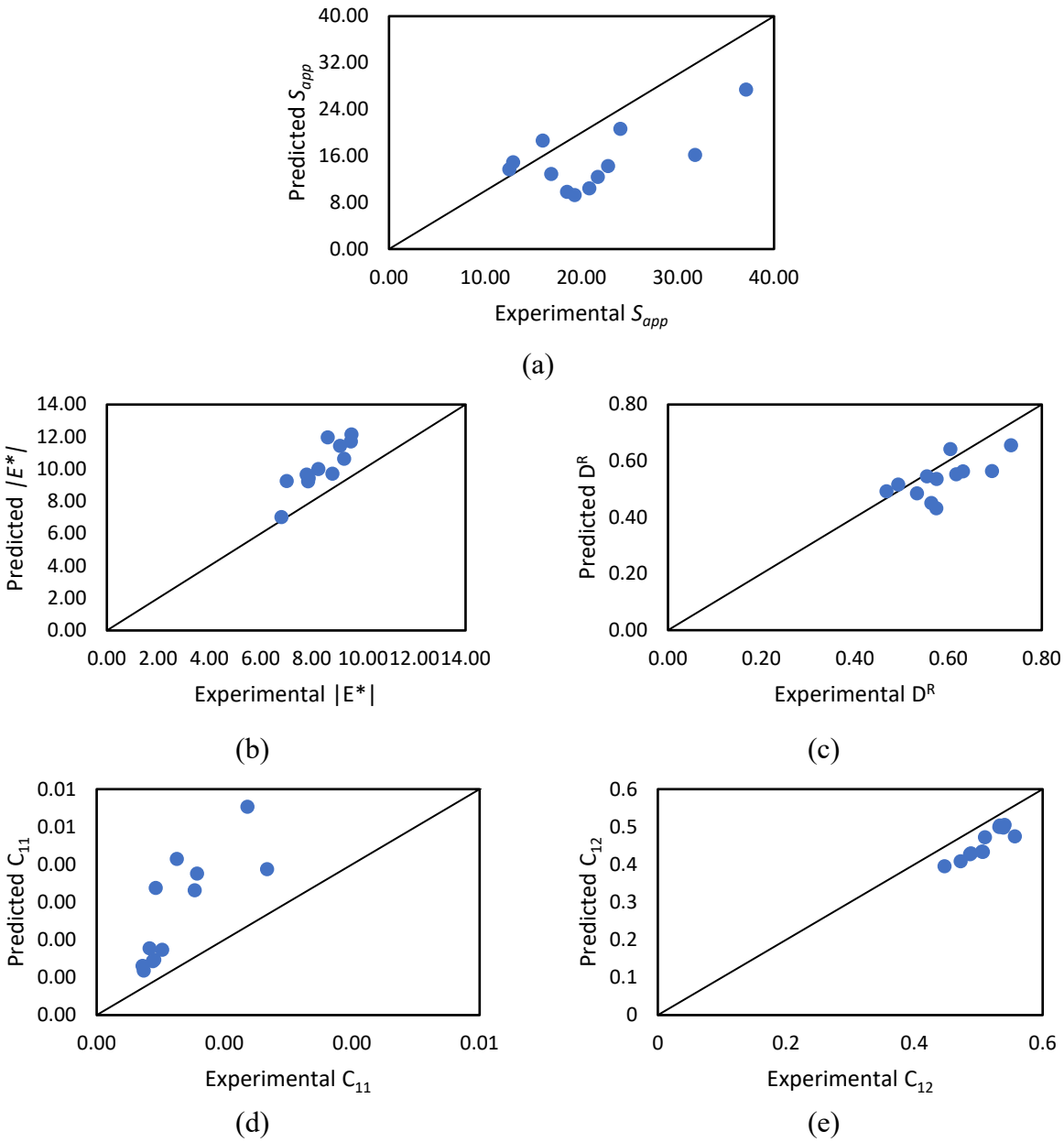

Figure 65. Predicted vs. Experimental comparison for (a) S_{app}, (b) $|E^*|$, (c) D^R, (d) C_{11}, and (e) C_{12} parameters.

5.4. NAWS Equivalent Oven Aging Duration

Table 12 presents the results of the equivalent aging duration determination. An average aging duration of 3.3 days at 95°C was obtained for all the mixtures, and no considerable difference was observed when analyzing by base binder type. However, high variability was observed for each additive mixture type. The obtained equivalent durations ranged between 0.8 days for the Binder 1 Additive 4 mixture and 7 days for the Binder 5 Additive 3 mixture.

Table 12. Equivalent NAWS aging duration of the loose mixture in a 95°C oven

Mix	Days	
	B1	**B5**
Ctrl	1.6	1.1
Ad1	1.8	4.7
Ad2	5.2	5.2
Ad3	5.1	7.0
Ad4	0.8	1.3
Ad5	4.1	1.1
Average	**3.1**	**3.4**
Stdev	**1.9**	**2.6**
Average	**3.3**	
Stdev	**2.2**	

Figure 66 compares the predicted and experimental variables for calculating the equivalent aging duration after optimizing S_{app}. It is observed that when aiming for the same predicted and experimental S_{app} values (Figure 66a), the model predicts stiffer mixtures and higher C_{11} values than those obtained in the laboratory, as evident in Figure 66b and Figure 66d. Although the predicted and obtained D^R values yielded similar results, the model predicted slightly higher values than those obtained in the laboratory. These results indicate that the fatigue cracking performance does not depend only on the mixture's stiffness and can't be evaluated by single parameters but by

their combined effects. Stiffer mixtures with higher C_{11} and D^R values could result in comparable cracking performances when evaluating using the S_{app} parameter.

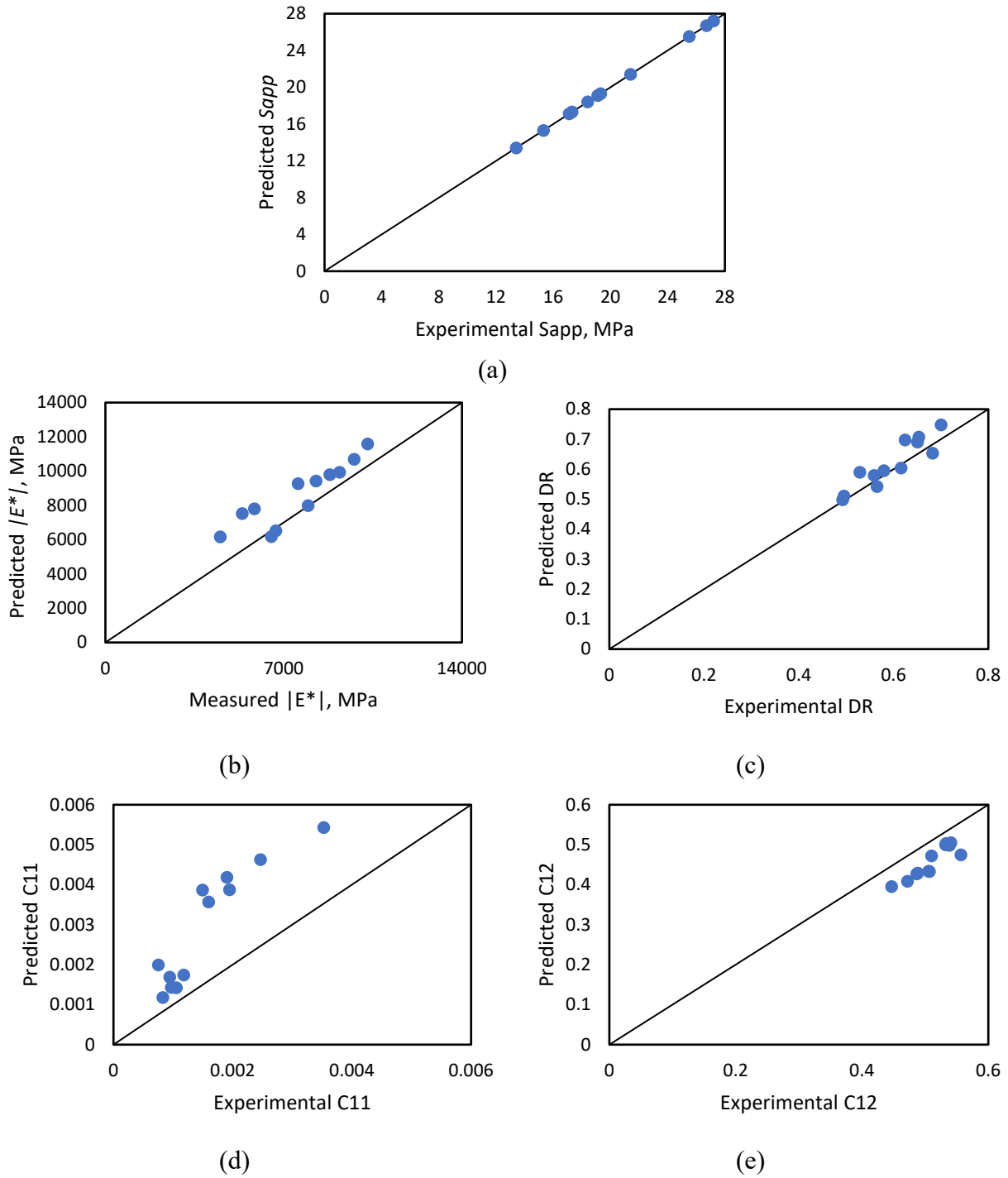

Figure 66. Comparison between predicted and experimental (a) S_{app}, (b) $|E^*|$, (c) D^R, (d)C_{11}, and (e) C_{12} parameters for equivalent aging duration calculation.

CHAPTER 6 - CONCLUSIONS AND RECOMMENDATIONS

This study aimed to determine the effect of five different technologies on the aging susceptibility and fatigue cracking resistance when incorporated into asphalt mixtures after long-term aging. Laboratory testing was conducted to characterize the performance of each studied mixture through performance indicators and damage curves. The complete study consisted of selecting two base binders to evaluate the additive technologies, the binder evaluation, and finally, the asphalt mixture performance evaluation of the technologies. This last experiment section was described in this thesis.

The technologies were evaluated by comparing the laboratory testing results of modified asphalt mixtures after three aging conditions (i.e., STOA, LTOA, and NAWS) to the unmodified control mixtures. Dynamic Modulus and phase angle determination through AMPT testing was conducted to characterize the mechanical properties of the mixtures. Glover-Rowe for the mixtures and black space diagrams were obtained from the results of this testing. Additionally, Cyclic Fatigue testing, also using the AMPT equipment, enabled the determination of the damage accumulation characteristics of each mixture and the calculation of the fatigue cracking performance indicator, S_{app}. Aging and effectiveness indicators for each were calculated from $G\text{-}R_m$ and S_{app} parameters. Damage predictions were calculated using the FlexPAVE software, considering the mixture's initial properties, traffic, climate, and pavement structure effects. Finally, the experimental LTOA S_{app} results were compared to predicted results from the AMAC and PAM models. Using these same models, an equivalent duration of oven-aged loose mixture at 95°C was determined for the NAWS aging conditioning method.

All testing results indicated that, in general, the additive technologies improved the mixture's characteristics related to improved fatigue cracking and aging resistance. However, the

effectiveness of the additives in improving mechanical properties and aging resistance depended on the base binder and each additive's nature.

6.1. Key Findings

- All the additives reduced the mixture's stiffness after aging, related to improved cracking resistance. The effectiveness of the additive depended on the base binder and the aging conditioning method. Additive 2 only effectively reduced the mixture's stiffness when evaluating the LTOA condition. Similarly, Additive 1 reduced the mixture's stiffness after LTOA, but only when blended with Binder 1.
- Similar results were obtained when considering the phase angle using the $G\text{-}R_m$ parameter. Improved characteristics related to cracking resistance were obtained after aging for all the additive technologies except for Additive 2. Additive 1 was only effective with Binder 1 when the mixtures were LTOA-aged. Additive 3 improved the cracking performance except for Binder 1 mixtures after NAWS. A summary of these findings is shown in Table 13, where a specific color differentiates each additive.

Table 13. Summary of Dynamic Modulus Fatigue Cracking Resistance Findings.

Base Binder	Lower E* (wr=10Hz)		Lower $G\text{-}R_m$	
	LTOA	NAWS	LTOA	NAWS
Binder 1	Ad3 Ad5 Ad4 Ad1 Ad2	Ad5 Ad4 Ad3	Ad3 Ad5 Ad4 Ad1	Ad5 Ad4
Binder 5	Ad3 Ad4 Ad5 Ad2	Ad4 Ad3 Ad5	Ad3 Ad4 Ad5	Ad4 Ad3 Ad5

Regarding aging resistance, Table 14 summarises the results of the $|E^*|$ aging ratio and the $G\text{-}R_m$ aging index for each mixture.

- The mixture's aging resistance was improved when incorporating the additive technologies. Both indicators suggest that Additives 1, 2, and 3 reduced aging susceptibility after LTOA.
- After NAWS conditioning, results indicate that the effect of the additive depends on the base binder. Additive 4 reduces aging susceptibility to NAWS aging in both base binders except for base binder 1 mixtures according to the $G\text{-}R_m$ aging index. Additive 5 reduces aging susceptibility to NAWS for Binder 1 but not Binder 5 mixtures. Similarly, Additive 3 reduces aging susceptibility to NAWS for Binder 5 but not Binder 1 mixtures. Finally, Additive 2 improves NAWS aging resistance only for Binder 5 mixtures according to the $G\text{-}R_m$ aging index.

Table 14. Summary of Dynamic Modulus Aging Susceptibility Findings

Base Binder	$\|E^*\|$ aging ratio		$G\text{-}R_m$ aging index	
	LTOA	NAWS	LTOA	NAWS
Binder 1	Ad1 Ad3 Ad2	Ad5 Ad4	Ad1 Ad3 Ad2	Ad5
Binder 5	Ad1 Ad2 Ad3	Ad4 Ad3	Ad1 Ad2 Ad3	Ad4 Ad3 Ad2

- Results when considering the damage accumulation characteristics of the mixtures indicate that the additive technologies effectively improve fatigue cracking performance. The summary of the mixtures that yielded improved mixture properties determined by D^R and S_{app} parameters is presented in Table 15.

- The D^R parameter indicates that Additives 3, 4, and 5 would improve cracking resistance after aging. According to the D^R parameter, additives 1 and 2 would improve cracking resistance after NAWS aging.
- The S_{app} parameter, a better fatigue cracking indicator, indicates that Additives 3 and 5 improve the fatigue cracking resistance of the asphalt mixtures independently of the aging method and base binder of the mixture. The same indicator suggests that Additive 4 improves cracking resistance when blended with Binder 1. Additive 1 improves cracking resistance with Binder 1, but only when evaluated with the NAWS method.

Table 15. Summary of Fatigue Cracking Resistance Findings.

Base Binder	D^R		S_{app}	
	LTOA	NAWS	LTOA	NAWS
Binder 1	Ad3 Ad5 Ad4	Ad4 Ad3 Ad5 Ad1 Ad2	Ad3 Ad5 Ad4	Ad4 Ad3 Ad5 Ad1
Binder 5	Ad5 Ad3 Ad4	Ad5 Ad4 Ad3	Ad3 Ad5	Ad5 Ad4 Ad3

- Aging resistance was defined with the D^R and S_{app} aging index, which indicates the changes in the aging parameters. A summary of the mixtures with improved aging resistance is presented in Table 16.
- Although the results in Table 15 indicated improved cracking resistance, only Additives 1, 4, and 5 yielded improvements in the aging resistance compared to the corresponding control mixtures. All the technologies resulted in higher aging susceptibility than the

control mixtures when evaluating aging through the LTOA method and with the S_{app} aging index.

Table 16. Summary of Fatigue Damage Aging Susceptibility Findings

Base Binder	D^R aging index		S_{app} aging index	
	LTOA	NAWS	LTOA	NAWS
Binder 1	Ad5	Ad4 Ad1		Ad4 Ad1
Binder 5		Ad5 Ad4		

FlexPAVE simulations provided cracking performance information considering not only the mixture's properties, as in the previous results, but also their interaction with other variables, such as the pavement structure, traffic, and climate.

- Results of predicting the fatigue cracking performance after the simulation of 20 years of service life indicated that only Binder 5 with Additive 4 mixtures led to higher percent damage at the end of the analysis period. The rest of the technologies reduced the percent damage after the FlexPAVE simulation, translating into life extension benefits when incorporating the additives into the mixture.

Limitations on the results of damage simulation using FlexPAVE are related to not considering the aging effect in the model. The input variables of this model were the STOA characteristics and were not affected by the aging effects during the simulation. As found in this study, improved characteristics at the initial stages of the asphalt mixture services life could benefit pavement performance; however, aging susceptibility could affect performance over extended periods if the technology benefits are not maintained over time. Considering aging during the FlexPAVE simulation, it is recommended that this limitation be addressed when the FlexPAVE 2.0 software version is available.

The $log|G^*|$ from STOA extracted binder and the experimental S_{app} results were used to evaluate and predict fatigue cracking parameters using the AMAC and PAM models. The analysis and comparison of the predicted and laboratory-obtained results led to the following key findings:

- The PAM estimations indicated that all the additive technologies reduced the aging susceptibility compared to the control mixture independently of the base binder. Aging susceptibility was determined by calculating the M_{blend} parameter, a fitting parameter of the PAM related to aging susceptibility.
- Improved aging susceptibility for all the additive-modified mixtures determined by the PAM model would indicate that future simulations in FlexPAVE, considering the effect of aging using this model, could maintain the trends of lower damage for the modified than the control mixtures.
- The prediction of the S_{app} parameter using the AMAC model required the prediction of three parameters (i.e., $|E^*|$, *C vs. S* curves, D^R) used in the S_{app} calculation. Each prediction led to approximation errors accumulated to the final S_{app} estimation. In general, the model predicted stiffer mixes, higher *Cvs.S* curves, and lower D^R values for most of the mixtures, which are characteristics related to lower cracking resistance and led to lower S_{app} values or an underestimation of the model compared to the experimental results.
- The model approximates the effect of aging in the mixture properties based on the changes in $log|G^*|$ obtained from DSR testing. Therefore, the underestimation of the S_{app} parameter could be related to improved characteristics caused by the additives that the model does not capture.
- The AMAC model calculated the equivalent days of oven aging at 95°C of a loose mixture, which led to the same S_{app} values obtained after NAWS conditioning. An average duration

of 3.3 days of oven aging was obtained with similar results obtained when separating by base binder. However, a high variability of durations was obtained for each additive technology, ranging from 0.8 to 7 days of aging.

- Similar trends of each parameter estimation were obtained on the NAWS and LTOA approximations (i.e., $|E^*|$ and C_{11} overestimation). However, the difference between both was found in the D^R predictions. The LTOA S_{app} predictions underestimated D^R, leading to lower S_{app} values than the experimental values. The NAWS method, which optimized the predicted S_{app} to be the same as the experimental, indicated an overestimation of the D^R parameter. This difference in the accuracy of predicting S_{app} and the estimation of D^R suggests that a more accurate prediction of the D^R parameter by the model could lead to better S_{app} predictions.
- The $|E^*|$ curve prediction at aged conditions requires the fitting parameter *c.* The level 2 method was used for this study, in which a constant value of 1.71 was used. The *c* parameter could be calibrated using the LTOA data to improve the model aged $|E^*|$ approximations.

In conclusion, the findings presented in this study offer valuable insights into the aging and cracking behavior of asphalt mixtures, particularly in response to the LTOA and NAWS laboratory conditioning. The outcomes of this study could be further refined and applied through correlation with previous binder testing and extracted binder evaluations. Additional cracking laboratory testing, such as Ideal-CT, could also help validate the findings of this study.

REFERENCES

AASHTO, A. A. o. S. H. a. T. O. (2019a). Determining the Dynamic Modulus for Asphalt Mixtures Using Small Specimens in the Asphalt Mixture Performance Tester (AMPT). In (Vol. T132). Washington, DC: Technical Subcommittee: 2d, Proportioning of Asphalt–Aggregate Mixtures.

AASHTO, A. A. o. S. H. a. T. O. (2019b). Standard Method of Test for Determining the Damage Characteristic Curve and Failure Criterion Using Small Specimens in the Asphalt Mixture Performance Tester (AMPT) Cyclic Fatigue Test. In *American Association of State Highway and Transportation Officials. Technical Subcommittee: 2d, Proportioning of Asphalt–Aggregate Mixtures* (Vol. T-133). Washington, DC.

AASHTO, A. A. o. S. H. a. T. O. (2019c). Standard Practice for Mixture Conditioning of Hot Mix Asphalt (HMA). In (Vol. R30). Washington, DC: American Association of State Highway and Transportation Officials.

AASHTO, A. A. o. S. H. a. T. O. (2019d). Standard Practice for Preparation of Small Cylindrical Performance Test Specimens Using the Superpave Gyratory Compactor (SGC) or Field Cores. In (Vol. PP-99). Washington, DC: American Association of State Highway and Transportation Officials. Technical Subcommittee: 2d, Proportioning of Asphalt–Aggregate Mixtures.

AASHTO, A. A. o. S. H. a. T. O. (2021). Developing Dynamic Modulus Master Curves for Asphalt Mixtures Using the Asphalt Mixture Performance Tester (AMPT). In (Vol. R84-17(2021)). Washington, DC: American Association of State Highway and Transportation Officials.

AASHTO, A. A. o. S. H. a. T. O. (2022). Standard Practice for Mixture Conditioning of Asphalt Mixtures. In. Washington, DC.

Ahmed, R. B., & Hossain, K. (2020). Waste cooking oil as an asphalt rejuvenator: A state-of-the-art review. *Construction and Building Materials, 230*, 116985. doi:10.1016/j.conbuildmat.2019.116985

Alamri, M., Lu, Q., & Xin, C. (2020). Preliminary Evaluation of Hot Mix Asphalt Containing Reclaimed Epoxy Asphalt Materials. *Sustainability, 12*(9). doi:10.3390/su12093531

Anderson, R., King, G., Hanson, D., & Blankenship, P. (2011). Evaluation of the Relationship Between Asphalt Binder Properties and Non-Load Related Cracking. *Asphalt Paving Technology: Association of Asphalt Paving Technologists-Proceedings of the Technical Sessions, 80*.

Anderson, R. M., King, G. N., Hanson, D. I., & Blankenship, P. B. (2011). Evaluation of the relationship between asphalt binder properties and non-load related cracking. *Journal of the Association of Asphalt Paving Technologists, 80*.

Apeagyei, A. K. (2011). Laboratory evaluation of antioxidants for asphalt binders. *Construction and Building Materials, 25*(1), 47-53. doi:https://doi.org/10.1016/j.conbuildmat.2010.06.058

Apostolidis, P., Liu, X., Erkens, S., & Scarpas, T. (2022). Oxidative aging of epoxy asphalt. *International Journal of Pavement Engineering, 23*(5), 1471-1481. doi:10.1080/10298436.2020.1806278

Apostolidis, P., Liu, X., Kasbergen, C., & Scarpas, A. T. (2017). Synthesis of Asphalt Binder Aging and the State of the Art of Antiaging Technologies. *Transportation Research Record, 2633*(1), 147-153. doi:10.3141/2633-17

Arámbula-Mercado, E., Kaseer, F., Epps Martin, A., Yin, F., & Garcia Cucalon, L. (2018). Evaluation of recycling agent dosage selection and incorporation methods for asphalt mixtures with high RAP and RAS contents. *Construction and Building Materials, 158*, 432-442. doi:https://doi.org/10.1016/j.conbuildmat.2017.10.024

Baek, C., Underwood, B. S., & Kim, Y. R. (2012). Effects of Oxidative Aging on Asphalt Mixture Properties. *Transportation Research Record, 2296*(2296), 77-85. doi:10.3141/2296-08

Barghabany, P., Zhang, J., Mohammad, L. N., Cooper, S. B., & Cooper, S. B. (2022). Chemical and Rheological Characterization of Asphalt Binders: A Comparison of Asphalt Binder Aging and Asphalt Mixture Aging. *Transportation Research Record: Journal of the Transportation Research Board*, 036119812110679. doi:10.1177/03611981211067977

Behnood, A. (2019). Application of rejuvenators to improve the rheological and mechanical properties of asphalt binders and mixtures: A review. *Journal of Cleaner Production, 231*, 171-182. doi:https://doi.org/10.1016/j.jclepro.2019.05.209

Bell, C. A. (1989a). *Aging of Asphalt-Aggregate Systems*. Retrieved from Corvallis, OR:

Bell, C. A. (1989b). *Summary report on aging of asphalt-aggregate systems*. Retrieved from Washington, D.C:

Bell, C. A., AbWahab, Y., M.E., C., & Sosnovske, D. (1994). *Selection of Laboratory Aging Procedures for Asphalt-Aggregate Mixtures*. Retrieved from Corvallis, OR:

Butz, T., Muller, J., & Riebesehl, G. (2012). *Innovative method for producing crumbed rubber modified asphalt.* Paper presented at the 5th Eurasphalt & Eurobitume Congress.

C. J. Glover, E. M., A. Chowdhury et al. (2009). *Evaluation of binder aging and its influence in aging of hot mix asphalt concrete: literature review and experimental design*. Retrieved from College Station, TX, USA,:

Cai, X., Zhang, J., Xu, G., Gong, M., Chen, X., & Yang, J. (2019). Internal aging indexes to characterize the aging behavior of two bio-rejuvenated asphalts. *Journal of Cleaner Production, 220*, 1231-1238. doi:https://doi.org/10.1016/j.jclepro.2019.02.203

Camargo, I. G. D., Ben Dhia, T., Loulizi, A., Hofko, B., & Mirwald, J. (2021). Anti-aging additives: proposed evaluation process based on literature review. *Road Materials and Pavement Design, 22*(sup1), S134-S153. doi:10.1080/14680629.2021.1906738

Camargo, I. G. d. N., Ben Dhia, T., Loulizi, A., Hofko, B., & Mirwald, J. (2021). Anti-aging additives: proposed evaluation process based on literature review. *Road Materials and Pavement design*, S134-S153.

Camargo, I. G. D. N., Dhia, T. B., Loulizi, A., Hofko, B., & Mirwald, J. (2021). Anti-aging additives: proposed evaluation process based on literature review. *Road Materials and Pavement Design, 22*(sup1), S134-S153. doi:10.1080/14680629.2021.1906738

Cao, W., Mohammad, L. N., Barghabany, P., & Cooper, S. B. (2019). Relationship between laboratory and full-scale fatigue performance of asphalt mixtures containing recycled materials. *Materials and Structures, 52*(1). doi:10.1617/s11527-019-1327-z

Cao, W., Norouzi, A., & Kim, Y. R. (2016). Application of viscoelastic continuum damage approach to predict fatigue performance of Binzhou perpetual pavements. *Journal of Traffic and Transportation Engineering (English Edition), 3*(2), 104-115. doi:https://doi.org/10.1016/j.jtte.2016.03.002

Cavalli, M. C., Zaumanis, M., Mazza, E., Partl, M. N., & Poulikakos, L. D. (2018). Effect of ageing on the mechanical and chemical properties of binder from RAP treated with bio-based rejuvenators. *Composites Part B: Engineering, 141*, 174-181. doi:https://doi.org/10.1016/j.compositesb.2017.12.060

Chavez, F., Marcobal, J., & Gallego, J. (2019). Laboratory evaluation of the mechanical properties of asphalt mixtures with rubber incorporated by the wet, dry, and semi-wet process. *Construction and Building Materials, 205*, 164-174. doi:https://doi.org/10.1016/j.conbuildmat.2019.01.159

Chen, Y., Hossiney, N., Yang, X., Wang, H., & You, Z. (2021). Application of Epoxy-Asphalt Composite in Asphalt Paving Industry: A Review with Emphasis on Physicochemical Properties and Pavement Performances. *Advances in Materials Science and Engineering, 2021*, 3454029. doi:10.1155/2021/3454029

Christensen, D. W., Pellinen, T. K., & Bonaquist, R. F. (2003). *HIRSCH MODEL FOR ESTIMATING THE MODULUS OF ASPHALT CONCRETE*.

Cong, P., Chen, S., & Yu, J. (2011). Investigation of the properties of epoxy resin-modified asphalt mixtures for application to orthotropic bridge decks. *Journal of Applied Polymer Science, 121*(4), 2310-2316. doi:10.1002/app.33948

Copeland, A. (2011). Reclaimed Asphalt Pavement in Asphalt Mixtures: State of the Practice. Retrieved from https://rosap.ntl.bts.gov/view/dot/40918

Das, P. K. (2014). *Ageing of Asphalt Mixtures: Micro-scale and mixture morphology investigation.* (Doctoral Thesis). KTH Royal Institute of Technology, Stockholm.

Dehouche, N., Kaci, M., & Mokhtar, K. A. (2012). Influence of thermo-oxidative aging on chemical composition and physical properties of polymer modified bitumens. *Construction and Building Materials, 26*(1), 350-356. doi:https://doi.org/10.1016/j.conbuildmat.2011.06.033

Diab, A., Enieb, M., & Singh, D. (2019). Influence of aging on properties of polymer-modified asphalt. *Construction and Building Materials, 196*, 54-65. doi:https://doi.org/10.1016/j.conbuildmat.2018.11.105

Elkashef, M., Podolsky, J., Williams, R. C., & Cochran, E. (2017). Preliminary examination of soybean oil derived material as a potential rejuvenator through Superpave criteria and asphalt bitumen rheology. *Construction and Building Materials, 149*, 826-836. doi:https://doi.org/10.1016/j.conbuildmat.2017.05.195

Elkashef, M., Williams, R. C., & Cochran, E. (2018). Effect of Asphalt Binder Grade and Source on the Extent of Rheological Changes in Rejuvenated Binders. *Journal of Materials in Civil Engineering, 30*(12), 04018319. doi:10.1061/(asce)mt.1943-5533.0002526

Elwardany, M. D. (2017). *Phenomenological Modeling and Laboratory Simulation of Long-Term Aging of Asphalt Mixtures.* (Doctor of Philosophy). North Carolina State University, Raleigh, NC.

Elwardany, M. D., Yousefi Rad, F., Castorena, C., & Kim, Y. R. (2017). Evaluation of asphalt mixture laboratory long-term ageing methods for performance testing and prediction. *Road Materials and Pavement Design, 18*(sup1), 28-61. doi:10.1080/14680629.2016.1266740

Epps Martin, A., Kasser, F., Arambula-Mercado, E., Bajaj, A., Garcia Cucalon, L., Yin, F., . . . King, G. (2020). *Evaluating the Effects of Recycling Agents on Asphalt Mixtures with High RAS and RAP Binder Ratios*. Washington, D.C.: Transportation Research Board.

Feng, Z., Xu, S., Sun, Y., & Yu, J. (2012). Performance Evaluation of SBS Modified Asphalt with Different Anti-aging Additives. *Journal of Testing and Evaluation, 40*(5), 728-733. doi:10.1520/JTE20120047

Fornai, D., Sangiorgi, C., Mazzotta, F., Bermejo, J., & Saiz, L. (2016). *A new era for rubber asphalt concretes for the green public procurement in road construction.* Paper presented at the Proceedings of the 1st European Road Infrastructure Congress, Leeds, UK.

Garcia Cucalon, L., Kaseer, F., Arámbula-Mercado, E., Epps Martin, A., Morian, N., Pournoman, S., & Hajj, E. (2019). The crossover temperature: significance and application towards engineering balanced recycled binder blends. *Road Materials and Pavement Design, 20*(6), 1391-1412. doi:10.1080/14680629.2018.1447504

Glover, C. J. D. R. R. D. C. H. R. Y. J. P. K. D. B. J., Sung Hoon. (2005). *Development of a New Method for Assessing Asphalt Binder Durability with Field Validation* (FHWA/TX-05/1872-2). Retrieved from College Station, Texas: https://library.ctr.utexas.edu/hostedpdfs/tti/0-1872-2.pdf

Hand, A. J. T., Aschenbrener, Timothy B. (2021). *Succesful Use of Reclaimed Asphalt Pavement in Asphalt Mixtures*. Retrieved from Reno, Nevada: http://hdl.handle.net/11714/8000

Houston, W., Mirza, M., Zapata, C., & Raghavendra, S. (2005). NCHRP Web-Only Document 113: Environmental Effects in Pavement Mix and Structural Design Systems. *Transportation Research Board of the National Academies, Washington, DC*.

Hu, Z., Zhang, H., Wang, S., & Xu, T. (2020). Thermal-oxidative aging mechanism of asphalt binder based on isothermal thermal analysis at the SARA level. *Construction and Building Materials, 255*, 119349. doi:https://doi.org/10.1016/j.conbuildmat.2020.119349

Huh, J.-D., & Robertson, R. E. (1996). Modeling of Oxidative Aging Behavior of Asphalts from Short-Term, High-Temperature Data as a Step toward Prediction of Pavement Aging. *Transportation Research Record: Journal of the Transportation Research Board, 1535*(1), 91-97. doi:10.1177/0361198196153500112

Im, S., Zhou, F., Lee, R., & Scullion, T. (2014). Impacts of rejuvenators on performance and engineering properties of asphalt mixtures containing recycled materials. *Construction and Building Materials, 53*, 596-603. doi:https://doi.org/10.1016/j.conbuildmat.2013.12.025

Jin, D., Ge, D., Wang, J., Malburg, L., & You, Z. (2023). Reconstruction of Asphalt Pavements with Crumb Rubber Modified Asphalt Mixture in Cold Region: Material Characterization, Construction, and Performance. *Materials, 16*(5), 1874. doi:10.3390/ma16051874

Jin, X., Han, R., Cui, Y., & Glover, C. J. (2011). Fast-Rate–Constant-Rate Oxidation Kinetics Model for Asphalt Binders. *Industrial & Engineering Chemistry Research, 50*(23), 13373-13379. doi:10.1021/ie201275q

Jing, R., Varveri, A., Liu, X., Scarpas, A., & Erkens, S. (2021). Differences in the Ageing Behavior of Asphalt Pavements with Porous and Stone Mastic Asphalt Mixtures. *Transportation Research Record: Journal of the Transportation Research Board, 2675*(12), 1138-1149. doi:10.1177/03611981211032218

Kaseer, F., Garcia Cucalon, L., Arambula, E., Epps Martin, A., & Epps, J. (2018). Practical Tools for Optimizing Recycled Materials Content and Recycling Agent Dosage for Improved Short-and Long-Term Performance of Rejuvenated Binder Blends and Mixtures. *Asphalt Paving Technology: Association of Asphalt Paving Technologists-Proceedings of the Technical Sessions, 87*. doi:10.12783/aapt2018/33816

Kaseer, F., Martin, A. E., & Arámbula-Mercado, E. (2019a). Use of recycling agents in asphalt mixtures with high recycled materials. *Construction and Building Materials*, 974-987.

Kaseer, F., Martin, A. E., & Arámbula-Mercado, E. (2019b). Use of recycling agents in asphalt mixtures with high recycled materials contents in the United States: A literature review. *Construction and Building Materials, 211*, 974-987. doi:https://doi.org/10.1016/j.conbuildmat.2019.03.286

Kaseer, F., Yin, F., Arámbula-Mercado, E., & Epps Martin, A. (2017). Stiffness Characterization of Asphalt Mixtures with High Recycled Material Content and Recycling Agents. *Transportation Research Record, 2633*(1), 58-68. doi:10.3141/2633-08

Keuliyan, F. (2022). *Rheological and Chemical Evaluation of Aging Resistant Binder Technologies.* (Master of Science). Auburn University, Auburn, AL.

Kim, S.-S., & Sargand, S. (2003). *PERFORMANCE EVALUATION OF POLYMER MODIFIED SUPERPAVE MIXES USING LABORATORY TESTS AND ACCELERATED PAVEMENT LOAD FACILITY*.

Kim, S., Sholar, G. A., Byron, T., & Kim, J. (2009). Performance of Polymer-Modified Asphalt Mixture with Reclaimed Asphalt Pavement. *Transportation Research Record, 2126*(1), 109-114. doi:10.3141/2126-13

Kim, Y. R., Castorena, C., Elwardany, M., Yousefi Rad, F., Underwood, B. S., Gundla, A., . . . Glaser, R. R. (2017). *Long-Term Aging of Asphalt Mixtures for Performance Testing and Prediction*. Retrieved from Washington, DC:

Kim, Y. R., Castorena, C., Saleh, N. F., Braswell, E., Elwardany, M., & Rad, F. Y. (2021). *Long-Term Aging of Asphalt Mixtures for Performance Testing and Prediction*. Retrieved from Raleigh, NC:

Kim, Y. R. Y. W. B. S. U. (2019). *Cyclic Fatigue Index Parameter (Sapp) for Asphalt Performance Engineered Mixture Design* (FHWA-HIF-19-091). Retrieved from Washington, D.C.:

Lesueur, D. (2009). *Evidence of the Colloidal Structure of Bitumen*.

Li, Y., Li, L., Zhang, Y., Zhao, S., Xie, L., & Yao, S. (2010). Improving the aging resistance of styrene-butadiene-styrene tri-block copolymer and application in polymer-modified asphalt. *Journal of Applied Polymer Science, 116*(2), 754-761. doi:https://doi.org/10.1002/app.31458

Lin, P., Liu, X., Apostolidis, P., Erkens, S., Ren, S., Xu, S., . . . Huang, W. (2021). On the rejuvenator dosage optimization for aged SBS modified bitumen. *Construction and Building Materials, 271*, 121913. doi:https://doi.org/10.1016/j.conbuildmat.2020.121913

Lo Presti, D. (2013). Recycled Tyre Rubber Modified Bitumens for road asphalt mixtures: A literature review. *Construction and Building Materials, 49*, 863-881. doi:https://doi.org/10.1016/j.conbuildmat.2013.09.007

Lu, X., & Isacsson, U. (2002). Effect of ageing on bitumen chemistry and rheology. *Construction and Building Materials, 16*(1), 15-22. doi:https://doi.org/10.1016/S0950-0618(01)00033-2

Mensching, D. J., Rowe, G. M., & Sias Daniel, J. (2017). A mixture-based Black Space parameter for low-temperature performance of hot mix asphalt. *Road Materials and Pavement Design, 18*(sup1), 404-425. doi:10.1080/14680629.2016.1266770

Mogawer, W., Bennert, T., Daniel, J. S., Bonaquist, R., Austerman, A., & Booshehrian, A. (2012). Performance characteristics of plant produced high RAP mixtures. *Road Materials and Pavement Design, 13*(sup1), 183-208. doi:10.1080/14680629.2012.657070

Mogawer, W. S., Austerman, A., Roque, R., Underwood, S., Mohammad, L., & Zou, J. (2015). Ageing and rejuvenators: evaluating their impact on high RAP mixtures fatigue cracking characteristics using advanced mechanistic models and testing methods. *Road Materials and Pavement Design, 16*(sup2), 1-28. doi:10.1080/14680629.2015.1076996

Moraes, R. (2014). *Investigation of Mineral Filler Effects on the Aging Process of Asphalt Mastics. Ph.D. Thesis*. Madison, Wisconsin: University of Wisconsin-Madison.

Moraes, R., & Bahia, H. (2015). Effect of Mineral Fillers on the Oxidative Aging of Asphalt Binders. *Transportation Research Record: Journal of the Transportation Research Board, 2506*(1), 19-31. doi:10.3141/2506-03

Moraes, R., & Bahia, H. (2018). Developing Simple Binder Indices for Cracking Resistance of Asphalt Binders at Intermediate and Low Temperatures. *Transportation Research Record, 2672*(28), 311-323. doi:10.1177/0361198118792999

Moraes, R., & Yin, F. (2022, 2022//). *Evaluation of Epoxy Asphalt Binders for Open-Graded Friction Course (OGFC) Application.* Paper presented at the Proceedings of the RILEM International Symposium on Bituminous Materials, Cham.

Morian, N., Hajj, E. Y., Glover, C. J., & Sebaaly, P. E. (2011). Oxidative Aging of Asphalt Binders in Hot-Mix Asphalt Mixtures. *Transportation Research Record, 2207*(1), 107-116. doi:10.3141/2207-14

Newcomb, D., Arambula-Mercado, E., Martin, A. E., Yuan, M., Tran, N., & Yin, F. (2019). *Field Verification of Proposed Changes to the AASHTO R30 Procedures for Laboratory Conditioning of Asphalt Mixtures*. Retrieved from

Nooralhuda, S. (2022). *Quality Assurance Aspects of Performance-Related Specificaton and Oxidative Aging of Asphalt Pavements.* (Doctor of Philosophy). North Carolina State University, Raleigh, North Carolina.

Nsengiyumva, G., Haghshenas, H. F., Kim, Y.-R., & Kommidi, S. R. (2020). Mechanical-Chemical Characterization of the Effects of Type, Dosage, and Treatment Methods of Rejuvenators in Aged Bituminous Materials. *Transportation Research Record, 2674*(3), 126-138. doi:10.1177/0361198120909110

Obaid, A., Nazzal Munir, D., Abu Qtaish, L., Kim Sang, S., Abbas, A., Arefin, M., & Quasem, T. (2019). Effect of RAP Source on Cracking Resistance of Asphalt Mixtures with High RAP Contents. *Journal of Materials in Civil Engineering, 31*(10), 04019213. doi:10.1061/(ASCE)MT.1943-5533.0002817

Olard, F., & Di Benedetto, H. (2003). General "2S2P1D" Model and Relation Between the Linear Viscoelastic Behaviours of Bituminous Binders and Mixes. *Road Materials and Pavement Design, 4*(2), 185-224. doi:10.1080/14680629.2003.9689946

Ongel, A., & Hugener, M. (2015). Impact of rejuvenators on aging properties of bitumen. *Construction and building materials*, 467-474.

Oshone, M., Sias, J. E., Dave, E. V., Epps Martin, A., Kaseer, F., & Rahbar-Rastegar, R. (2019). Exploring master curve parameters to distinguish between mixture variables. *Road Materials and Pavement Design, 20*(sup2), S812-S826. doi:10.1080/14680629.2019.1633784

Ouyang, C., Wang, S., Zhang, Y., & Zhang, Y. (2006). Improving the aging resistance of styrene–butadiene–styrene tri-block copolymer modified asphalt by addition of antioxidants. *Polymer Degradation and Stability, 91*(4), 795-804. doi:https://doi.org/10.1016/j.polymdegradstab.2005.06.009

Park, H. J., Eslaminia, M., & Kim, Y. R. (2014). Mechanistic evaluation of cracking in in-service asphalt pavements. *Materials and Structures, 47*(8), 1339-1358. doi:10.1617/s11527-014-0307-6

Petersen, J. C. (2009). A Review of the Fundamentals of Asphalt Oxidation: Chemical, Physicochemical, Physical Property, and Durability Relationships. *Transportation research circular*.

Petersen, J. C., Harnsberger, P. M., & Robertson, R. E. (1996). Factors affecting the kinetics and mechanisms of asphalt oxidation and the relative effects of oxidation products on age hardening. *Preprints of Papers, American Chemical Society, Division of Fuel Chemistry, 41*(CONF-960807-; Journal ID: ACFPAI; ISSN 0569-3772; CNN: Contract DTFH61-92-C-00170; TRN: 97:000003-0020 2009-12-16), Medium: X; Size: pp. 1232-1244. Retrieved from https://www.osti.gov/biblio/430341

Pfeiffer, J. P., & Saal, R. N. J. (1940). Asphaltic Bitumen as Colloid System. *The Journal of Physical Chemistry, 44*(2), 139-149. doi:10.1021/j150398a001

Picado-Santos, L. G., Capitão, S. D., & Neves, J. M. C. (2020). Crumb rubber asphalt mixtures: A literature review. *Construction and Building Materials, 247*, 118577. doi:https://doi.org/10.1016/j.conbuildmat.2020.118577

Pszczoła, M., Jaczewski, M., Szydłowski, C., Judycki, J., & Dołżycki, B. (2017). Evaluation of Low Temperature Properties of Rubberized Asphalt Mixtures. *Procedia Engineering, 172*, 897-904. doi:https://doi.org/10.1016/j.proeng.2017.02.098

Rahbar-Rastegar, R., Sias Daniel, J., & Reinke, G. (2017). Comparison of asphalt binder and mixture cracking parameters. *Road Materials and Pavement Design, 18*(sup4), 211-233. doi:10.1080/14680629.2017.1389071

Randy C. West, P. D., P.E. (2018). Aging: Avoiding the Inevitable. *Asphalt Technology News, 30(1)*.

Rathore, M., Zaumanis, M., & Haritonovs, V. (2019). Asphalt Recycling Technologies: A Review on Limitations and Benefits. *IOP Conference Series: Materials Science and Engineering, 660*(1), 012046. doi:10.1088/1757-899X/660/1/012046

Reed, J. (2010). *Evaluation of the Effects of Aging on Asphalt Rubber Pavements.* (M.S.). Arizona State University, United States -- Arizona. Retrieved from http://spot.lib.auburn.edu/login?url=https://www.proquest.com/dissertations-theses/evaluation-effects-aging-on-asphalt-rubber/docview/822753385/se-2?accountid=8421

https://resolver.ebscohost.com/openurl?ctx_ver=Z39.88-2004&ctx_enc=info:ofi/enc:UTF-8&rfr_id=info:sid/ProQuest+Dissertations+%26+Theses+Global&rft_val_fmt=info:ofi/fmt:kev:mtx:dissertation&rft.genre=dissertations&rft.jtitle=&rft.atitle=&rft.au=Reed%2C+Jordan&rft.aulast=Reed&rft.aufirst=Jordan&rft.date=2010-01-01&rft.volume=&rft.issue=&rft.spage=&rft.isbn=978-1-124-37147-4&rft.btitle=&rft.title=Evaluation+of+the+Effects+of+Aging+on+Asphalt+Rubber+Pavements&rft.issn=&rft_id=info:doi/ ProQuest Dissertations & Theses Global database. (1483476)

Riekstins, A., Baumanis, J., & Barbars, J. (2021). Laboratory investigation of crumb rubber in dense graded asphalt by wet and dry processes. *Construction and Building Materials, 292*, 123459. doi:https://doi.org/10.1016/j.conbuildmat.2021.123459

Roberts, F. L. K., Prithvi S.; Lee, Dah-Yinn; Kennedy, Thomas W. (1996). *Hot Mix Asphalt Materials Mixture Design and Construction Second Edition*. Lanham, Maryland.

Saleh, N. F., Braswell, E., Elwardany, M., Yousefi Rad, F., Castorena, C., & Kim, Y. R. Field calibration and validation of a pavement aging model. *International Journal of Pavement Engineering*, 1-18. doi:10.1080/10298436.2022.2027416

Saleh, N. F., Keshavarzi, B., Yousefi Rad, F., Mocelin, D., Elwardany, M., Castorena, C., . . . Kim, Y. R. (2020). Effects of aging on asphalt mixture and pavement performance. *Construction*

and Building Materials, 258, 120309. doi:https://doi.org/10.1016/j.conbuildmat.2020.120309

Shen, J., Amirkhanian, S., & Tang, B. (2007). Effects of rejuvenator on performance-based properties of rejuvenated asphalt binder and mixtures. *Construction and Building Materials, 21*(5), 958-964. doi:https://doi.org/10.1016/j.conbuildmat.2006.03.006

Sirin, O., Paul, D. K., & Kassem, E. (2018a). State of the Art Study on Aging of Asphalt Mixtures and Use of Antioxidant Additives. *Advances in Civil Engineering, 2018*, 1-18. doi:10.1155/2018/3428961

Sirin, O., Paul, D. K., & Kassem, E. (2018b). State of the Art Study on Aging of Asphalt Mixtures and Use of Antioxidant Additives. *Advances in Civil Engineering, 2018*, 3428961. doi:10.1155/2018/3428961

Sudarsanan, N., & Kim, Y. R. (2022). A critical review of the fatigue life prediction of asphalt mixtures and pavements. *Journal of Traffic and Transportation Engineering (English Edition), 9*(5), 808-835. doi:https://doi.org/10.1016/j.jtte.2022.05.003

Sultana, S., & Bhasin, A. (2014). Effect of chemical composition on rheology and mechanical properties of asphalt binder. *Construction and Building Materials, 72*, 293-300. doi:10.1016/j.conbuildmat.2014.09.022

Tarar, M. A., Khan, A. H., & Rehman, Z. u. (2022). Evaluation of effects of soybean derived oil and aggregate petrology on the performance of asphalt mixes. *Road Materials and Pavement Design, 23*(2), 308-334. doi:10.1080/14680629.2020.1826346

Tia, M., Roque, R., Sirin, O., & Kim, H.-J. (2002). *Evaluation of Superpave mixtures with and without polymer modification by means of accelerated pavement testing*. Retrieved from Gainesville, Florida:

Timm, D. H., Yin, F., Tran, N., Foshee, M., & Rodezno, C. (2022). Comparison of Relative Structural Characterization Methods for Additive-Modified Asphalt Mixtures. *Transportation Research Record, 2676*(11), 676-688. doi:Artn 03611981221094583
10.1177/03611981221094583

Tran, N. H., Taylor, A., & Willis, R. (2012). *Effect of rejuvenator on performance properties of HMA mixtures with high RAP and RAS contents*. Retrieved from Auburn, AL:

Von Quintus, H. L., Mallela, J., & Buncher, M. (2007). Quantification of Effect of Polymer-Modified Asphalt on Flexible Pavement Performance. *Transportation Research Record, 2001*(1), 141-154. doi:10.3141/2001-16

Wang, L., Chang, C.-q., & Xing, Y.-m. (2009). Viscoelastic Mechanical Properties of Crumb Rubber Modified Asphalt Mixture. In *ICCTP 2009* (pp. 1-6): American Society of Civil Engineering.

Wang, L., Shan, M., & Li, C. (2020). The cracking characteristics of the polymer-modified asphalt mixture before and after aging based on the digital image correlation technology. *Construction and Building Materials, 260*, 119802. doi:https://doi.org/10.1016/j.conbuildmat.2020.119802

Wang, Y. D., Keshavarzi, B., & Kim, Y. R. (2018). Fatigue Performance Prediction of Asphalt Pavements with FlexPAVETM, the S-VECD Model, and DR Failure Criterion. *Transportation Research Record: Journal of the Transportation Research Board, 2672*(40), 217-227. doi:10.1177/0361198118756873

Wang, Y. D., Underwood, B. S., & Kim, Y. R. (2020). Development of a fatigue index parameter, Sapp, for asphalt mixes using viscoelastic continuum damage theory. *International Journal of Pavement Engineering, 23*(2), 438-452. doi:10.1080/10298436.2020.1751844

Wang, Y. D., Underwood, B. S., & Kim, Y. R. (2022). Development of a fatigue index parameter, Sapp, for asphalt mixes using viscoelastic continuum damage theory. *International Journal of Pavement Engineering, 23*(2), 438-452. doi:10.1080/10298436.2020.1751844

Wu, B., Luo, C., Pei, Z., Xia, J., Chen, C., & Kang, A. (2021). Effect of Different Polymer Modifiers on the Long-Term Rutting and Cracking Resistance of Asphalt Mixtures. *Materials, 14*(12). doi:10.3390/ma14123359

Wuang, Y. (2019). *Development of the Framework of Performance-Engineered Mixture Design for Asphalt Concrete* (Doctor of Philosophy). North Carolina State University, Raleigh, NC.

Xiang, Q., & Xiao, F. (2020). Applications of epoxy materials in pavement engineering. *Construction and Building Materials, 235*, 117529. doi:https://doi.org/10.1016/j.conbuildmat.2019.117529

Xiao, Y., van de Ven, M. F. C., Molenaar, A. A. A., Su, Z., & Zandvoort, F. (2011). Characteristics of two-component epoxy modified bitumen. *Materials and Structures, 44*(3), 611-622. doi:10.1617/s11527-010-9652-2

Xu, G., & Wang, H. (2017). Molecular dynamics study of oxidative aging effect on asphalt binder properties. *Fuel, 188*, 1-10. doi:https://doi.org/10.1016/j.fuel.2016.10.021

Yin, F., Kaseer, F., Arámbula-Mercado, E., & Epps Martin, A. (2017). Characterising the long-term rejuvenating effectiveness of recycling agents on asphalt blends and mixtures with high RAP and RAS contents. *Road Materials and Pavement Design, 18*(sup4), 273-292. doi:10.1080/14680629.2017.1389074

Yousefi Rad, F., Elwardany, M. D., Castorena, C., & Kim, Y. R. (2017). Investigation of proper long-term laboratory aging temperature for performance testing of asphalt concrete. *Construction and Building Materials, 147*, 616-629. doi:https://doi.org/10.1016/j.conbuildmat.2017.04.197

Youtchef, J., Gibson, N., Shenoy, A., & Al-Katheeb, G. (2006). The Evaluation of Epoxy Asphalt and Epoxy Asphalt Mixtures. *Proceedings of the Canadian Technical Asphalt Association, 51*, 351-368.

Zaumanis, M., & Mallick, R. B. (2015). Review of very high-content reclaimed asphalt use in plant-produced pavements: state of the art. *International Journal of Pavement Engineering, 16*(1), 39-55. doi:10.1080/10298436.2014.893331

Zaumanis, M., Mallick, R. B., & Frank, R. (2014). Determining optimum rejuvenator dose for asphalt recycling based on Superpave performance grade specifications. *Construction and Building Materials, 69*, 159-166. doi:https://doi.org/10.1016/j.conbuildmat.2014.07.035

Zaumanis, M., Mallick, R. B., & Frank, R. (2015). Evaluation of different recycling agents for restoring aged asphalt binder and performance of 100 % recycled asphalt. *Materials and Structures, 48*(8), 2475-2488. doi:10.1617/s11527-014-0332-5

Zhang, R., Sias, J. E., & Dave, E. V. (2021). Development of a rheology-based mixture aging model for asphalt material cracking performance evaluation. *Materials and Structures, 54*(4). doi:10.1617/s11527-021-01743-5

Zhou, F., Newcomb, D., Gurganus, C., Banihashemrad, S., Park, E. S., Sakhaeifar, M., & Lytton, R. L. (2016). *Experimental Design for Field Validation of Laboratory Tests to Assess Cracking Resistance of Asphalt Mixtures*. Retrieved from College Station, TX:

Zhu, J., Birgisson, B., & Kringos, N. (2014). Polymer modification of bitumen: Advances and challenges. *European Polymer Journal, 54*, 18-38. doi:https://doi.org/10.1016/j.eurpolymj.2014.02.005

Ziari, H., Moniri, A., Bahri, P., & Saghafi, Y. (2019a). The effect of rejuvenators on the aging resistance of recycled asphalt mixtures. *Construction and Building Materials, 224*, 89-98. doi:https://doi.org/10.1016/j.conbuildmat.2019.06.181

Ziari, H., Moniri, A., Bahri, P., & Saghafi, Y. (2019b). The effect of rejuvenators on the aging resistance of recycled asphalt mixtures. *Construction and Building Mterials*, 89-98.

CHAPTER 7 - Appendices

7.1. Appendix 1.

Comparison of measured and predicted LTOA dynamic modulus (|*E|) in log-log scale for (a) control, (b) additive 1, (c) additive 2, (d) additive 3, (e) additive 4, and (f) additive 5 mixes with base binder 1.**

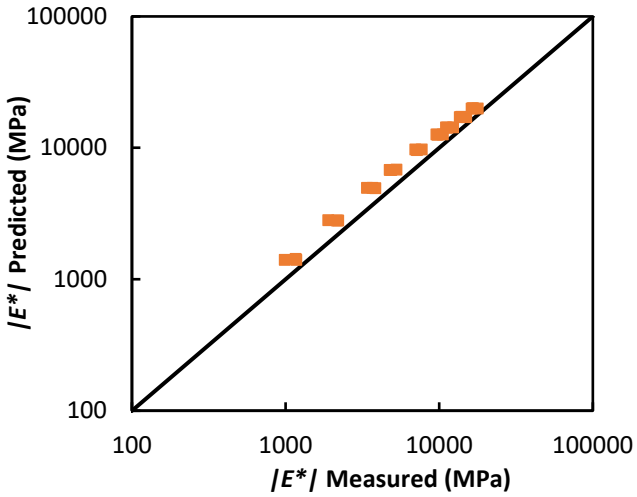

(a)

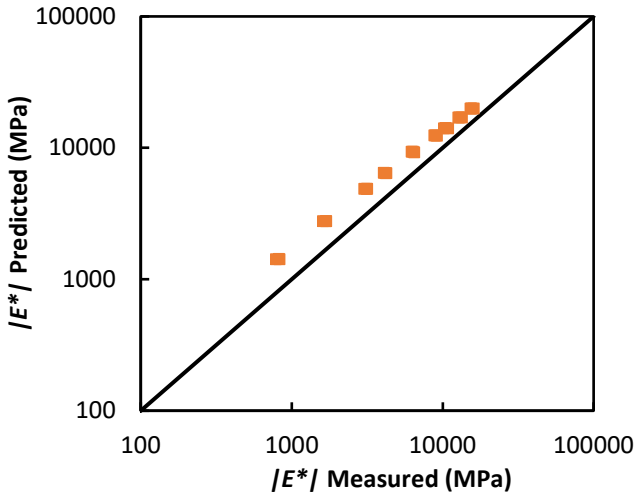

(b)

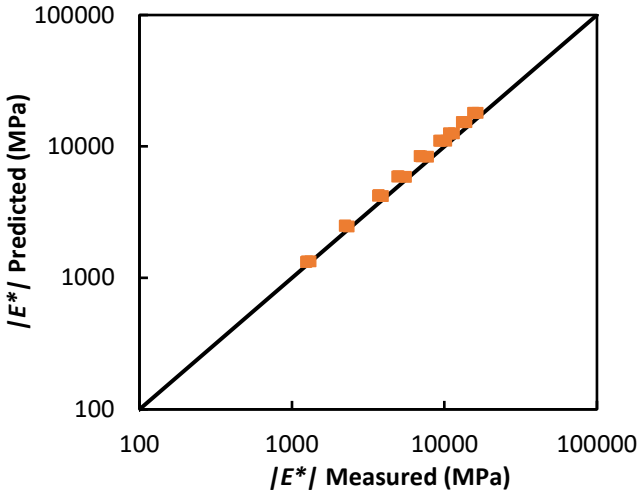

(c)

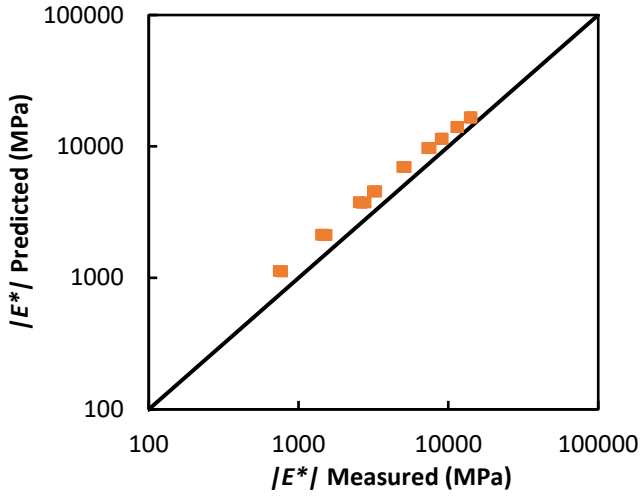

(d)

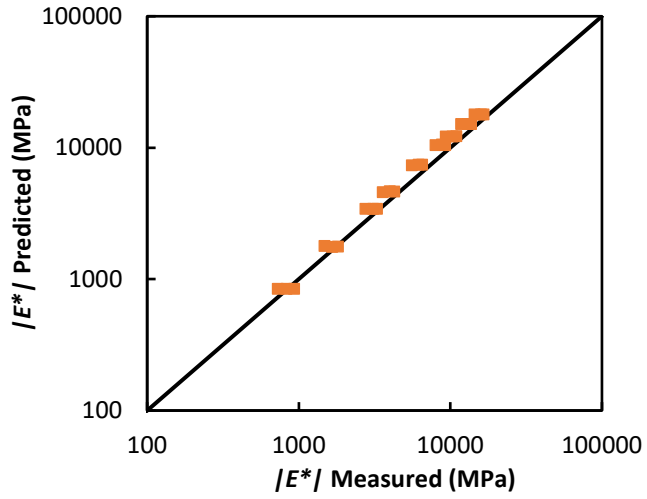

(e)

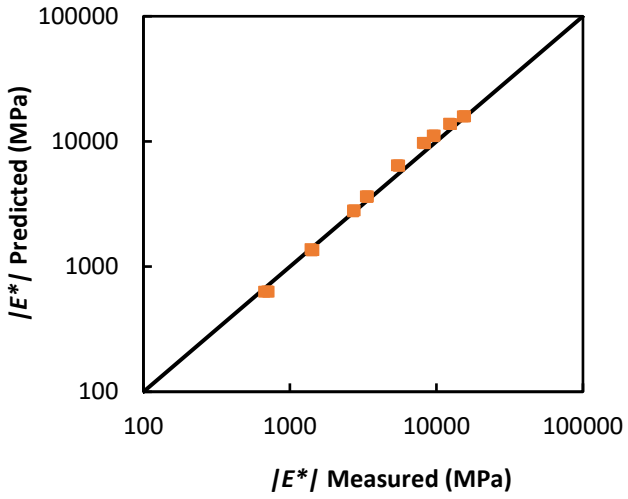

(f)

Comparison of measured and predicted LTOA dynamic modulus (|*E|) in log-log scale for (a) control, (b) additive 1, (c) additive 2, (d) additive 3, (e) additive 4, and (f) additive 5 mixes with base binder 5.**

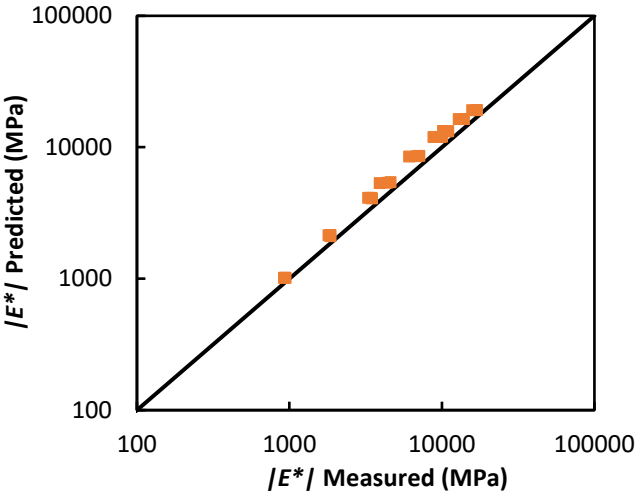

(a)

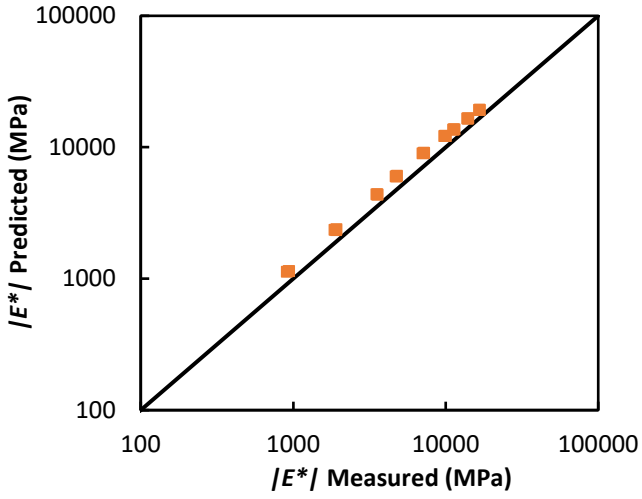

(b)

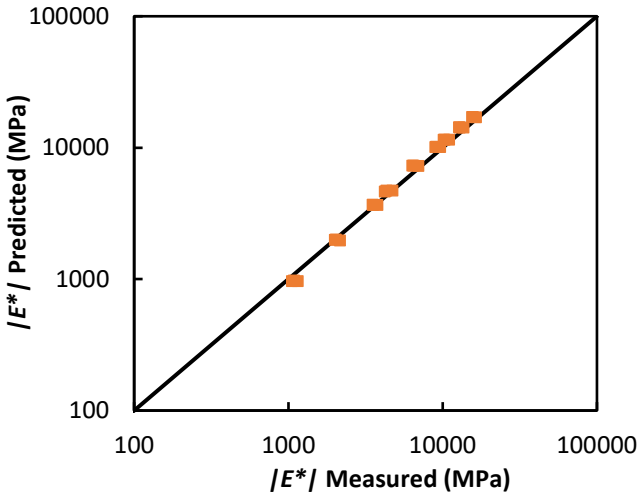
100000
10000
1000
100
100
1000
10000
100000
/E*/ Predicted (MPa)
/E*/ Measured (MPa)

(c)

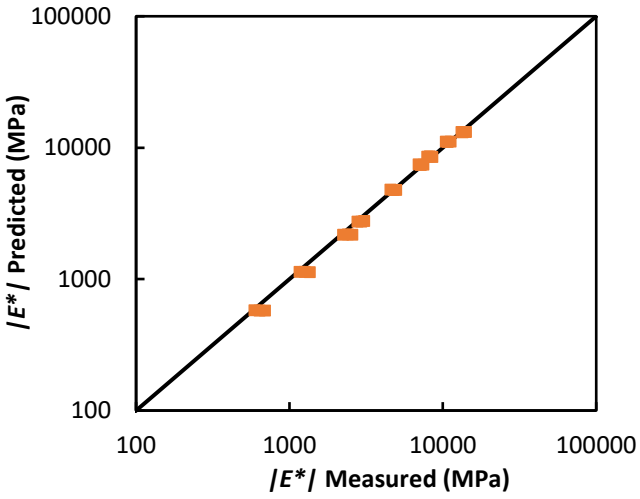
100000
10000
1000
100
100
1000
10000
100000
/E*/ Predicted (MPa)
/E*/ Measured (MPa)

(d)

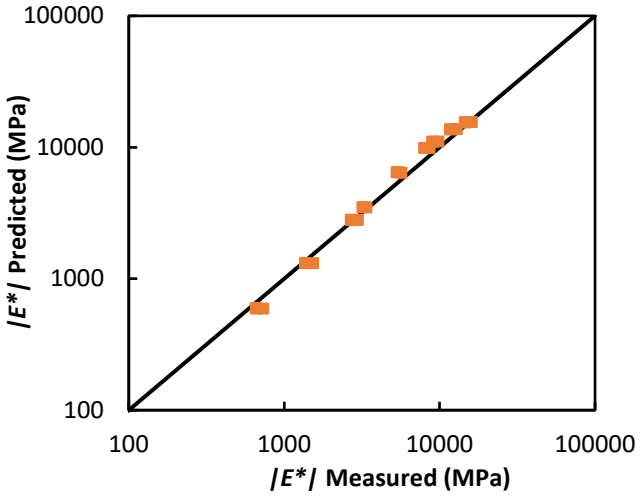
100000
10000
1000
100
100
1000
10000
100000
/E*/ Predicted (MPa)
/E*/ Measured (MPa)

(e)

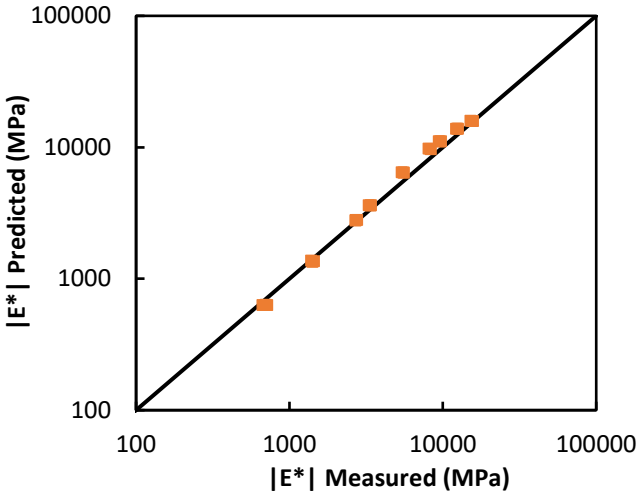
100000
10000
1000
100
100
1000
10000
100000
|E*| Predicted (MPa)
|E*| Measured (MPa)

(f)